NATIONAL AERONAUTICS AND SPACE ADMINISTRATION

Space Programs Summary 37-53, Vol. IV

Flight Projects

For the Period July 1 to August 31, 1968

JET PROPULSION LABORATORY
CALIFORNIA INSTITUTE OF TECHNOLOGY
PASADENA, CALIFORNIA

September 30, 1968

NATIONAL AERONAUTICS AND SPACE ADMINISTRATION

Space Programs Summary 37-53, Vol. I

Flight Projects

For the Period July 1 to August 31, 1968

JET PROPULSION LABORATORY
CALIFORNIA INSTITUTE OF TECHNOLOGY
PASADENA, CALIFORNIA

September 30, 1968

JPL SPACE PROGRAMS SUMMARY 37-53, VOL. I

Prepared Under Contract No. NAS 7-100
National Aeronautics & Space Administration

Preface

The Space Programs Summary is a multivolume, bimonthly publication that presents a review of technical information resulting from current engineering and scientific work performed, or managed, by the Jet Propulsion Laboratory for the National Aeronautics and Space Administration. The Space Programs Summary is currently composed of four volumes:

Vol. I. *Flight Projects* (Unclassified)

Vol. II. *The Deep Space Network* (Unclassified)

Vol. III. *Supporting Research and Advanced Development* (Unclassified)

Vol. IV. *Flight Projects and Supporting Research and Advanced Development* (Confidential)

Contents

PLANETARY–INTERPLANETARY PROGRAM

ADVANCED STUDIES

I. *Mariner* Mars 1969 Project

PLANETARY–INTERPLANETARY PROGRAM

A. Introduction

1. Mission Description

The primary objective of the *Mariner* Mars 1969 Project is to make two flyby exploratory investigations of Mars in 1969, which will set the basis for future experiments—particularly those relevant to the search for extra-terrestrial life. The secondary objective is to develop Mars mission technology.

The spacecraft design concept is modeled after the successful *Mariner IV* spacecraft, considerably modified to meet the 1969 mission requirements and to enhance mission reliability.

The launch vehicle is the *Atlas/Centaur* SLV-3C, used for the *Surveyor* missions. This vehicle, developed by General Dynamics/Convair Company for the Lewis Research Center, has a single- or double-burn capability in its second stage and a considerably increased performance rating over the *Atlas D/Agena D* used in the *Mariner IV* mission.

Mariner Mars 1969 missions will be supported by the Air Force Eastern Test Range launch facilities at Cape Kennedy, the tracking and data acquisition facilities of the Deep Space Network, and other NASA facilities.

The six planetary-science experiments, selected by NASA for the *Mariner* Mars 1969 missions, are listed in Table 1.

2. Project Status

During this reporting period, the first system test on the first flight spacecraft was completed and space simulator testing was begun. The proof-test model (PTM) test program was completed, and the spacecraft was disassembled for assembly-level tests, including the completion of type-approval requirements and life tests. (The PTM spacecraft is to be reassembled in December for mission support operations.) Assembly of the second flight spacecraft was completed and the first system test was started; buildup of the third was completed except for the science payload and the temperature control flux monitor.

A series of launch vehicle/spacecraft integration tests, using flight spacecraft adapters, was conducted in August and continued into the next period.

Table 1. *Mariner* Mars 1969 science experiments and investigators

Experiment	Investigator	Affiliation
Television	R. B. Leighton[a]	CIT
	B. C. Murray	CIT
	R. P. Sharp	CIT
	N. H. Horowitz	CIT
	A. G. Herriman	JPL
	R. K. Sloan	JPL
	M. E. Davies	Rand Corp.
	C. Leovy	Rand Corp.
	B. A. Smith	New Mexico State University
Infrared spectrometer	G. C. Pimentel[a]	UCB
	K. C. Herr	UCB
Ultraviolet airglow spectrometer	C. A. Barth[a]	University of Colorado
	F. C. Wilshusen	University of Colorado
	K. Gause	University of Colorado
	K. K. Kelly	University of Colorado
	R. Ruehle	University of Colorado
	J. B. Pearce	University of Colorado
	E. F. Mackey	Packard-Bell Electronics Corp.
	W. G. Fastie	Johns Hopkins University
Infrared radiometer	G. Neugebauer[a]	CIT
	G. Munch	CIT
	S. C. Chase	Santa Barbara Research Center, Hughes Aircraft Co.
S-band occultation	A. J. Kliore[a]	JPL
	G. Fjeldbo	Stanford University
	S. I. Rasool	Goddard Institute of Space Studies
Celestial mechanics	J. D. Anderson[a]	JPL
	W. L. Martin	JPL

[a]Principal investigator.

Development, documentation, and test planning for the Mission Operations System (MOS) and the Tracking and Data System continued during this period. The MOS test readiness review, a design review of the encounter sequence, and the ninth project quarterly review are scheduled for September 1968.

B. Project Engineering

1. Launch Vehicle Integration

Efforts of launch vehicle integration for the *Mariner* Mars 1969 Project include the continuing negotiation and documentation of interface design agreements and the negotiation and coordination of interface tests and operational conditions between the spacecraft system and the *Atlas/Centaur* launch vehicle system. The *Mariner* spacecraft are to be launched by vehicles AC-19 and AC-20.

During the period, updated revisions of the spacecraft launch vehicle hardware interface control document, the interface control drawing, and the interface schedule were released. A large number of technical agreements was made, and a number of important interface tests was completed.

Air-conditioning tests were performed at the Air Force Eastern Test Range using the AC-17 launch vehicle. The telemetry design verification test was also completed. Following the spacecraft separation and match-mate tests conducted with the development-test model spacecraft in a previous reporting period (SPS 37-51, Vol. I, p. 2), detailed flight-equipment match-mate operations were begun during the present period at General Dynamics/Convair, San Diego. The first flight adapter was mated to the AC-19 vehicle, and a composite test and data review were conducted late in August. Mechanical match-mate of AC-20 with two other flight adapters was also conducted.

2. Spacecraft System Test and Operations

a. Introduction. Mariner Mars 1969 spacecraft system test operations progressed on schedule (SPS 37-50, Vol. I, Fig. 10, p. 42) during July and August 1968. Some electrical test operations were performed ahead of schedule on the flight and flight spare spacecraft due to early delivery of some spacecraft subsystems.

Phase I of the proof-test model (PTM) spacecraft (M69-1) test program was completed in early August. Selected subsystems were removed from the spacecraft for additional testing in the subsystem laboratories. The spacecraft will be reassembled for flight-support testing, which is scheduled to start in January 1969.

Flight spacecraft assembly and test operations proceeded smoothly during July and August. The first flight spacecraft (M69-2) completed its first system test and had virtually completed part I of the space simulation test during the reporting period. The second flight spacecraft (M69-3) was well into its first system test by the end of August, while assembly and test of the flight spare spacecraft (M69-4) was well underway.

b. Spacecraft M69-1 (PTM). System test 3 was conducted at the JPL Spacecraft Assembly Facility from July 1 to 9 to verify the functional performance of the

spacecraft as an integrated system within the constraints imposed by the test equipment and the earth-based environment. During the test, the spacecraft was exercised in all major elements of a nominal flight sequence. Three different types of trajectory-correction maneuvers were performed, as well as two types of far- and near-encounter sequences. Encounter data were played back, using both the normal low-rate capability and the block-coded high-rate (86.4-kbit/s) capability.

A series of preliminary compatibility tests was held between the M69-1 spacecraft and Compatibility Test Area 21 of the Deep Space Instrumentation Facility (DSIF) during the period July 10–17. The purpose of the tests was to establish the degree to which the telecommunications portions of the spacecraft and DSIF designs met the requirements of the *Mariner* Mars 1969 Project and to establish the design compatibility between a preliminary version of the DSIF telemetry and command processor operational software and the spacecraft data stream.

A power transient survey was performed on July 18 to obtain oscilloscope pictures and oscillograph recordings of the power transients produced during the turn-on of spacecraft subsystems. A secondary objective was to verify that the transients produced were insufficient to cause the spacecraft battery and spacecraft solar panel supplies to go into a sharing mode, even when the total spacecraft power load was at or near maximum.

A free mode test was held on July 19 to: (1) demonstrate the correct operation of the spacecraft on solar power, (2) verify the functional integrity of the spacecraft in the absence of any support equipment electrical connections, and (3) verify that the system test complex and associated cabling did not affect spacecraft data readouts. To meet the test objectives, the spacecraft solar panels were installed in protective boxes, placed outside the test facility, and oriented toward the sun (Fig. 1). The electrical power produced by the solar panels was used to operate the spacecraft, which was located inside the facility on its low-level positioner. Data analysis was performed via the telemetry link.

During the periods July 22–23 and 29–30, parameter variation tests were performed on the M69-1 spacecraft. The purpose of the tests was to vary selected spacecraft parameters above and below the nominal operating range to evaluate spacecraft system performance margins and subsystem interactions under specific tolerance variations.

Fig. 1. Solar panels in protective boxes oriented toward sun during free mode test

Television subsystem calibration was verified on July 25 and 26. The verification included all elements of the television picture-taking system.

During the alignment of the scan platform instruments on July 31, the line-of-sight of all planetary instruments mounted on the platform was measured with respect to each other and to a reference plane on the scan platform.

A scan control subsystem telemetry calibration was conducted on August 5 to provide accurate data concerning the correlation between the telemetered scan platform position data and the actual position of the scan platform clock and cone axes.

The umbilical and inflight separation connector transient test was conducted on August 2; the spacecraft was operated in the launch mode while specific transients were introduced into each separation connector function. In addition, each connector wire was grounded to the chassis in a separate test. Spacecraft performance was monitored to verify that the transients and grounding produced no deleterious effects.

Spacecraft cleaning and disassembly were performed from August 6 to 10. In addition to the usual cleaning methods utilized on the spacecraft temperature control

surfaces, a new ultrasonic procedure was tried experimentally. Selected spacecraft subsystems were removed and returned to the subsystem laboratories for additional testing. The remainder of the spacecraft was placed in bonded storage in the JPL Spacecraft Assembly Facility pit, where it will remain until reassembled in December 1968 for flight-support testing in January 1969.

c. Spacecraft M69-2. Assembly of the first flight spacecraft (M69-2) continued throughout July and August as flight-qualified equipment became available for installation. By the start of system test 1 on July 26, most of the flight equipment had been assembled.

Initial power application and subsystem interface testing began on June 7 (SPS 37-52, Vol. I, p. 5) and continued through July as new subsystems were installed on the spacecraft. After the interfaces had been verified, subsystem tests were performed on each newly installed subsystem. In addition, tests of several interrelated subsystems were performed in July in preparation for the first system test.

During July, spacecraft telemetry channel calibrations were verified and, when necessary, corrected. During the end-to-end calibrations, data were obtained that allowed verification of computer-derived curves describing the relationship between the data numbers telemetered by the flight telemetry subsystem and the engineering parameter (e.g., voltage, temperature, or pressure) being transduced on the spacecraft.

System test 1 was performed from July 26 to August 1; the functional performance of the spacecraft as an integrated system was verified. The spacecraft was operated in all of the major elements of a nominal flight sequence. The spacecraft was exercised through the central-computer-and-sequencer and direct-command-controlled encounter sequences and computer-only, sequencer-only, tandem, and aborted tandem trajectory-correction maneuvers.

The spacecraft was prepared for space simulation testing in the JPL 10-ft space simulator from August 17 to 23. Over 75 instrumentation thermocouples and about 35 auxiliary heaters for spacecraft temperature control and analysis were installed on the spacecraft and associated support equipment was installed in the space simulator. Preliminary spacecraft preparation was performed at the JPL Spacecraft Assembly Facility. The spacecraft was moved to the 10-ft space simulator and installed on the endbell support ring on August 19. Following connection of electrical cabling to the spacecraft, preliminary test equipment and spacecraft verifications were performed. Preparation was complete when the spacecraft system verification test, designed to verify the proper operation of all spacecraft subsystems, was successfully conducted.

Part I of the space simulation test began on August 23 with the evacuation of the 10-ft space simulator. The purpose of part I was to demonstrate long-term (at least 250 h) spacecraft functional performance while operating in a simulated space environment. During part I, the spacecraft was operated through all nominal modes several times while data were compiled for analysis. The nominal simulated space environment was a pressure of less than 5×10^{-5} torr and a cold-wall temperature of about $-300°F$.

d. Spacecraft M69-3. Assembly of the second flight spacecraft (M69-3) continued throughout July and August as flight-qualified equipment became available for installation. By the start of system test 1 on August 28, most of the flight equipment had been assembled.

Initial power application to spacecraft M69-3 subsystems commenced on June 27 and continued through July and August. Following verification of the subsystem interfaces, which began in early July, a detailed subsystem test was conducted on the newly installed subsystems.

Scan control subsystem telemetry calibration was performed during the period August 19–23 to: (1) calibrate telemetry measurements relative to the physical positions of the scan platform, (2) determine the scale factor of scan platform movement in response to command pulses, and (3) measure far-encounter planet sensor tracking performance and susceptibility to electromagnetic interference.

System test 1, designed to verify the functional performance of the spacecraft as an integrated system within the constraints imposed by test equipment and the earth-based environment, began on August 28.

e. Spacecraft M69-4. Assembly of the flight spare spacecraft (M69-4) began on August 12 when the spacecraft octagon was installed on its low-level positioner inside a portable, laminar downflow clean room, which is used for all flight spacecraft assembly operations. Assembly continued throughout August as flight-qualified equipment became available for installation.

A power subsystem test was performed on August 19 and 20 to verify proper operation of the spacecraft power subsystem before applying spacecraft power to other spacecraft subsystems.

Initial power application to spacecraft subsystems began on August 21 and continued throughout the remainder of the month as equipment was installed. Shortly after initial power application began, subsystem interface tests were begun and continued throughout August. The duration of the individual interface tests is dependent on the availability of the subsystems involved and the number and complexity of the interfaces. More than 290 subsystem interfaces were verified by the end of August.

C. Systems

1. System-Test-Complex Data System

During this reporting period, the system-test-complex data system (STCDS) supported the proof-test model (PTM) system testing, conducted following the series of tests recommended in the June 18 summary review. In addition, the initial system test of the M69-2 (first flight) spacecraft was supported after checkout and acceptance of the operational interfaces of data input subsystem A (DIS-A) with the new system-test-complex 2 (STC-2) equipment. Near the end of the reporting period, DIS-A was again moved from the JPL Spacecraft Assembly Facility (SAF) back to the 10-ft space simulator for operation in STC-1 during the simulator tests of the M69-2 spacecraft.

Assembly of DIS-B was completed, including interconnection of the signal and data input circuits, and operational acceptance tests were conducted on the new hardware modules. Interface tests with STC-3 were run successfully and the capability to operate DIS-B with the CDC 3300 computers and STC-3 was essentially completed by August 20. This included demonstrating the operational status of the associated test-director display.

The analog low-speed module is not yet being used for any type of test support; however, the signal interfaces with STC-3 were connected, and operational tests with the RF subsystem operational support equipment (OSE) were conducted. Extension of this capability to other spacecraft subsystem OSE depends on resolution of interface incompatibility problems.

A requirement was identified for an additional telemetry input module to permit extension of the so-called "minor support configuration"; i.e., engineering telemetry data acquisition concurrent with complete data acquisition from a second spacecraft. This configuration is needed during combined operations of STC-2 and STC-3 while DIS-A is located in the space simulator. Construction of the additional module is near completion.

A new program (assembly G) was introduced, which significantly improved operational capability and reliability, starting with the M69-2 system test. The succeeding program (assembly H), containing additional capability, was also assembled and checkout was started to enable its use in test operations during the next period.

Some operational constraints were levied on the STCDS during encounter tests to ensure against computer system saturation or recurrence of previous troubles. Some of the constraints were relaxed as operational experience was obtained. Development was continued on the program to provide supplementary plotting capability (in nonreal time) using the Scientific Computing Facility and its high-speed cathode-ray tube plotter. The program for providing ultraviolet/infrared spectrometer spectral plots using the image processing laboratory formatted tapes was improved and reached operational status. Another program was developed to accept decommutated format tapes from the STCDS and produce raw (spacecraft data number) plots of spacecraft engineering telemetry data.

The marginal capability of the STCDS to support tests on request (SPS 37-52, Vol. I, p. 9) has improved somewhat, although significant problems with computer system down-time continue. The air conditioning in the computer room is still somewhat unreliable and suffers from lack of adequate air distribution to some of the computer system components.

The problems associated with specific hardware and software malfunctions have been significantly reduced. The problems of the main STC line printer associated with STC-1/STC-2 were alleviated by the interchange of printer controllers. Troubles in the DIS controller that receives the high-rate telemetry and hardline data were eliminated, and a control problem, manifested by unreliability in the computer-controlled connect/disconnect function of the DIS modules, was solved by software changes. Some of the difficulties associated with processing high-rate data were found to be attributable to deficient interface circuits between OSE and STCDS, which distorted the signal waveforms; changes to the drivers were made to remedy these problems.

Other known, documented interface difficulties still remain to be investigated and resolved. Access to the STCDS for interface investigations, trouble shooting or repairs, improvements and additions, or maintenance continues to be very limited because of the first priority requirement for providing all requested real-time and nonreal-time support.

The tape recorder/reproducer system intended to provide simulation data for checkout of new program assemblies did not reach useful operational status because of problems with maintaining waveform and dc level with the direct-recording techniques necessary for handling the high-rate data. Some work is continuing on dc restoration of the reproduced waveforms.

Excessive computer running time was required during nonreal-time processing of the high-rate data, especially the decoding of the 86.4-kbit/s block-coded data. Some of these run-time problems were caused by anomalous recorded data resulting from TV subsystem, spacecraft block-coder, or data storage subsystem problems, or because of the hardware interface problem previously mentioned. The high-rate-processor operating time on good recorded data has now been reduced from about 30 times real time to 4 times real time. Selective tabulation of recorded engineering telemetry data is processed at about 10 times the real-time acquisition rate. Considerable nonreal-time processing was accomplished on a computer being used concurrently for test data processing of a spacecraft in the nonencounter mode.

Requirements on the STCDS are described in a series of documents called "User Service Requests." There is now a total of 41 such requests, which describe most of the supplementary data processing requirements beyond those provided by the software operating system and many various utility routines. All requests have been programmed and are either in use or are in the forthcoming assembly.

Programming was completed to interface existing software capability with the raw telemetry stream received via high-speed data line in block multiplexed form (i.e., containing intermingled blocks of engineering, science, and ground data system status information) from the Deep Space Instrumentation Facility telemetry and command processors. This capability will be used after launch to permit processing of spacecraft engineering telemetry by the CDC 3300 systems at the Air Force Eastern Test Range. The necessary communication terminal (modem and error detection decoder) to receive the data was installed in the SAF.

The Spacecraft Checkout Computer Facility (UNIVAC 1219 Data Processing System), previously used in the *Surveyor* system test and flight operations applications, is now being used to supplement the STCDS by performing real-time block decoding of the high-rate telemetry data on request by the test directors. This function provides a simplified version of the STCDS nonreal-time processing, permitting real-time evaluation of the block-decoding function on each 32-symbol word and of the degree of success in frame-synchronizing the 972- and 6804-bit science frames by recognizing the pseudonoise sequences. Application of the Spacecraft Checkout Computer Facility may be extended by providing additional nonreal-time processing capability for the STCDS log tapes to relieve STCDS peak processing load conditions.

2. Mission Operations Planning

Planning for the *Mariner* Mars 1969 mission operations has continued on schedule since the last reporting period. Activity has been focused on preparation for the training and testing phase of the mission operations for maximum readiness to support the first launch in February 1969.

The Mission Operations Training Plan, the Mission Operations Training Schedule, the Space Flight Operations Test Plan, and the Mission Operations Test Schedule were released during the period. The Space Flight Operations Plan was revised (Revision 2) to reflect recent changes in the mission sequence and to refine and expand the procedures and sequence of events to be utilized during space flight operations.

The Phase IA simulation program for the EMR 6050 computer, which was described in SPS 37-51, Vol. I, p. 10, is progressing as scheduled. The request for programming (RFP) and detail design document have been released. Computer coding of the program is complete and the first portion of the program, which produces edited digital tapes, was acceptance-tested on August 2, 1968. Acceptance-testing of the second portion of the program, the operational simulator, is scheduled for late August.

Digital computer tapes, containing data recorded during spacecraft testing are being produced by the system-test-complex data system. These tapes are being input to the Phase IA Edit program together with card modification data to produce final simulation digital tapes. The

operational simulator program will then process these final simulation digital tapes along with card inputs to produce teletype and high-speed data outputs or serial pulse-code-modulated outputs. These data will then be used for mission operations testing.

The Phase I simulation program acceptance-testing was completed on May 31, 1968. The program is being used to produce analog test tapes for Compatibility Test Area 21 integration tests, Air Force Eastern Test Range down-range station tests, and telemetry and command processor acceptance tests and to align the automatic data switching system synchronizer.

The Phase II RFP review of the engineering telemetry portion was conducted on June 26; review of the detail design document was conducted on July 31 and August 1, and coding is in process. Work on the RFP for the science telemetry portion of the Phase II program will be started in the next reporting period.

Pulse-code-modulated analog data were recorded during the M69-2 spacecraft system tests, and duplicate tapes have been provided to the Deep Space Instrumentation Facility for Deep Space Network (DSN) testing.

All DSN command libraries have been produced, verified, and delivered to the DSN. These libraries of read–write–verify command tapes will be located at each deep space station committed to support *Mariner* Mars 1969. All direct, quantitative, and certain coded commands that will be transmitted to the *Mariner* Mars 1969 spacecraft during the space flight operations will come from this DSN command library.

D. Engineering Mechanics

1. V-Band Assembly

a. Introduction. The spacecraft is attached to the launch-vehicle/spacecraft adapter at eight points by V-blocks held in position by a circumferential stainless-steel band. The entire assembly is called the V-band assembly. A single attach point is shown in Fig. 2. A tension of 2500 lb is applied to the circumferential band by two turnbuckles. At the attach points, this tension becomes a radial force; through the wedging action of the V-blocks, it becomes an axial force, clamping the spacecraft and the adapter together. Separation is accomplished by pyrotechnically releasing the circumferential band at two points, thus allowing the blocks to retract simultaneously.

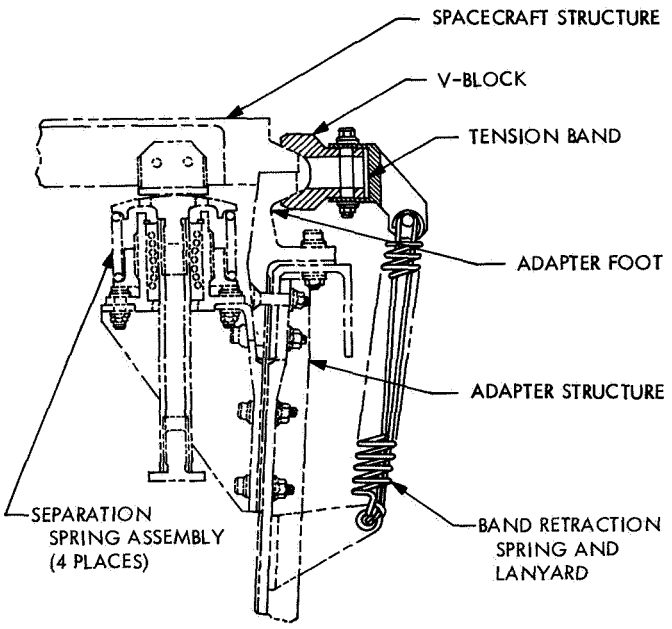

Fig. 2. Spacecraft separation joint

b. Design modifications. The V-band release method was first used on the *Mariner IV* and was again flown, unmodified, on *Mariner V*. The design of this system was, at that time, under the control of Lockheed Missiles and Space Company (LMSC) with the delivery and installation of this hardware being under their cognizance. Although JPL assumed direct responsibility of this area for *Mariner* Mars 1969, the basic design was kept intact with only minor modifications.

The change from an *Agena* final stage on the *Mariner* Mars 1964 and *Mariner* Venus 67 to the *Centaur* for the *Mariner* Mars 1969 made it necessary to revise the adapter interface. The *Mariner* Mars 1969 adapter design combines many of the spacecraft-interface features of the previous *Mariners* and most of the launch-vehicle-interface features of the *Surveyors*.

The most noteworthy design change resulted from a new, but subsequently relaxed, requirement that the V-band be tensioned to 3000 lb instead of the previously established 2500 lb; this requirement resulted primarily from a consideration of a heavier *Mariner* Mars 1969 spacecraft. The band material was changed from 7075-T6 aluminum alloy to A286 high-strength steel and also the turnbuckle size was increased from ¼- to 5/16-in. diameter. The pyrotechnic release devices, although considered marginal at this tension, were retained to minimize development effort and take advantage of previous test and flight data. However, as a result of subsequent testing,

which indicated some degree of tension relaxation in the device, the design requirements were reappraised and modified to the original 2500-lb tension specified on previous *Mariner* programs.

c. Qualification testing. V-band assemblies have undergone a complete series of developmental, type-approval, and flight-acceptance tests. All bands have been statically proof-loaded to 3450 lb a minimum of 6 times. Type-approval vibration testing of a complete development-test model and proof-test model spacecraft mounted on flight adapters with both 2500- and 3000-lb tensions has been successfully completed with only the previously mentioned load relaxation being noted.

Static and dynamic separation tests have been performed with a fully configured spacecraft using the flight-type V-band. Approximately 21 pyrotechnic releases have been logged with accelerometer, rate gyro, and fastax movies being used to record data. In all cases, including tests using only one pyrotechnic release device and one squib, the V-band properly released, allowing the spacecraft to separate.

d. V-band operational support equipment. Band tension is monitored during assembly and post-assembly operations by means of foil strain gages attached to the flat strap segments. During installation, tension readings are taken from gages mounted on each of the eight segments of the V-band assembly to ensure even distribution of load while tightening. These same gages are again monitored during critical tests, such as complete vehicle vibration, to verify no loss in load that might indicate an impending failure. A third requirement, newly established for *Mariner* Mars 1969, is the blockhouse monitoring, via umbilical lines, of tension on two of the eight gages during launch countdown.

Strain gage readout consoles used by LMSC for the previous *Mariners* were made available for use by JPL if the new design requirements were compatible. However, a detailed study of the applicability of this equipment for such service as driving sufficient power through the long cables to the blockhouse, maintaining adequate stability on imbalanced umbilical lines, and providing proper sensitivity during installation resulted in the design and fabrication of new monitoring equipment. In addition to allowing design improvement in the above areas, it allowed the incorporation of parallel-channel independent circuitry that would ensure reliable operation of the remotely located, transfer room equipment.

Two sets of operational-support/launch-complex monitoring equipment have been fabricated and delivered. Both sets have been thoroughly tested with actual installation exercises and blockhouse/spacecraft interfaces have been verified as operational.

2. Spacecraft Structural Elements

a. Octagon structure assembly. All of the flight octagon structures (see SPS 37-52, Vol. I, Fig. 4, p. 13) have been assembled, inspected, and delivered to the JPL Spacecraft Assembly Facility. The design-test model and proof-test model have been tested without any structural failures.

The only major differences between the *Mariner* Mars 1969 octagon structure and the *Mariner* Mars 1964 structure are the larger and heavier scan platform attachment structure and a new adjustable midcourse motor mounting scheme. Since the fabrication techniques are essentially the same as in the previous program, there were very few problems. The difficulties that were encountered were in the new areas (motor mount and scan platform support) and were primarily tooling problems.

b. Superstructure assembly. The superstructure, for supporting the high-gain antenna, is a truss structure (Fig. 3) consisting of swaged aluminum tubing riveted to machined aluminum end-fittings.

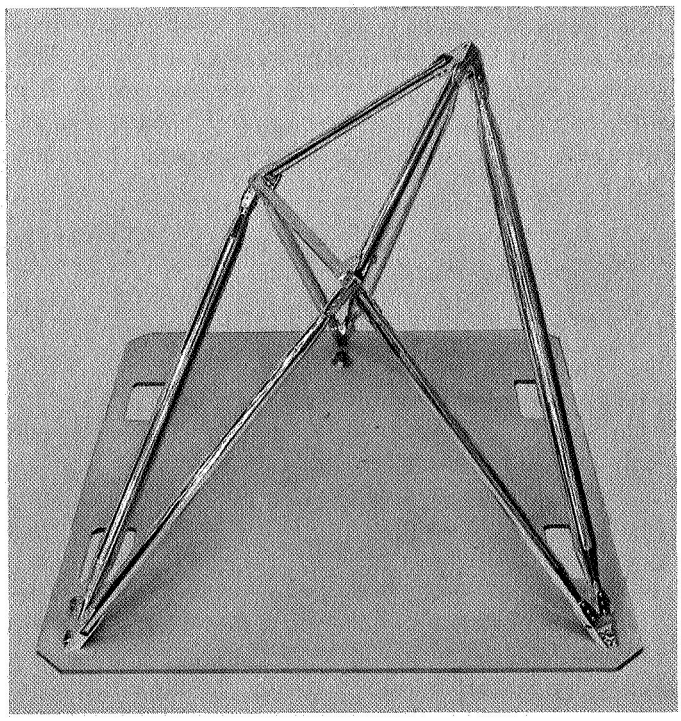

Fig. 3. Superstructure assembly

Assembly of the superstructure was accomplished by supporting the machined end-fittings in their relative positions by accurately machined tooling, and riveting the tubes to their respective fittings. The only problem encountered was a rivet that could not be drawn due to inadequate gun clearance. This rivet was replaced with a chemically expanded type.

The superstructures were completed ahead of schedule and have been tested with no failures.

c. Cable trough assembly. The *Mariner* Mars 1969 cable trough is an eight-sided polygon that is constructed from aluminum sheet metal and formed into a channel. This structure houses the spacecraft upper cable ring and mounts on the top of the octagon. The cable trough structure without the assembled cable ring is shown in Fig. 4. The holes in the outer surface of the trough are for connector mounting. The sheet metal segments are spot-welded together and are secured to the octagon structure by machined aluminum clips riveted to the trough.

No particular difficulty was encountered in fabricating the cable trough; however, a late change caused a connector location to be shifted. This made it necessary to patch the existing hole and relocate the mounting. There was no structural degradation associated with these modifications and the cable trough passed its structural test requirements.

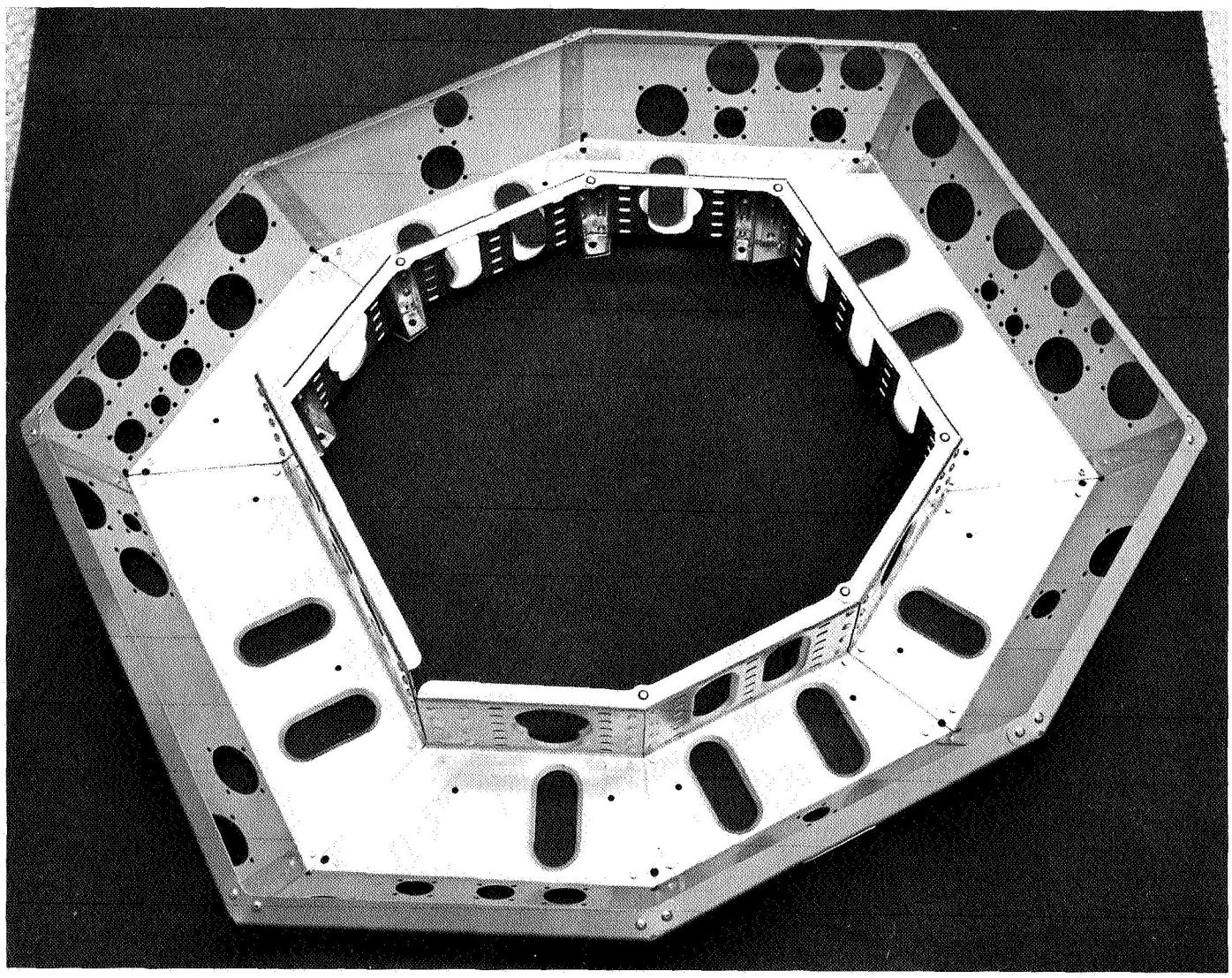

Fig. 4. Cable trough structure

3. Separation-Initiated Timer

a. Introduction. The primary function of the separation-initiated timer (SIT) is to provide a time delay between arming and firing of the pyrotechnics subsystem. This allows the capacitors to acquire the required charge. The SIT consists of a spring-loaded hydraulic timer and a set of electrical switches. The switch end of the timer shaft protrudes from the timer and holds the switches in the energized position (Fig. 5a). The other end rests against the adapter. When separation occurs, the shaft moves (slowly) under the influence of the timer spring and hydraulic damping. The switches move to the de-energized position (Fig. 5b) sequentially as the switch end of the shaft withdraws into the timer body.

The *Mariner* Mars 1969 SIT is only slightly different from the *Mariner* Mars 1964 SIT described in SPS 37-27, Vol. VI, p. 13. Two modifications have been made to the latter design: (1) a bellows-type volume compensator was added, and (2) a simple circuit was removed. Tests on the *Mariner* Mars 1964 SIT showed that high temperatures produced high pressures in the hydraulic fluid. No leakage occurred, but the volume compensator was added to the *Mariner* Mars 1969 design to increase the allowable temperature range and assure adequate sealing. The *Mariner* Mars 1964 SIT contained a resistive–capacitive circuit to prevent a blocking of the event registers by the closed switch contacts. This was removed from the *Mariner* Mars 1969 SIT design and combined with the rest of the pyrotechnic circuitry. Here, it is packaged in a more standard manner and the mechanical and thermal environments are better controlled.

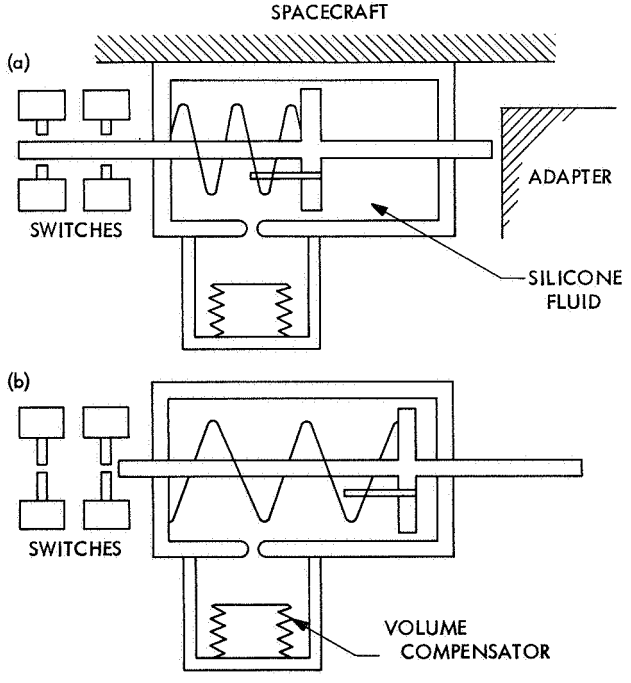

Fig. 5. Separation-initiated timer: (a) before separation, (b) after separation

b. Assembly operations. The SIT was not assembled satisfactorily from the drawings alone although JPL specification defines the assembly and checkout test procedures in considerable detail. Two assembly operations deserve special comment: filling the timer and adjustment of the microswitches.

Filling the timer and assembly in preparation for filling are the only assembly operations requiring a clean environment. Assembly is done in a class 10,000 clean area as defined in Federal Standard 209. The timer is assembled complete except for a cap. The timer is then placed in the vacuum fill apparatus (Fig. 6). The bell jar is evacuated to 30 or 40 μm pressure for about 2 h. This deaerates 9000-cS silicone fluid and evacuates the timer. The solenoid valve is operated, allowing the fluid to flow into the timer. The bell jar is repressurized with air to atmospheric pressure. This pressure collapses the bellows (a sealed evacuated type) to its midpoint, and additional fluid flows into the timer. To assure that fluid has completely filled the space on the far side of the capillary tube, the timer is capped, cocked, actuated, uncapped, and the fill cycle is repeated. There have been no difficulties due to incomplete filling.

Adjustment of the microswitches is somewhat difficult and requires considerable care. In the cocked configuration, the timer shaft must hold the microswitch actuator arms in the energized position and at the bottom of their overtravel (resting against the switch case). This is necessary to prevent switch chatter in the launch vibration environment. At the same time, the load between the timer shaft and the actuator arm must not be excessive. If it is, the drag on the shaft will produce erratic timing, or the side load will force the shaft against the O-ring gland causing galling when the shaft moves.

c. Test criteria. The test criteria for the SIT are defined by design and environmental requirements established by the *Mariner* Mars 1969 Project.

Switch resistance constraints have been established at 100 mΩ maximum for closed circuits and at 100 MΩ minimum for open circuits. Switch events must occur in sequence and at times specified.

(1) Switch 1 at 10 to 100 s after separation.

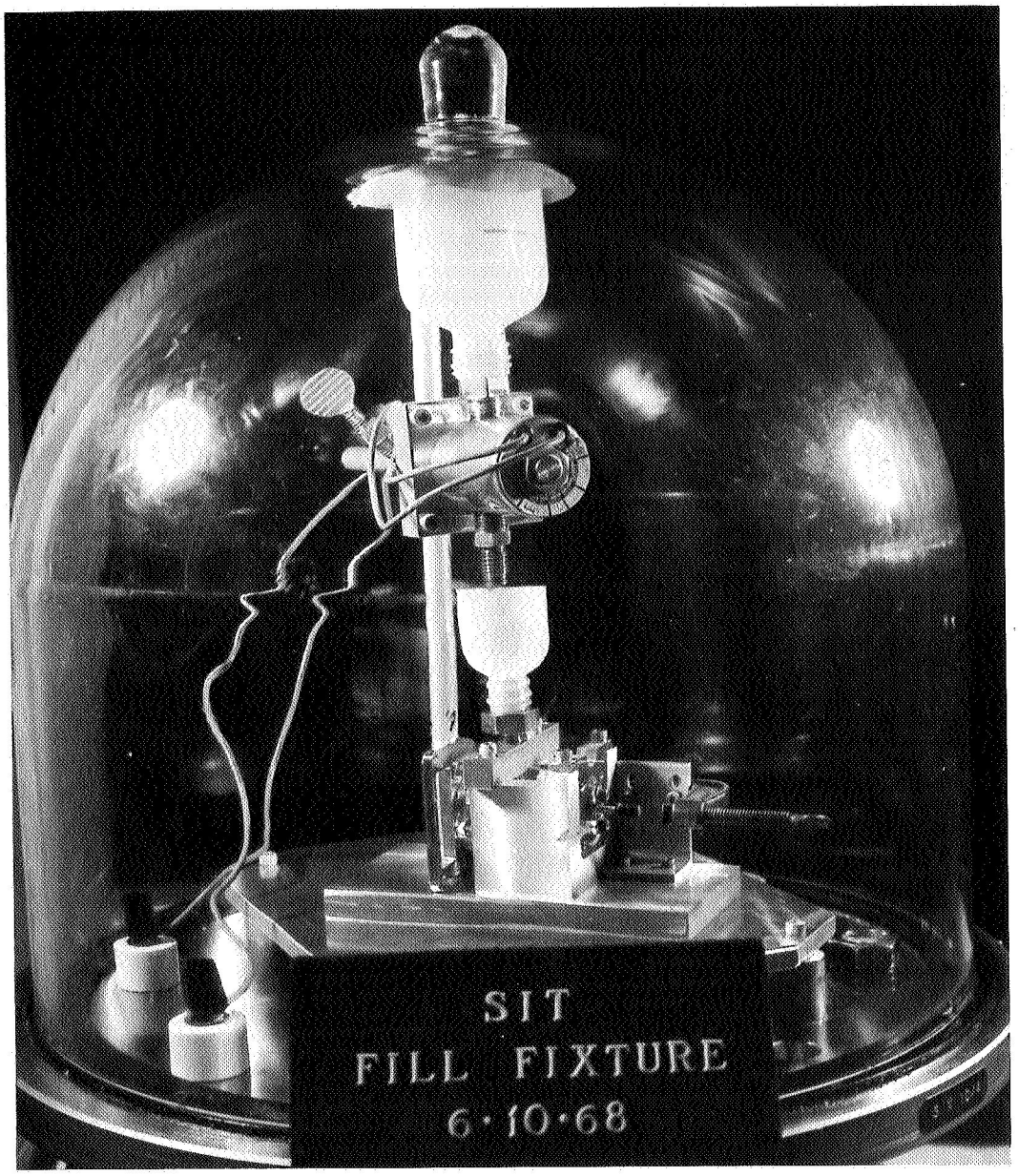

Fig. 6. Separation-initiated timer to fill fixture

(2) Switch 2 at 10 to 100 s after separation.

(3) Switch 3 at 100 to 450 s after separation.

(4) Switch 4 at 90 to 350 s after switch 2.

At any one temperature, the duration between any two events must be repeatable to within 20 s.

The SIT must also operate within these specifications over a temperature range of 32 to 131°F, and must meet resistance and leakage requirements over a range of −4 to 167°F. In addition, it must survive a three-axis sine vibration and three axes of random vibrations with no contact chatter of the switches.

d. Test results. Testing of the SIT revealed several problems. All but three were extremely minor and were corrected by part modifications or assembly procedure changes. The three remaining problems are switch chatter, improper microswitch adjustment (*Paragraph b*), and closed-circuit resistance above the 100 mΩ maximum.

Contact chatter was observed on switch 1 during vibration tests. The SIT is vibration-tested in the cocked configuration, which places all switches in the energized position. The chatter observed was a sequence of switch openings of approximately a ¼-ms duration. Figures 7a and b show the internal configuration of the microswitches in the de-energized and energized positions, respectively. To stop the chatter, the actuating arm was bent to place a greater load on the contact. However, bending the arm is not recommended as a permanent, flight-worthy solution, since the switch can be easily damaged and the mating geometry of the normally open contact can be altered. Further, the high-resistance anomaly problem tended to prove that bending the arm was indeed detrimental. Bending the arm was discontinued, and the chatter problem was satisfactorily solved by selecting a switch with at least a 0.005-in. overtravel for switch 1. The problem existed only with this switch because it is the only switch wired to the normally open contact.

The most puzzling problem encountered was erratic closed-circuit resistance. The specifications require that the closed-circuit resistance be no more than 100 mΩ. For switches of the same type, the normal resistance was found to be about 20 mΩ, including the contact resistance of the SIT connector, the mating connector, and the wiring in the SIT. It was found that the resistance of such a switch would vary from actuation to actuation over the range of 20 to 300 mΩ. The switches had all passed the screening specification (75 mΩ maximum) and were all 7 mΩ.

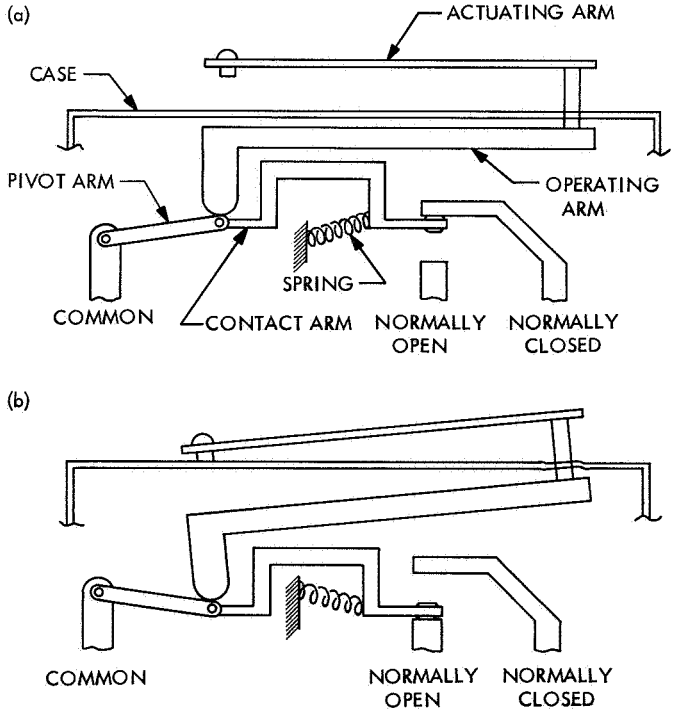

Fig. 7. Microswitch: (a) de-energized, (b) energized

The bridges used to measure closed-circuit resistance in the SIT applied a maximum of 6 and 11 V (to an open circuit) and supplied 175 and 215 mA through the closed contacts. A two-wire system was used. Investigation showed that, if the resistance is measured as described, the switch resistances are erratic and vary up to nearly 300 mΩ, but the resistance does not get higher as the switches are repeatedly actuated. In addition, if the resistance is measured at 1 A, the value is the "normal" 7 mΩ.

Since all the SIT circuits operate properly with 10 Ω in place of the closed-circuit switches, the "high-resistance" SITs were accepted for spacecraft use.

e. Operational support equipment. The operational support equipment for the SIT consists of equipment needed to operate the SIT in support of spacecraft assembly and testing. There are four items of SIT operational support equipment: the SIT cocking tool, the SIT/pyrotechnic arming switch (PAS) function simulator, the SIT remote actuator, and the SIT/PAS operational support equipment panel.

The spreader on the cocking tool puts the microswitches in the energized position and a thumbscrew moves the shaft into the cocked position against the SIT spring. The SIT/PAS function simulator is a box of manually operated switches with connectors so it can be plugged into the spacecraft cabling in place of the SIT and PAS and is easier to operate than the SIT and PAS. Since the switches are individually operable, it provides more flexibility for spacecraft electrical checkouts. The SIT remote actuator is a mechanism that holds the SIT in the cocked configuration and releases the shaft (thus simulating spacecraft separation) when a solenoid is activated. It is a one-shot device, and is used only to support the space simulator tests. The SIT/PAS operational support equipment panel is the power supply and switches needed to operate the SIT remote actuator.

4. Pyrotechnic Arming Switch

The pyrotechnic arming switch (PAS) has two primary functions: arming the pryotechnic subsystem (turning it on) and initiating the sun acquisition sequence. The PAS consists of four microswitches and two leaf springs

mounted in a housing. When the spacecraft is mated to the adapter, the switches are held in the energized position (Fig. 8). Upon separation, the springs and microswitches are released and the PAS moves to the deployed configuration.

The only significant difference between the *Mariner* Mars 1964 and *Mariner* Mars 1969 PAS designs was the addition of the inner spring (Fig. 8). Switch chatter was a problem in the *Mariner* Venus 67 Project, which used an unmodified *Mariner* Mars 1964 design. The outer spring (the only spring in the *Mariner* Mars 1964 design) has two broad leaves, each of which actuated two microswitches. The inner spring has four narrower leaves so that each switch is individually actuated. There has been no switch chatter problem on *Mariner* Mars 1969.

Assembly of the PAS is very simple and requires only the assembly drawing as a procedure. There is one relatively easy adjustment that must be made carefully during assembly. The mounting holes in the springs are large so the springs can be adjusted before the nuts are torqued. It was found that to prevent switch chatter during vibration the springs must be set at the extreme position in which they apply the most load on the switches.

The test criteria for the PAS are the same as for the separation-initiated timer (SIT), except for the timing

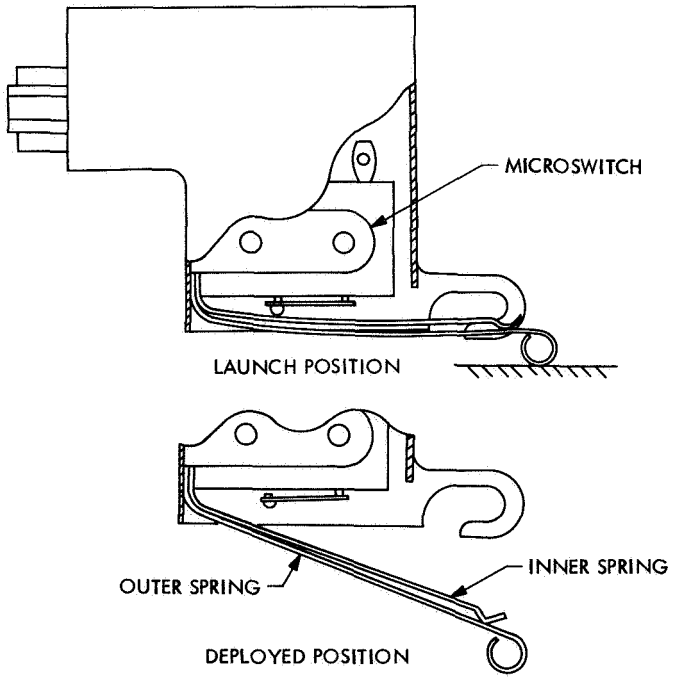

Fig. 8. Pyrotechnic arming switch

requirements. The only problem of significance revealed during testing of the PAS was the high-resistance problem (see *Subsection 3*).

There are three items of PAS operational support equipment: the SIT/PAS function simulator, the SIT/PAS operational support equipment panel, and the PAS remote actuator. The first two items are described in *Subsection 3*. The PAS remote actuator is a mechanism to release and reset the PAS during space simulator tests. It employs a two-coil latching solenoid that is operated from the SIT/PAS operational support equipment panel.

5. Mechanical Fasteners

The design of the *Mariner* spacecraft requires extensive use of mechanical fastener devices that must meet high reliability and performance requirements. In many instances these requirements are beyond the maximum qualification limits established by military specifications. It is important, therefore, to closely examine the selection of fasteners to minimize the inherent problems that exist when assembling spacecraft hardware.

The basic types of structural fasteners selected for use on the *Mariner* Mars 1969 spacecraft are illustrated in Figs. 9 and 10. A significant change from the *Mariner* Venus 67 spacecraft project is the use of the 12-point external-wrenching bolt in place of the hexagon-socket internal-wrenching bolt. Subsystems on the *Mariner* spacecraft are installed and removed a considerable number of times and the 12-point bolt provides a much more durable bolt-head wrenching configuration to satisfy the reusability requirement.

The primary structural fastener material in use on the *Mariner* Mars 1969 spacecraft is A286 corrosion-resistant steel. This is another significant change from the *Mariner* Venus 67 spacecraft, which used titanium alloy fasteners. Because the weight factor on the *Mariner* Mars 1969 spacecraft was not critical per se, A286 material was selected primarily for economy.

The performance of the fasteners used on *Mariner* Mars 1969 has been generally satisfactory; however, some problems were encountered. The three most common problems were nutplate failure, burrs on self-locking screws, and galling.

The nutplate failure involved a miniature, commercially available floating nutplate (Fig. 10). This nutplate is a three-piece assembly consisting of the basket, the floating self-locking nut, and a cap (or dome) brazed to the nut.

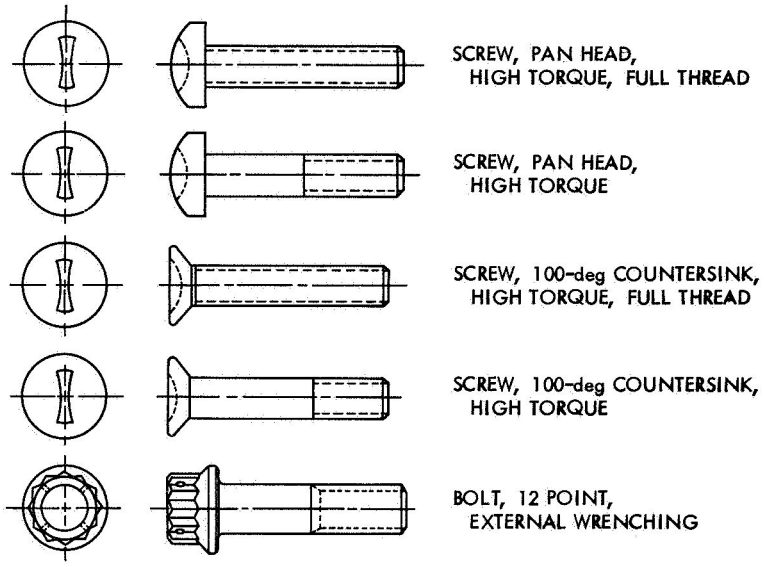

Fig. 9. External-threaded structural fasteners

A capped nutplate is used to trap any debris that is generated during assembly and disassembly of the screw into the nutplate. During a rivet removal operation on the octagon structure, a cap fell off a nutplate. Examination revealed a poorly brazed joint such that the shock of punching out a drilled rivet was sufficient to break loose the cap.

As a result of this failure, a test procedure was established to evaluate the brazed joint of the cap to the nut. All nutplates, including those installed in hardware and those remaining in stock, were subjected to this test. Approximately 20% of the nutplates were defective and were discarded.

The manufacturing inspection procedures applied to this part consisted of taking an acceptable-quality-level sample of each manufactured lot. An axial load of x pounds was applied to the cap of each sample part. If no failure occurred, the lot was accepted. If a failure did occur, the entire lot was inspected for defective parts. However, this method is now considered inadequate to assure detection of defective parts. Therefore, all nutplates are now inspected because of their critical spacecraft applications.

The burrs on self-locking screws are a constant problem. The *Mariner* Mars 1969 uses a very large number of self-locking screws ranging in size from 0.086 (No. 2) through 0.25 in. in diameter. Excessive burrs (resulting from drilling or milling operations) in the vicinity of the locking device affect the reusability performance of the screw. Burrs can also cause galling of the screw and

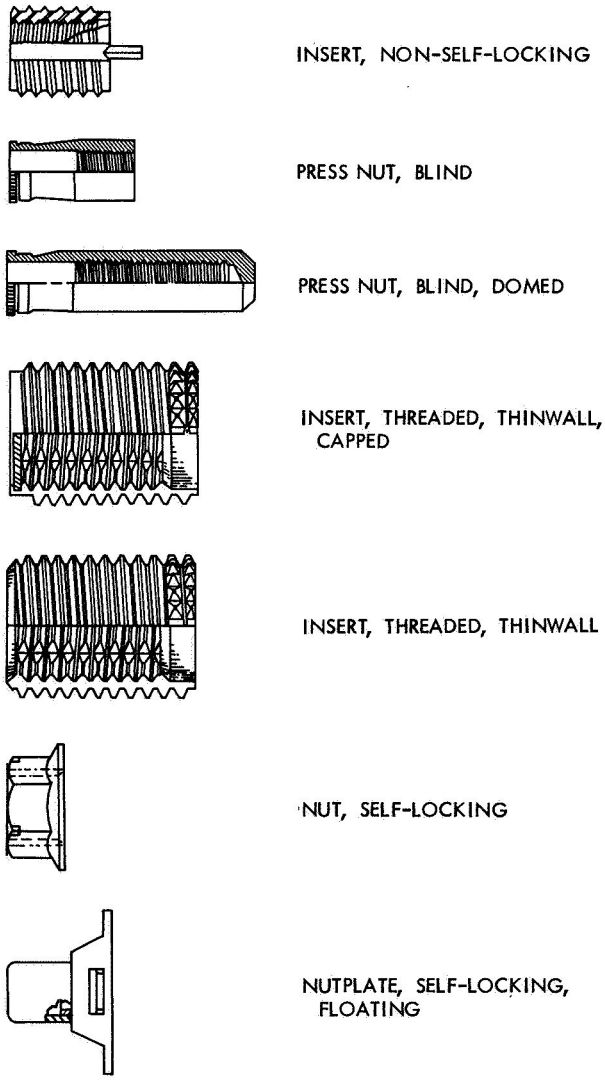

Fig. 10. Internal-threaded structural fasteners

mating part, as well as create a cleanliness problem around the spacecraft. To preclude these problems, it has been necessary to continue to procure, at a premium, "burr-free" self-locking screws, and to constantly monitor the manufacturing process to maintain the quality of workmanship required on these parts. A relatively new "bonded on" self-locking device may eliminate this problem on future spacecraft projects.

The galling problems experienced on the *Mariner* Mars 1969 spacecraft were of the type to be expected when using corrosion-resistant steel fasteners, particularly when installed in like material. The problems were resolved by using lubricants suitable for spacecraft environments.

6. Operational Support Equipment Cabling

The purpose of the operational support equipment (OSE) cables is to route power and signals from the OSE to the spacecraft. Two restraints governed their design:

(1) Shielded wires are to be grounded at the spacecraft end of the cable.

(2) For direct access and umbilical cables, a male connector (pins) is to be on the cable end nearest the spacecraft.

The OSE cables were categorized into: (1) console cables, (2) umbilical cables, (3) direct-access cables, and (4) hood cables. Figure 11 shows the application of each group.

Due to the late requirement inputs from the various subsystems, some innovations were introduced to the *Mariner* Mars 1969 OSE cabling effort. First, in an effort to "standardize" the cabling as much as possible, and thereby enable a supplier to lay and jacket (in one effort) enough cable to fabricate many assemblies, all OSE to computer data subsystem cables were made of 20 TPSJ wires with 24-61SW or PW connectors. Second, a grommet-compression clamp adapter[1] was substituted for the potted-type backshell used in the past. This change was made to reduce the initial fabrication time and because most of the cables rejected on the *Mariner* Venus 67 were due to faulty potting and miswires. In both cases the original connector and backshell had to be scrapped and replaced. Using the Glenair shell precludes the necessity of replacing the connector and backshell in case of a miswire.

7. Packaging of Integrated Circuits: Stick Module

a. Introduction. The increased use of integrated circuits on JPL spacecraft required that an approach to the packaging of integrated circuits be developed. The result of this development is a stick module, which was described in SPS 37-34, Vol. IV, pp. 96–101.

The stick module is a molded tray (approximately 5 × 1 × ¼ in.), which is used for mounting integrated circuits and small discrete components. Besides providing

[1]Supplied by Glenair, Inc., Glendale, Calif.

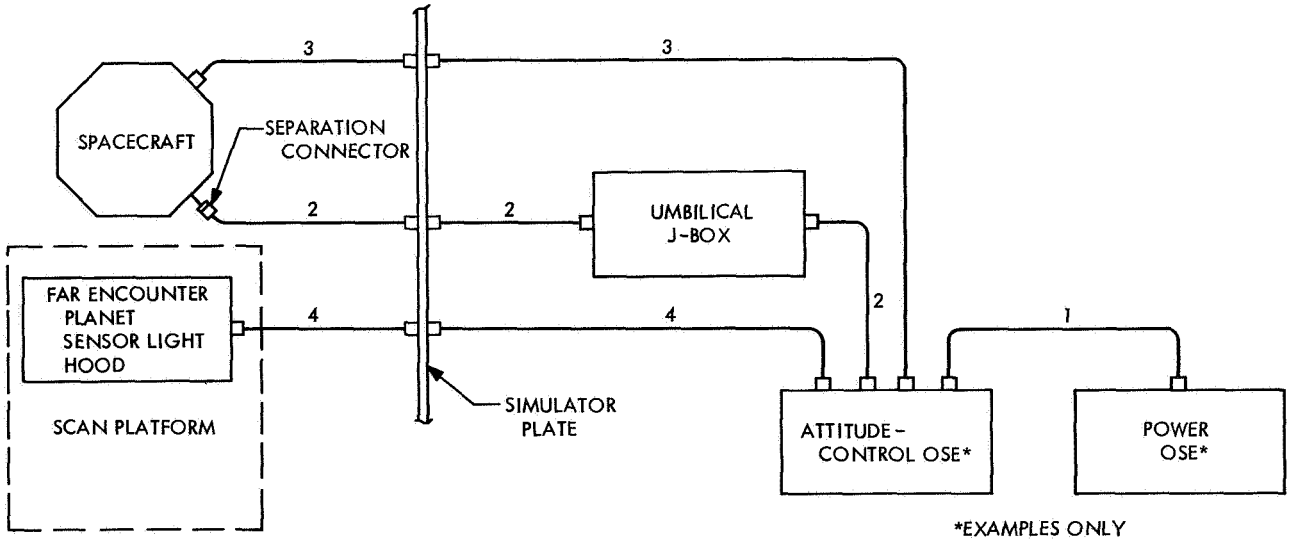

Fig. 11. Typical OSE cable layout

the means to interconnect the circuits and components within each stick module, they can be used to make direct interconnections between stick modules.

The stick module is suitable in applications where substantial quantities of integrated circuits are used in comparison with the quantity of discrete components. For *Mariner* Mars 1969, the stick module is used in seven different applications.

The use of the stick module for packaging integrated circuits and small discrete components results in a modular system that has the following characteristics:

(1) Flexibility.

(2) Repair capability at the component level.

(3) Short design and fabrication time.

(4) Reliability.

(5) Inspectability and ease of electrical checkout.

b. Circuit and component. Interconnect terminals are used to mount and interconnect the integrated circuits and discrete components. These terminals are accessible from both sides of the stick module. Figure 12 shows the wiring, and integrated-circuit and discrete component sides of a stick module with interconnect terminals installed, circuits and components mounted, and interconnection wiring done. The circuits and components are mounted on the front side of the stick module by either welding or soldering. Solderable magnet wire is used on the back side of the stick module to make the interconnections and to connect to the input–output terminals of the stick module. Input–output terminals are molded into the top edge of the stick module. The stick module also has two studs molded into the top edge and two module ears on the bottom edge. (See SPS 37-34, Vol. IV, pp. 96–101, for additional views of the stick module and parts.)

The first step in the design of a subassembly that employs stick modules consists of establishing the number and type of integrated circuits and discrete components required in the subassembly. The number of stick modules required to accommodate these components is then established. This number is then used to determine the size of the subchassis. The integrated circuits and their associated discrete components are then assigned to specific stick modules. The next step requires that the stick modules be arranged in a sequence that will optimize the intermodule connections. Each electrical function that requires intermodule connections is then assigned to a row of input–output terminals. Lastly, the circuits and components within each stick module are positioned within their respective tray in a sequence that will afford an optimum interconnection pattern within each stick module. This is done by minimizing the interconnection distances between associated circuits, components, and their related input–output terminals.

The above design process completes the physical layout of the subassembly. Stick module fabrication is the next step. The interconnect terminals are installed first. They are pushed through the flash coating of their assigned holes. The type of interconnect terminal installed in each hole depends on whether a discrete component or an integrated circuit has been assigned to that location in the stick module. Copper magnet wire with a solder-through polyurethane insulation is then used to interconnect the circuits and components within the stick module and to connect them to their assigned input–output terminals. All of the wiring is done on the back side of the stick module. The integrated circuit parts are then bonded into their assigned positions on the front side of the stick module and parallel-gap welded to their terminals. Discrete components are soldered into the bifurcations of their respective terminals. Both sides of the stick module are then conformally coated to provide electrical insulation, mechanical support, and environmental protection for the electrical parts and circuitry. Any module-level inspection or electrical testing is performed at this time.

The stick modules are now ready for final assembly into half-size (Fig. 13) or full-size (Fig. 14) subchassis. The two mounting studs located along the top edge of the stick module are used for attaching the stick module to the subchassis. The two module ears on the bottom edge of the stick module are used in conjunction with the locating pins to position the stick module correctly in its assigned location in the subchassis. Stranded insulated wire is then used to interconnect the stick modules. The wires are routed in straight parallel runs between the columns of input–output terminals and are soldered into the bifurcations of the terminals. Any electrical functions that route out of the subassembly are wired to the subassembly connectors. The final step consists of spot bonding the stick modules and the wire harness to the subchassis and insulation coating the input–output terminals.

A plug-in feature is used to test stick modules either singly, by subassembly, or by electrical function. Special

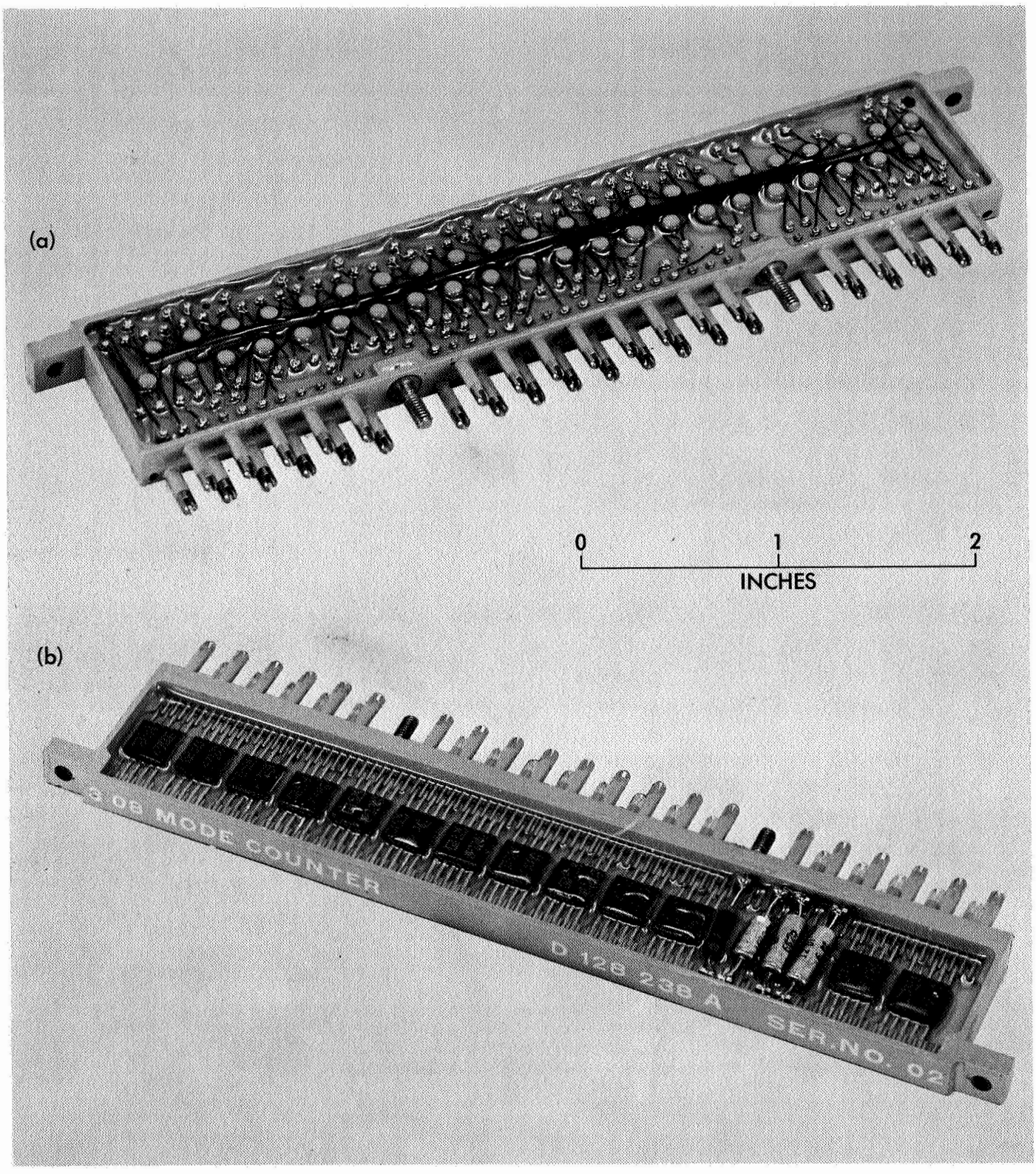

Fig. 12. Stick module: (a) wiring side, (b) component side

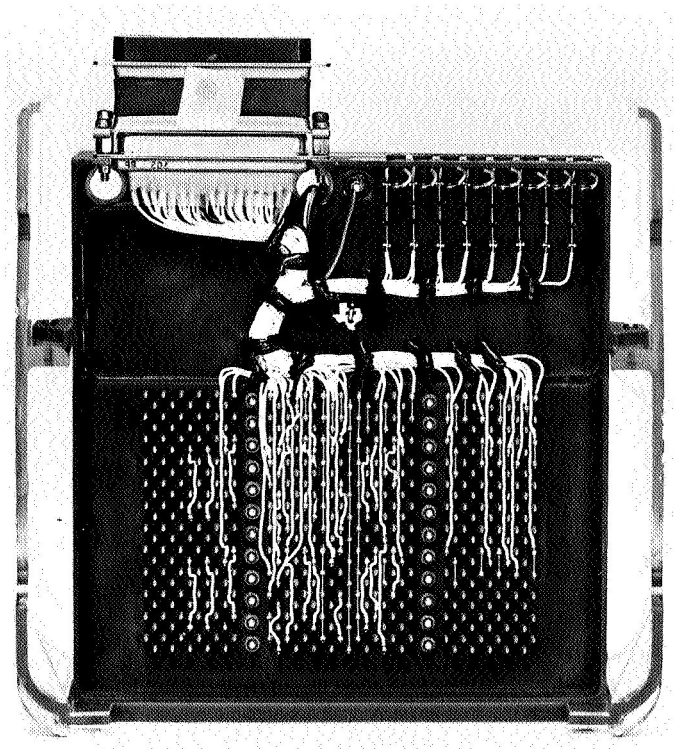

Fig. 13. Stick modules in half-size subchassis

Fig. 14. Stick modules in full-size subchassis

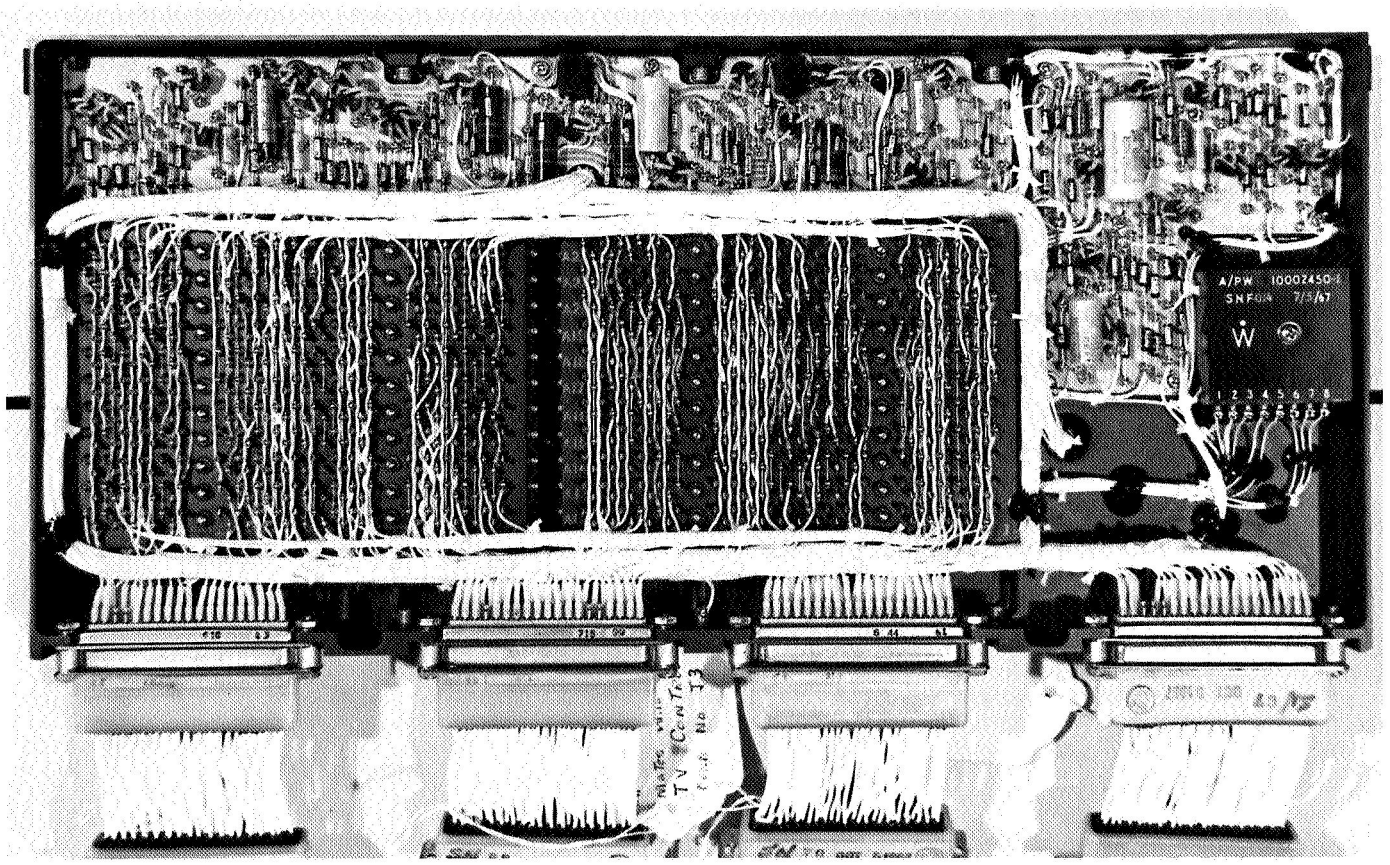

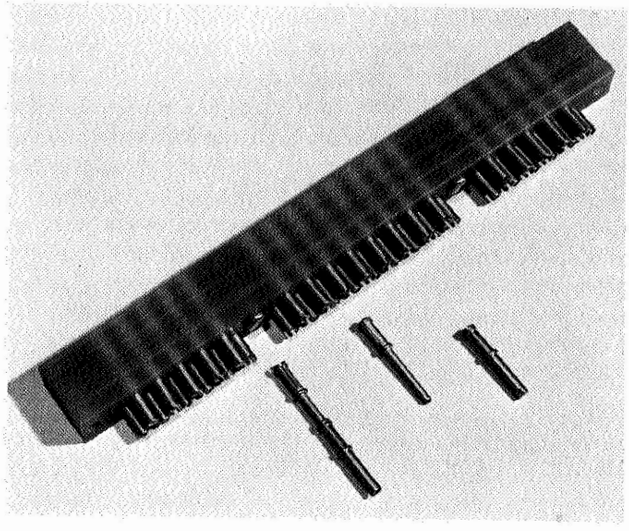

Fig. 15. Stick module test connector

test connectors (Fig. 15) and test setup (Fig. 16) were fabricated for this purpose.

c. Environmental criteria. Each subassembly or instrument that used stick modules was designed to be capable of passing the following series of environmental tests:

(1) Handling and transportation environment: package drops and simulated transportation vibration.

(2) Atmospheric: immersion in explosive and high-humidity atmospheres while normal electrical load was applied.

(3) Static acceleration: 9-*g* steady acceleration load for 5 min in each of 3 mutually perpendicular axes.

(4) Shock: 200-*g* shock pulse in each of 3 axes.

(5) Acoustic: reverberant field wideband acoustic noise.

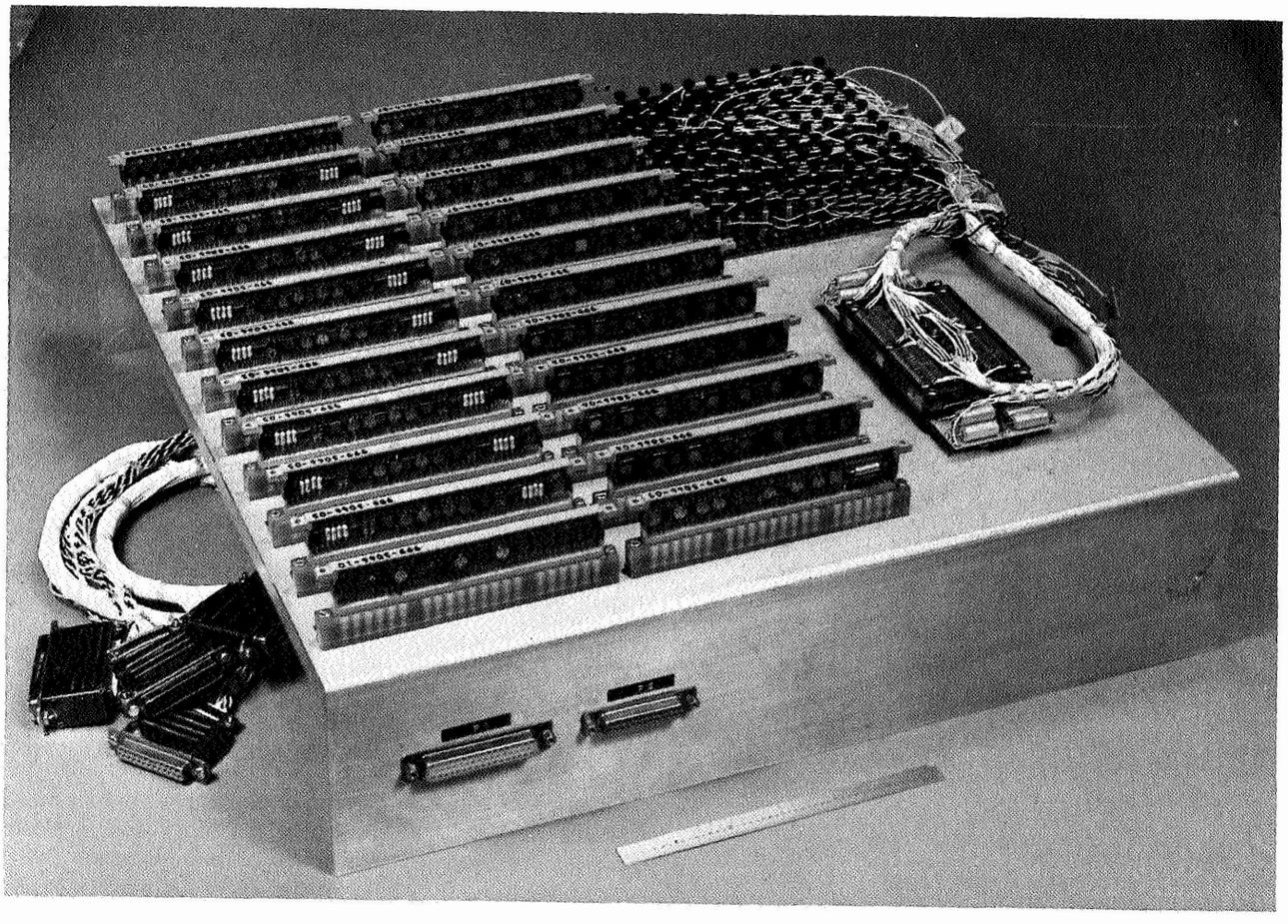

Fig. 16. Stick module test setup

(6) Vibration: Sine wave and random vibration conditions encountered at launch.

(7) Thermal/vacuum: −20°C (−4°F) for 24 h at pressure of 10^{-5} torr and to 75°C (167°F) for 12 days at pressure of 10^{-5} torr.

(8) Thermal shock: temperature cycle of 75°C (167°F) to −46°C (−50°F) to 75°C (167°F) at pressure of 10^{-5} torr.

(9) Radiation: electron and proton radiation.

d. Application. The choice of circuit packaging for the different subsystems and instruments in *Mariner* Mars 1969 was dependent on several factors. Some subsystem packaging techniques were selected on the basis of contractor experience with a particular technique or special circuit design criteria. However, where these constraints were not overriding, the main criterion was the relationship between the quantity of integrated circuits and discrete components used. Stick modules were used where a substantial number of integrated circuits were employed compared to the number of discrete components used. The exceptions to this rule were applications where small quantities of integrated circuits were required and the discrete-component packaging configuration employed made it difficult to accommodate a small number of integrated circuits. In these cases, the stick module was used but it was mounted laying on its side (Fig. 17). Lastly, the decision on whether to use or not to use stick modules for a particular *Mariner* Mars 1969 application was based on the interrelationship between the basic characteristics of the stick module and the particular packaging requirements. For example, the importance of being able to inspect the components and their interfaces, of being able to replace components and change wiring, and of being able to electrically check out the circuit easily had to be considered for each potential application.

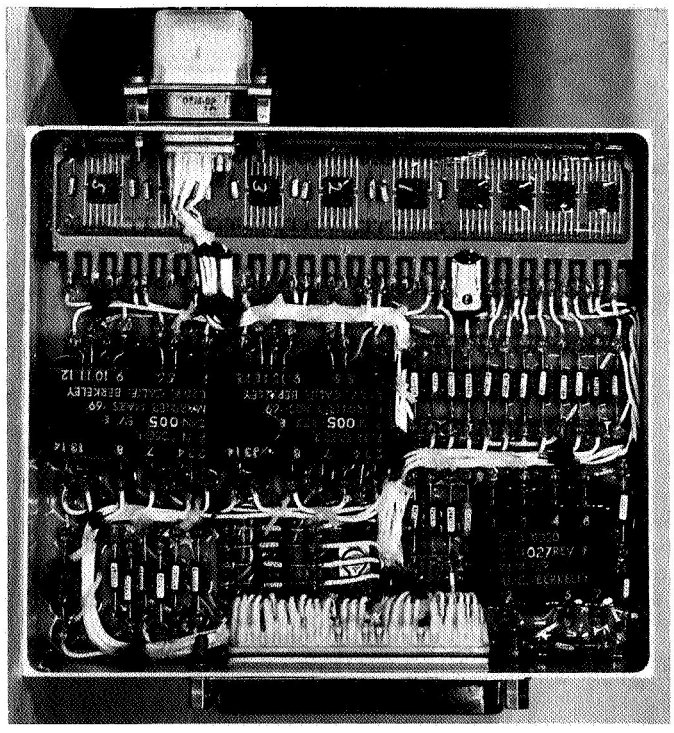

Fig. 17. Alternate stick module mounting configuration

The stick module was used for the *Mariner* Mars 1969 in the data storage subsystem, flight telemetry subsystem, television subsystem, central computer and sequencer subsystem, infrared spectrometer subsystem, Canopus tracker, and temperature control flux monitor.

The heat produced by the integrated circuits and discrete components of the central computer and sequencer subsystem required that a method (beyond normal heat transfer through the body of the stick module) for removing the heat be developed. The result was a 0.005-in. thick by 0.3-in. wide copper strip bonded to the body of the stick module on the component side. This heat sink was designed to take the heat from the components and transfer it to the subchassis where the module ears contact the subchassis.

The infrared spectrometer subsystem and the Canopus tracker are applications where stick modules were used because the discrete component packaging configuration made it difficult to accommodate a small number of integrated circuits. The stick module was mounted laying on its side as shown in Fig. 17.

The total stick module packaging for *Mariner* Mars 1969 consisted of 132½ stick modules, which contained 1503 integrated circuits and 351 discrete components.

8. Plug-In Equipment Electronic Assemblies

a. Introduction. It became apparent early that the *Mariner* Mars 1969 spacecraft configuration (based on the *Mariner* Mars 1964) would not adequately house the required electronic equipment, and that new packaging configurations would be required. The volume requirements became critical for the attitude control (AC)/central computer and sequencer (CC&S) and science equipment (data storage and data automation/television) electronic assemblies.

Two approaches were considered to gain the additional volume for the electronic equipment: (1) appending packages on top of the spacecraft octagon, and (2) increasing the volume within the AC/CC&S and science equipment electronic assemblies. The design study resulted in the decision to design new electronic assemblies for bays III and VII, which offered 20% additional volume for use in packaging electronic equipment (1220 in.^{3} for *Mariner* Mars 1964 compared to 1450 in.^{3} for the new *Mariner* Mars 1969 electronic assembly design). The additional volume required within the data storage electronic assembly for a second tape recorder was obtained by moving the two communications receiver subassemblies and the associated power supply into the radio electronic assembly, which was completely redesigned.

The design constraints for the new plug-in electronic assemblies were: (1) no decrease in electronic assembly packaging reliability (compared to the *Mariner* Mars 1964), and (2) minimum physical interface changes between the electronic assemblies and the spacecraft.

b. Assembly design. The new *Mariner* Mars 1969 plug-in equipment (PIE) electronic assembly was designed for a high degree of mechanical integration within the octagonal spacecraft structure. This integrated design concept was also a feature of the *Mariner* Mars 1964 electronic assembly, which utilized the chassis structure as an integrated shear plate (ISP) for the octagonal structure.

The spacecraft octagonal structure and the electronic assembly structures are physically interdependent in that they are not rigid as individual assemblies; but, when fastened together, they form a very rigid total spacecraft structural assembly. Figure 18 shows the PIE electronic assembly installed in a typical bay within the spacecraft octagonal structure. The separate outer shear plate fastens to the outboard flanges of the longerons and the outboard flanges of the upper and lower ring structures; the chassis fastens to the inboard longeron flanges. The mechanical integration of electronic subassemblies within the chassis and shear plate structures is more effective compared to previous JPL spacecraft designs.

Within a PIE electronic assembly, the electronic subassemblies are standardized. To optimize design and to reduce electrical interconnections, two profile standards are utilized. Subassembly thickness is varied to satisfy the individual subsystem equipment design requirements and packaging techniques. Figure 19 shows some of the outboard surfaces of electronic assembly III subassemblies. The AC electronics and the CC&S logic and power supply utilize full-size (14 in. wide) subassemblies; the gyro control assembly and the CC&S memory use a total of four half-size (6.5 in. wide) subassemblies.

The *Mariner* Mars 1964 ISP electronic assembly configuration required access within the spacecraft to the inboard side of the electronic assembly for removal of the

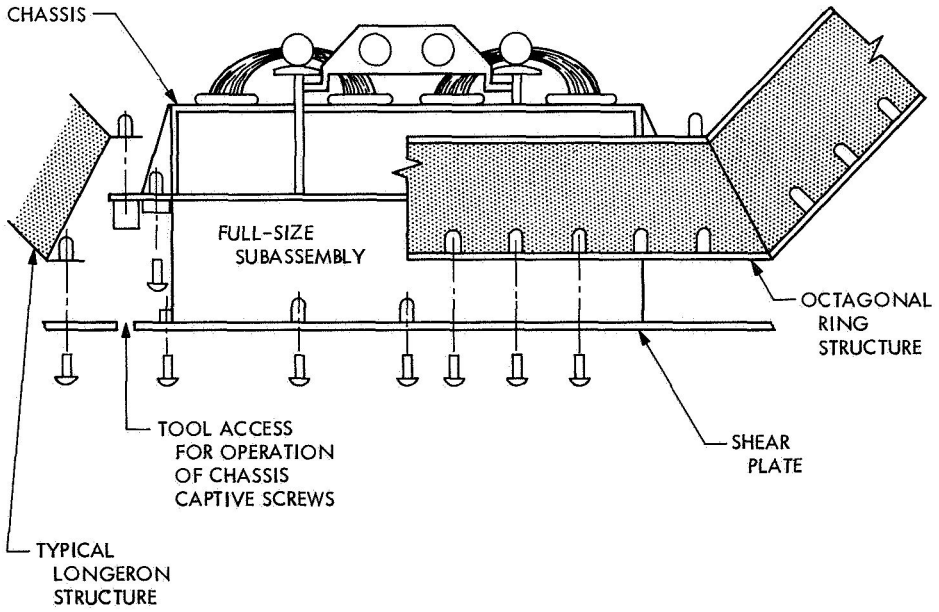

Fig. 18. Installation of PIE electronic assembly into octagonal structure bay

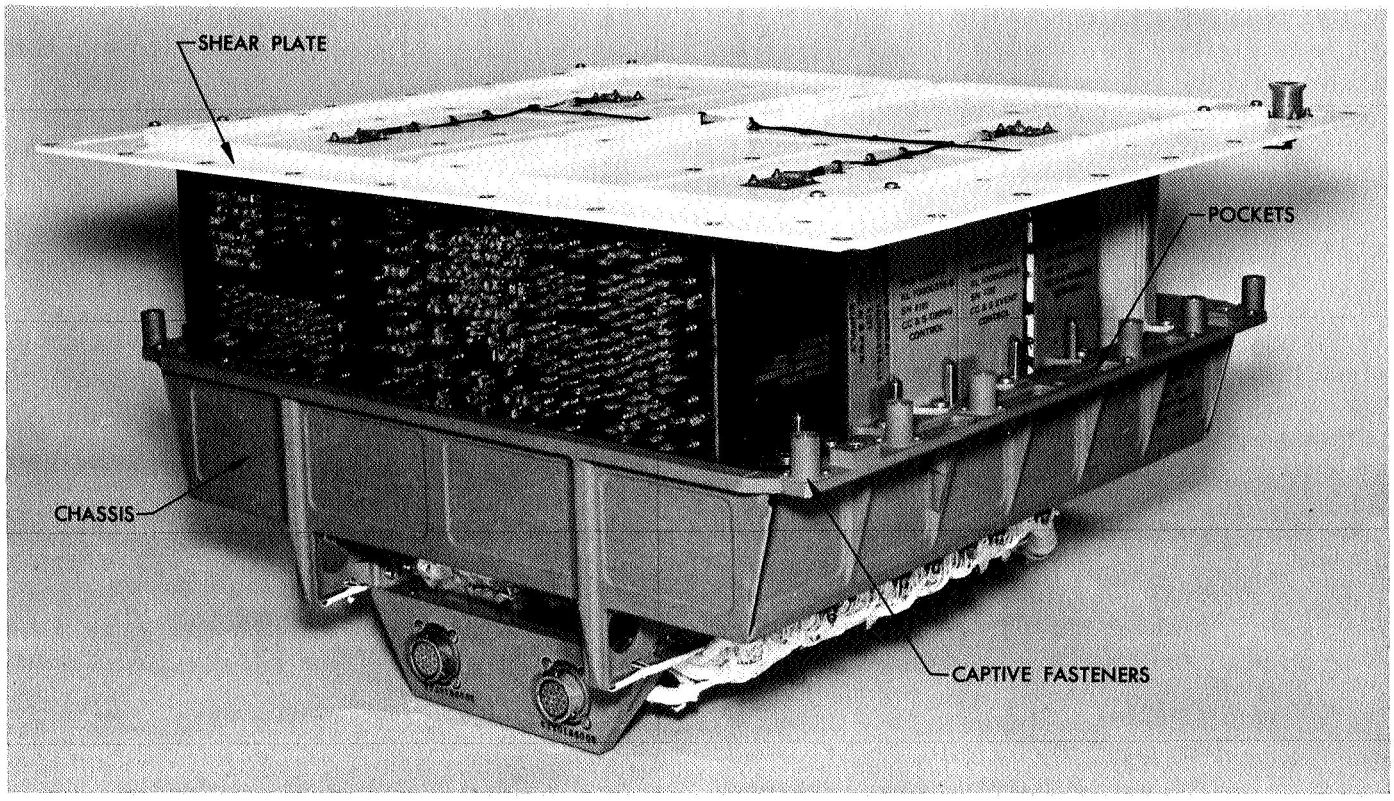

Fig. 19. Electronic assembly III with shear plate

assembly or the individual subassemblies. In some instances, the inboard access was sufficient so that an individual subassembly could be removed; in other instances, the entire electronic assembly had to be removed before the subassembly could be removed. The large science platform assembly on the *Mariner* Mars 1969 makes inboard access to the electronic assembly more difficult. All of the electronic assemblies have been designed (or redesigned) to require only outside access for installation. The spacecraft octagon and the electronic subassemblies for the newer PIE design may be removed and installed easily from outside the spacecraft during operational checkout. Prior to thermal vacuum test, vibration test, or flight, the new electronic assembly is removed from the spacecraft and additional screws are installed through the chassis and into the electronic subassemblies. Also, no cross-bolting through the upper and lower rings of the spacecraft octagonal structure is required for the PIE electronic assembly (compared to the other bays using the *Mariner* Mars 1964 design). This simplification is significant because the PIE electronic assembly can now be removed from the spacecraft without removing the spacecraft from its supporting adapter. The operational shortcoming of the PIE design, compared to the *Mariner* Mars 1964 configuration, is that after the shear plate is installed with its many associated fasteners, the entire shear panel must then be removed in order to replace an electronic subassembly; however, the only time it is necessary to install the shear plate is prior to environmental testing or flight. Overall, the new PIE electronic assembly is believed to be easier to work with than the *Mariner* Mars 1964 design.

A plug-in connector engagement design is used for interconnecting the electronic subassemblies to the hard-mounted electronic assembly cable harnesses. This feature of the PIE electronic assembly design gives the cabling increased resistance to environmental stress because of the rigid support and shorter length of the average conductor. The shorter conductors result in improved electrical performance and reduced weight. Two alignment pins are used with each subassembly connector to align each pair of mating connectors during installation. Operational tooling is used for the installation and removal of the electronic subassemblies because of the high connector engagement forces (up to 200 lb for a subassembly using a maximum of eight 50-pin connectors), and to ensure a straight and free engagement/disengagement of the mating subminiature rectangular connectors. Circular miniature connectors are used for operational support

equipment (OSE) checkout and for interconnection with spacecraft system cabling. The OSE connectors are rigidly mounted on a bracket at the top of the electronic assembly chassis subassembly; all interconnections to the upper ring harnesses are carried through pigtailed cables at the top of the chassis. Interconnections to the lower ring harness are accomplished with circular connectors rigidly mounted on a bracket at the lower end of the chassis. Figure 20 shows electronic assembly III cable harnesses mounted on the chassis; structural members on the back of the chassis are designed for both cable harness support and chassis stiffening.

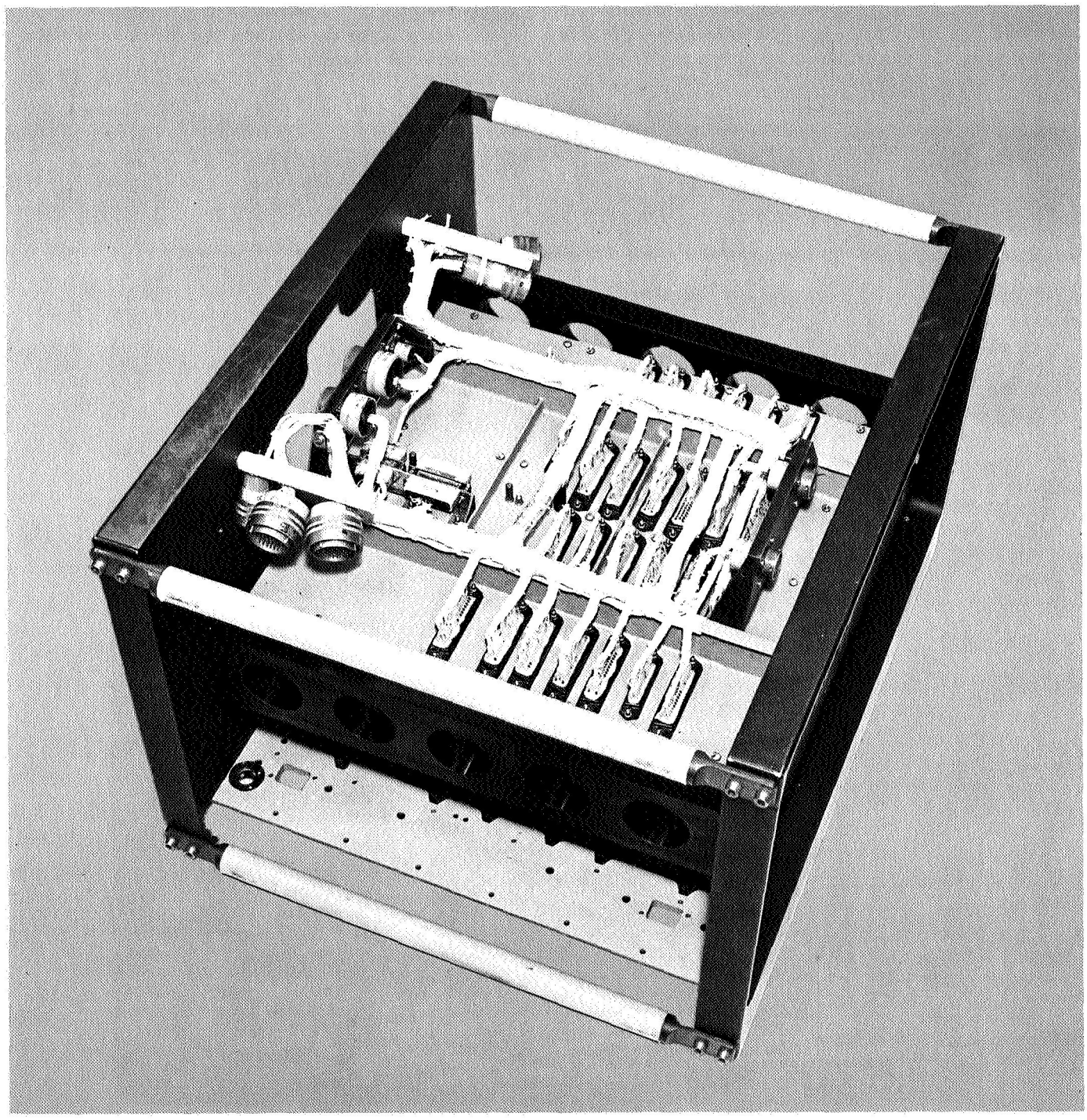

Fig. 20. Electronic assembly III cabling configuration

The PIE electronic assembly shear plate is shown in Fig. 19. The shear plate is very similar to the integral shear plate of the *Mariner* Mars 1964-type chassis. Four temperature transducers are mounted on the outboard surface of the shear plate. The major advantage in using a separate electronic assembly shear plate is that it can be left off during system checkout and operations to permit direct and easy access to each electronic subassembly. The shear plate is required to be semiflexible relative to an axis perpendicular to the plane of the plate because of tolerance variations and to allow the shear plate to make intimate contact with the outboard flanges of the octagonal structure. Figure 21 shows electronic assembly III mounted on the proof-test model spacecraft with the shear plate removed; an "extender module" has been installed to replace one of the CC&S subassemblies, which is shown installed in special support tooling to allow electrical checkout within the subassembly. Jumper cables are used to interconnect the extender modules to the functional subassembly.

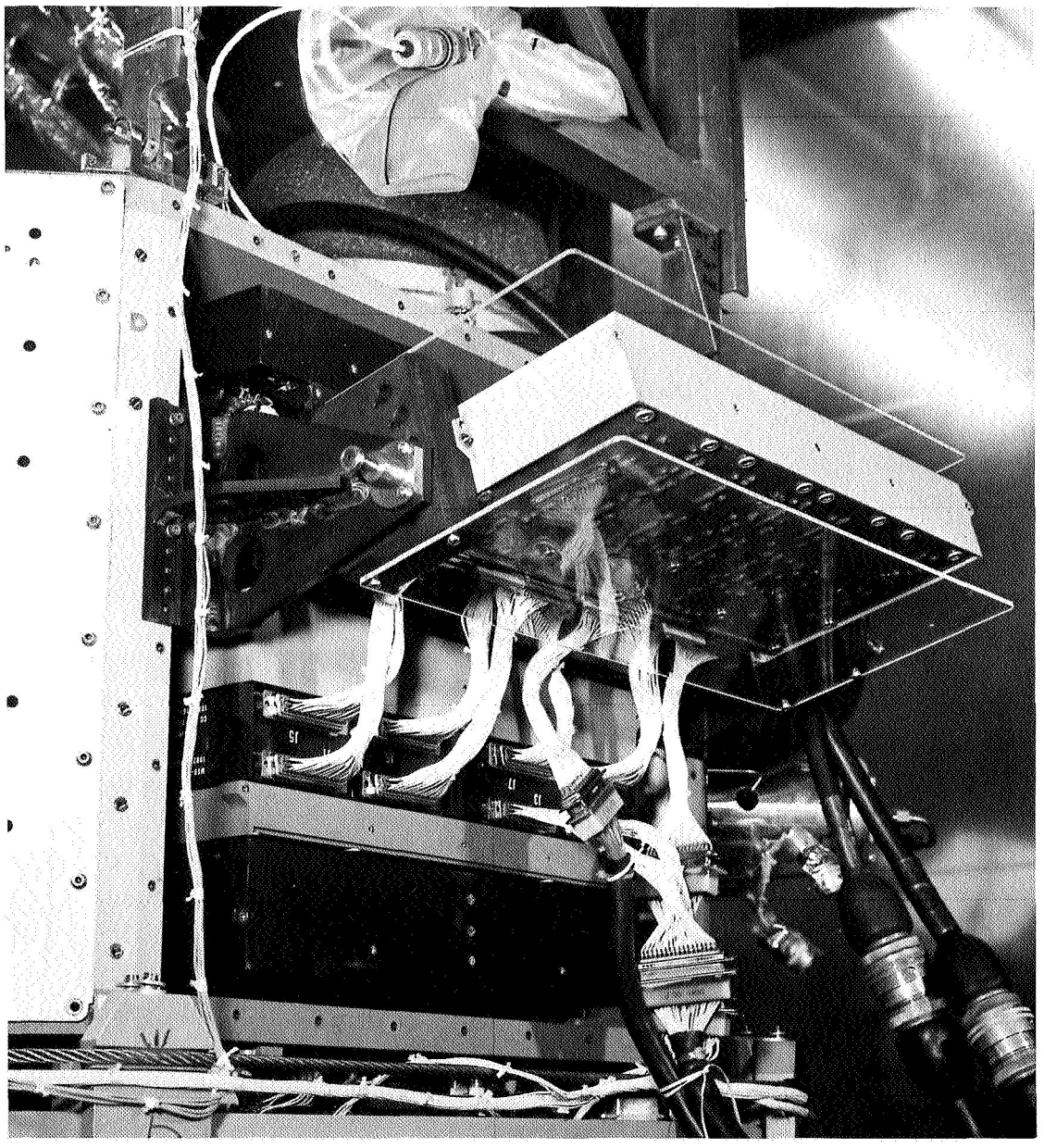

Fig. 21. Extender module assembly

c. Dynamic characteristics. The components within the PIE electronic subassemblies are protected from excessive dynamic loading due to low-frequency spacecraft resonances by dynamic decoupling. The subassemblies have a 400-Hz minimum resonant frequency requirement (same as *Mariner* Mars 1964-type units), which results in a transmissibility of one for the dynamic forces coming from the chassis and shear plate into the subassemblies up to 400 Hz. The 400-Hz requirement is generally easier to satisfy in the PIE electronic assembly because each subassembly is rigidly supported on two opposite sides (between the shear plate and chassis). The PIE electronic assembly has a minimum resonant frequency requirement of 300 Hz, which is comparable to the *Mariner* Mars 1964.

A design goal was set to have all chassis and shear plate resonances fall within the frequency range of 300 to 590 Hz or above 2000 Hz to take advantage of the vibration environmental requirements for *Mariner* Mars 1969. An additional design goal was to have characteristic resonant frequencies of the chassis, shear plate, and subassemblies different to minimize dynamic coupling (and associated high transmissibilities) and to take advantage of phase-shift damping within the electronic assembly. In general, the dynamic characteristics of the PIE electronic assembly are excellent.

The major problem that remains after the development phase is caused by resonances of the electronic assembly vibration fixture when the electronic assembly is tested. This fixture, developed for the *Mariner* Mars 1964-type electronic assembly, is too flexible to test the *Mariner* Mars 1969 PIE electronic assembly properly; fixture resonances occur that couple into some of the PIE electronic assembly characteristic resonances. The overall frequency response characteristics of the PIE electronic assembly was very similar to that of the *Mariner* Mars 1964 electronic assembly configuration.

d. Thermal characteristics. The thermal design characteristics of the PIE electronic assembly are similar to those of the *Mariner* Mars 1964 electronic assembly. The outboard thermal/shear plate is the primary temperature control member for the PIE electronic assembly. Four temperature transducers are mounted on the thermal/shear plate to measure "average" electronic assembly temperature. The outboard interface surface for mounting temperature control louvers on the thermal/shear plate is raised to ensure that no fastener or temperature transducer protrusions interfere with the operation of the louvers. The outboard surface of the thermal/shear plate is shown in Fig. 19.

Heat is transferred from the subassemblies to the shear plate primarily by conduction. As heat flows into the thermal/shear plate, it is further conducted across the surface and simultaneously radiated into space until steady-state thermal conditions are reached. The thermal impedances are quite low between the thermal/shear plate and subassemblies. The thermal impedances are approximately 3°F/W for each screw, with most of the heat conducted through the magnesium subchassis and the thermal/shear plate adjacent to these screws. The minimum number of screws through the shear plate into a full-size subchassis is three 6-32 and two 8-32 and through the thermal/shear plate into a half-size subchassis is one 6-32 and two 8-32. The minimum thermal/shear plate thickness in the area of any threaded fastener is 0.10 in. to control the "choking" of heat transfer. The inboard-mounted chassis is used to transfer heat between subassemblies, and also to assist in the transfer of heat between adjacent electronic assemblies through longeron flanges. In general, the new PIE electronic assembly design is thermally superior to the *Mariner* Mars 1964.

e. Subassembly design. The electronic subassemblies in the PIE electronic assembly are 6.6 in. high. The width can be either 14 in. for the full-size unit or 6.5 in. for the half-size unit. The subassembly thickness is determined from the number and size of rectangular connectors required and the volume requirements of each subassembly. Figure 22 shows electronic assembly III CC&S memory subassembly as a representative half-size unit; this subassembly is of special interest because all of the preferred electronic packaging techniques are utilized within this single unit. Figure 23 shows a representative full-size subassembly, which utilizes planar packaging of components.

The structural subchassis for the subassemblies are generally machined from AZ31B magnesium alloy. In special cases, where machining tolerances are extremely close, or improved physical properties are required, ZK60-T5 magnesium alloy is used.

Each subchassis within a PIE electronic assembly is designed as a structural member since the physical integrity of the electronic assembly relies on each subchassis as a load-bearing member. The minimum subchassis web thickness is 0.090 in. The functions of the subchassis web are to: (1) provide a stiff supporting substrate for components, (2) conduct heat from electrical components to the temperature control surfaces of the electronic assembly, and (3) contribute to the structural integrity of the electronic assembly.

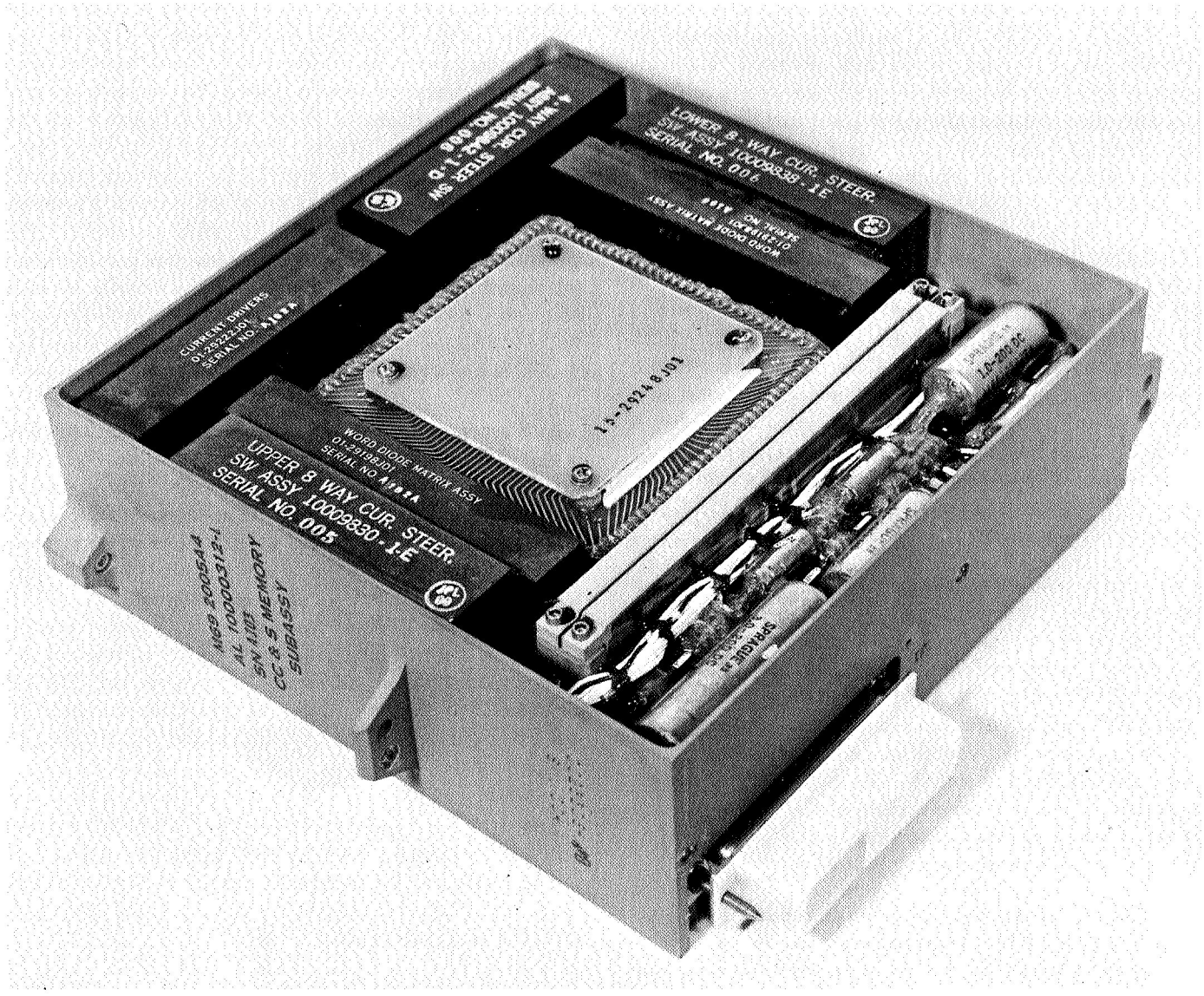

Fig. 22. Typical half-size electronic subassembly

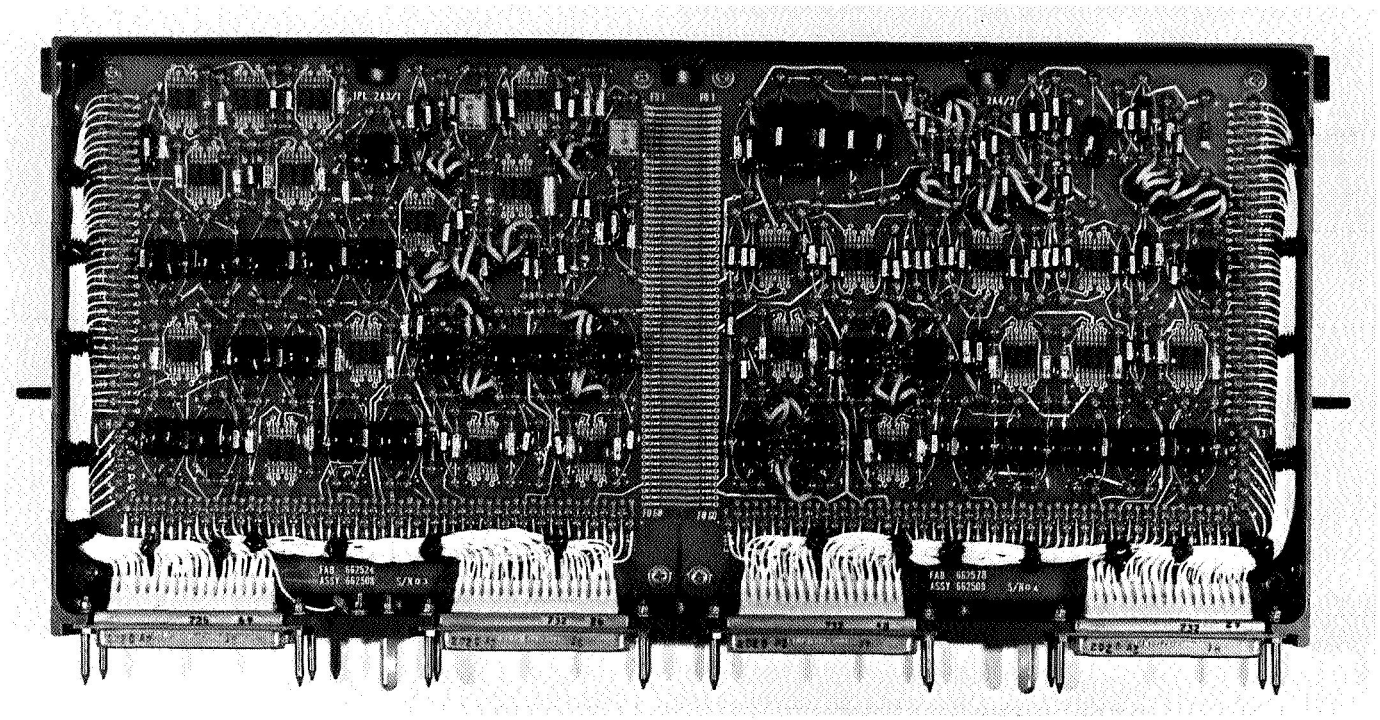

Fig. 23. Typical full-size electronic subassembly

Subassembly connector mountings, incorporating the plug-in connector engagement design (also see *Paragraph b*), are shown in Figs. 22 and 23. The connectors are recessed relative to the inboard subassembly surface to maintain the correct spacing with mating connectors on the chassis; the recessed connector installation also contributes to the localized stiffness of the connector supporting areas of the subchassis.

The cable harness connectors are installed against the back surface of the electronic assembly chassis with threaded fasteners and high-strength molded-plastic back shells, which are bonded to each electronic assembly cable harness rectangular connector. The rectangular connector assemblies are free to translate approximately 0.040 in. in any direction within the plane defined by the back surface of the chassis; this freedom of connector movement during subassembly installation allows the chassis-mounted cable harness connectors to align themselves with mating subassembly connector alignment pins before the connector pairs actually engage.

The plug-in connector design is a conservative one because of the use of screened close-tolerance connectors and close-dimensional tolerances. The design ensures proper connector engagement even in the worst-case tolerance buildup condition. No problems have occurred.

f. Chassis design. The PIE electronic assembly chassis are machined from ZK60-T5 magnesium alloy forged billets (Fig. 24). The surface finish is Dow 17 (anodized). The inboard (back) surface of the chassis functions as a structural shear plate, which ties the inboard sides of all subassemblies together.

Two integral beams run the length of the chassis; they are required to support the electronic assembly cable harnesses (Fig. 20), as well as to stiffen the back surface of the chassis to prevent excessive deflections during subassembly installation when forces up to 200 lb are imposed normal to this surface. Smaller flanges are used between the two major beams to provide additional local stiffening of the chassis, which is required during subassembly installation. The center flange (running parallel to the two large beams) is required to improve the chassis characteristics during vibration. (This flange was added after vibration testing to increase the resonant frequencies of all subassemblies by changing the inboard chassis/subassembly fastener points to allow them to function more like a fixed-end support and less like hinged ends.)

Pockets were added asymmetrically between some of the captive fasteners on the two flanges of the chassis (Fig. 19), which bear against the octagonal structure inboard longeron flanges. This was done to improve the

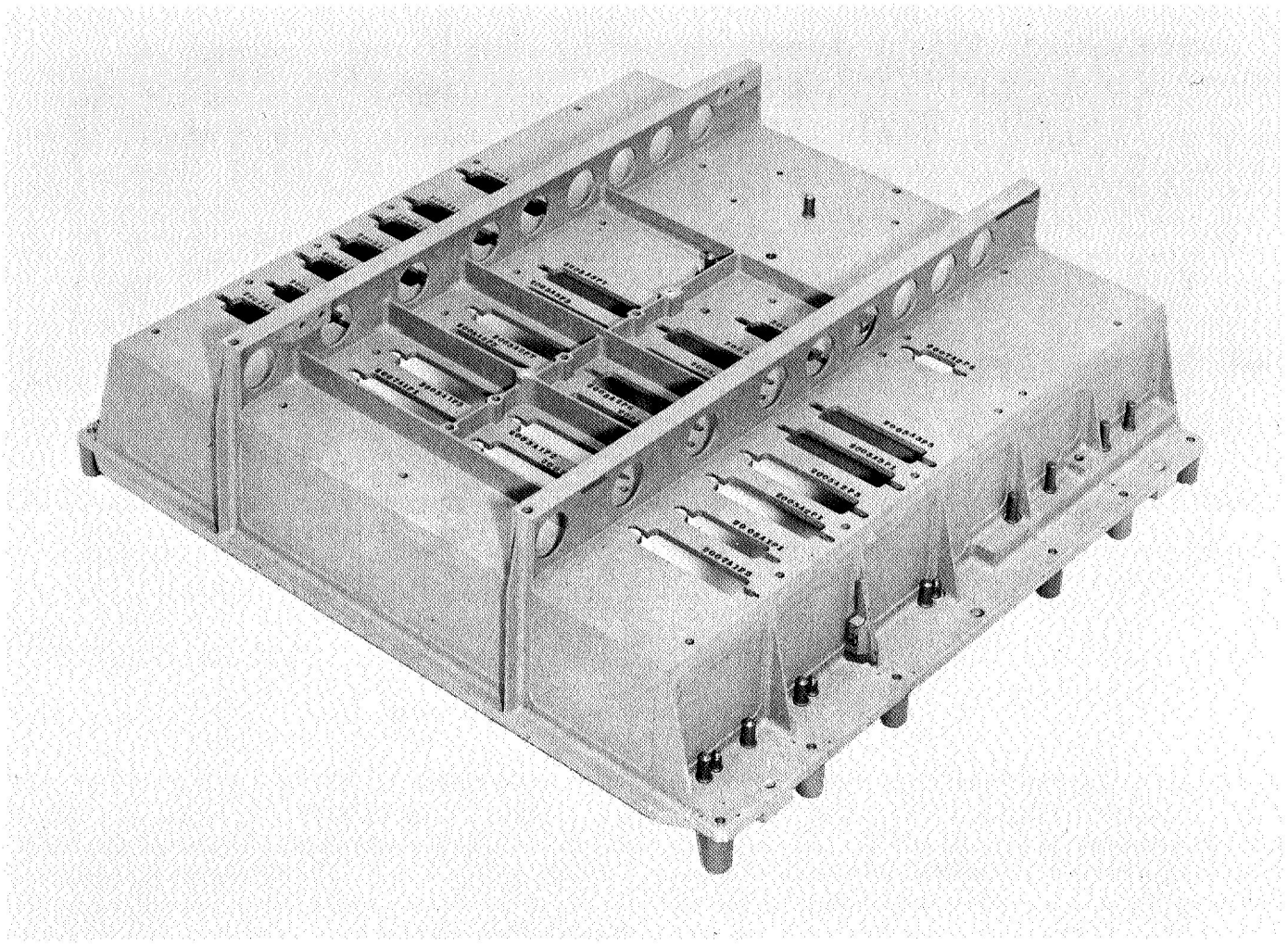

Fig. 24. Electronic assembly III chassis subassembly

electronic assembly dynamic performance when shaken in an axis perpendicular to the back surface of the chassis (*Y* axis).

Epoxy/fiberglass guide plates are bonded to opposite inside surfaces of the chassis to prevent scratching of the chassis during installation and removal of the subassemblies. Subassembly identification information is silk-screened on the guide plates. Two techniques are used to ensure that subassemblies are not inadvertently installed in the wrong direction or location. The primary technique is to vary location and orientation of connectors; the second technique is to use indexing/polarizing pins mounted on the subassembly, which match clearance holes in the chassis. Guide pins are temporarily installed on the two chassis flanges for use in aligning and supporting the subassemblies during installation and removal operations; the connector guide pins position and support the back of each subassembly. The guide pins are removed prior to environmental test and flight.

The *Mariner* Mars 1969 spacecraft design requires the use of blind engagement captive fasteners capable of resisting tension and shear forces between the two chassis flanges and the associated octagonal structure longeron flanges. A satisfactory captive fastener design was not available commercially, and a new captive structural screw design concept was developed at JPL. Twelve cast aluminum captive screw retainers are on the two chassis flanges (Fig. 19).

g. Cabling. The PIE electronic assembly cable harness design represents a significant advancement from that of the *Mariner* Mars 1964. The cable assemblies are completely hard-mounted on the electronic assembly chassis, except for the cable branches, which interconnect to the

upper ring harnesses (Figs. 19 and 20). Subminiature rectangular connectors are used for interconnections between the electronic subassemblies and the cable harnesses. Circular miniature connectors are used on the cables for OSE checkout functions and to interconnect to the upper and lower ring harnesses. Figure 19 shows the rigidly mounted connectors on a bracket at the lower end of the chassis that attach to cable branches from the lower ring harness, which is mounted on the lower ring of the spacecraft octagonal structure. Figure 20 also shows the rigidly mounted circular OSE connectors that are adjacent to the cable branches going to the upper ring harnesses.

The CC&S and the AC harnesses are designed and fabricated as individual subsystem harnesses for electronic assembly III; the cables are individually spot-tied with lacing cord during fabrication. Nylon cable straps and cable clamps are then used to mechanically integrate the cable harnesses to the chassis subassembly. Elements of the electronic assembly cables that cross between the two main cable trunks mounted on the chassis I-beams are supported at mid-span by standoffs, which attach to the back of the chassis. Figure 20 shows a portion of the AC harness that is mounted on top of the CC&S harness; both cables are then secured to the chassis I-beam by nylon straps. The rectangular connectors mounted on the back surface of the chassis are not potted. Plastic shrinkable tubing is used over both the connector solder pots and the associated wire; this tubing provides both mechanical support for the solder joints and insulation of the stripped portion of the wires. The backs of the rectangular connectors are sealed with silicone rubber to ensure complete insulation of conductors.

9. Materials Engineering

During fabrication of *Mariner* Mars 1969 squibs, intended for use as actuating devices on explosive valves on the propulsion subsystem, it became necessary to identify part materials that had already been joined by a complex and critical process. This critical process was the brazing of four metal pins into a ceramic header. The pins were fabricated of Ceramvar and the header material was aluminum oxide.

The Ceramvar pins are first nickel-plated and the aluminum oxide is metallized with molybdenum–manganese, which, in turn, is nickel-plated. The pins are then brazed into the header using a silver alloy. Due to the complexities of the operation and the stringent requirements of the joint (5400 psi proof pressure, as well as X-ray inspection), the production yield from this process is very low.

After a considerable number of these parts had been brazed and successfully passed inspection and proof requirements, it was revealed that there was a possibility that Kovar had been inadvertently substituted for Ceramvar as a pin material. Since Ceramvar more closely matches the aluminum oxide with respect to thermal expansion, it is a more desirable alloy for this application. In addition, previous *Mariner* hardware had used Ceramvar pins and a considerable test history was available and was being relied on for *Mariner* Mars 1969.

To discard these successfully brazed assemblies at this stage of fabrication would have delayed delivery and test schedules. Thus, an attempt was made to distinguish which alloy had been used. The nominal chemical compositions for Ceramvar and Kovar are given below:

Alloy	Composition, wt %		
	Nickel	Cobalt	Iron
Ceramvar	27	25	48
Kovar	29	17	54

Both alloys, being similar in composition, exhibit like characteristics with respect to magnetic, electrical, mechanical, and other properties. Thus, chemical means was the only way to distinguish between the two alloys. A nondestructive technique was required so as not to damage the parts in any way. With the pins already brazed into the header, and having been plated previously, only the pin ends on the opposite side of the header were accessible for analysis. The pin ends had been ground flush to the header on that side. Adding to the complexity were the bridge wires, which had already been welded in place across these ends on some assemblies. Also, there was no guarantee that a single header had pins from the same alloy; therefore, each pin had to be tested.

As can be seen in the table, the main difference in the two alloys is their respective cobalt content. The most sensitive instrumental technique for analysis in this range is X-ray fluorescence. The configuration of the squibs, however, did not conform to analysis by normal X-ray fluorescence units. Laboratory experience with the electron probe microanalyzer indicated a possibility that this instrument could excite, by electron beam, the X-ray emission of a spot on each flush pin tip, and measure the magnitude of the cobalt characteristic radiation emitted.

Ceramvar and Kovar wires were each subjected to examination using the electron probe microanalyzer to determine how successful this technique might be. The data indicated that for cobalt a very significant difference in output appeared. This showed that the pins could indeed be checked by reading the cobalt content indicated by the detector counts.

Special holders were fabricated for the instrument and fitted with four headers each. A small portion of a production lot of the pin-to-header brazements was subjected to analysis using the electron probe microanalyzer. The results of this preliminary number of samples indicated all the pins to be Ceramvar. It was decided that the entire questionable production lot of 89 headers be subjected to the same analysis. This amounted to nondestructive analysis of 356 pins, which was accomplished in 24 h. All pins in all headers were identified as Ceramvar. Destructive wet chemical analysis of certain selected test pins verified this analysis.

Based on the reliability of the nondestructive alloy determination, all parts were judged usable and production was immediately resumed.

10. Reliability Considerations in Electronic Transformers

a. Introduction. Two general categories of transformers are used in spacecraft: the quasi-catalog items and those made for specific applications. The catalog types are based on qualification tests and extensive usage. Units that fail during testing or use are very carefully dissected to determine the exact cause of failure. This information is then reported to the manufacturer. In some instances, the manufacturer uses this information to upgrade his entire line; in others, the manufacturer assigns a special number to upgraded units to identify the best transformer produced. The specially made transformers and inductors are generally of JPL design and incorporate all the materials and techniques that were developed over the years. They are generally of toroidal configuration; the fabrication techniques described in this study apply principally to this type.

The following *Paragraphs b* and *c* discuss the two ways to ensure that the components used are the best available.

b. Fabrication techniques. Built-in reliability is accomplished through control of design, materials, techniques, and processes. Many space experiments and equipment (such as cameras and infrared and ultraviolet experiments) are sensitive to materials that outgas, and, since space vehicles operate in airless regions, the use of materials with a low vapor pressure is a prime consideration. In addition to materials that outgas, transformers and inductors that are encapsulated or potted without having the winding impregnated will leak the enclosed air, regardless of the quality of the encapsulation. Many toroidal units are unimpregnated, especially inductors with critical inductance requirements; this type of unit cannot be incorporated in spacecraft.

Great care must be taken so that expansion and contraction stresses do not adversely affect the transformers. Studies have been made to determine which potting materials produce the least stresses at the lower temperature extreme. Internal movement can easily cause breakage when fine wires are involved, and, despite the unreliability of the finer wires, there are many applications where their use is unavoidable. To minimize breakage, fine wire must not be connected directly to a heavy one. Wires finer than a No. 36 require the splicing in of an intermediate size wire.

While many manufacturers use Mylar tape for wrapping coils and for insulation between windings, it is prohibited at JPL for two reasons. First, since Mylar is not porous, impregnation must go around unless the tape is wound too tightly, in which case there may be air voids within the transformer. Second, since epoxies do not bond to Mylar, an incipient fracture plane is produced in the impregnation.

Instead of Mylar, either polyester matte or woven glass tapes are used. These tapes are somewhat thicker than the Mylar film tape, but their advantages outweigh their disadvantages. Where high voltages are encountered, greater thickness is required for proper insulation; porous insulations, however, allow complete impregnation with consequent elimination of voids and absence of corona.

In winding transformers, several special precautions are taken. One of these is to place unimpregnated woven glass sleeving over each lead coming from the unit. This sleeving is not merely slipped on after the unit is wound; it is actually placed over the lead as soon as the lead is brought out, so that any subsequent winding will be over the sleeving (Fig. 25). The sleeving serves several purposes: (1) it helps to take stress off the lead, (2) it prevents sharp bending as the toroid is wound, and (3) it prevents abrasions of the insulation.

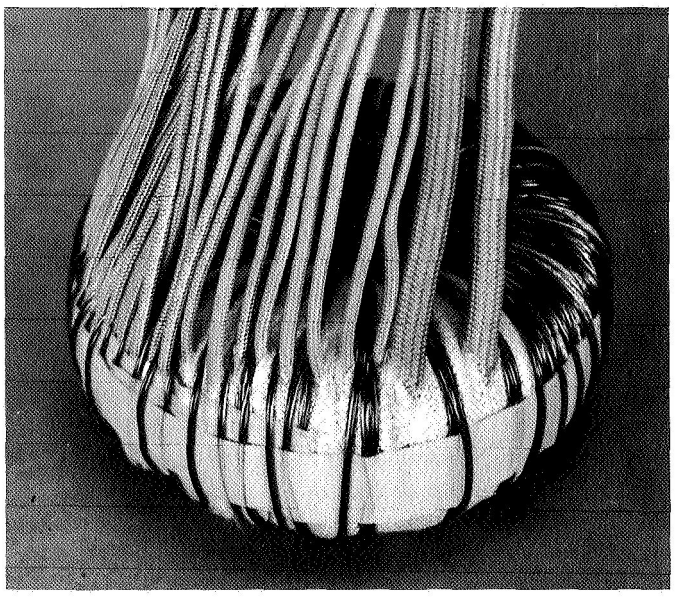

Fig. 25. Toroidal transformer showing lead breakout with sleeving

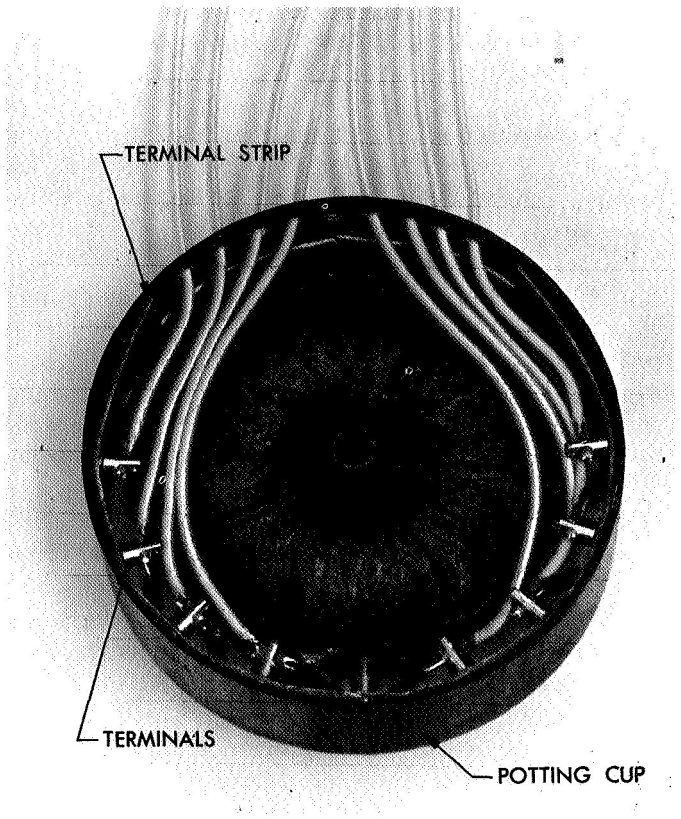

Fig. 26. Internal assembly of completed transformer

In attaching flexible leads to a winding, the common commercial practice is to solder the lead to the winding wire and then to insulate and anchor the joint with adhesive tape of one kind or another. Experience has shown that this method does not result in the most reliable type of assembly. Analysis of failed units showed that insulation between leads had been punctured, with consequent shorting of windings. To prevent this type of failure and to provide a suitable anchor point for the stranded wire, an internal terminal board is used that is made from a strip of epoxy fiberglass approximately 15–20 mils thick in which bifurcated terminals have been secured (Fig. 26). The strip also has a number of large holes to aid in the potting operation. This terminal strip is inserted between the toroid and the potting cup and spot-cemented to the cup (Fig. 26). The wires from the transformer, with the sleeving cut back to proper length, and the flexible external lead wires may then be connected to the appropriate terminals (Fig. 26). Prior to potting, the lead egress holes are sealed with a suitable removable Silastic.

c. Screening tests. In a typical screening test, the transformer or inductor is first subjected to a careful examination, usually using a 10× magnification. Cracks, chips, scraped or pinched leads, or anything that could conceivably affect the electrical operation are looked for and recorded if found. When any questionable area is found, it is usually examined under 20× magnification. Second in the test program is the electrical testing. It would be relatively simple but time consuming merely to check all of the electrical parameters. Equally meaningful but much faster is the testing of a few characteristics that singly or in combination reveal any fault in the unit. After many years of testing, a few characteristics stand out as being particularly meaningful:

(1) Turns ratio shows that each winding has the proper ratio of turns to every other winding on the transformer.

(2) Exciting current or primary inductance shows that the proper type of core material has been used, the gap, if any, is proper, the number of turns is correct, and there are no shorted turns of wire in the assembly. If primary inductance is measured, the unit is degaussed prior to test. This degaussing is repeated after any test in which the core is submitted to a dc field, such as occurs during resistance measurement.

(3) Direct current resistance shows that proper wire size has been used, also being related to transformer regulation.

(4) Insulation resistance or dielectric strength shows that insulation is proper for handling the voltages involved.

For many transformers, additional tests will be required (capacity, corona, rise and fall times, etc.). However, for the large majority of units, the tests listed above are sufficient.

After the initial electrical measurements, units are subjected to a 10-cycle thermal shock test. This test is conducted in accordance with the applicable test conditions of MIL-STD-202. During thermal shock, each transformer or inductor is continuously monitored for continuity during the high-temperature half of each cycle.

Following thermal shocks, units are normally tested for excitation current and insulation resistance. These two tests will reveal most of the faults that can occur. Then the units are placed in an oven for 168 h and run in a loaded condition at the temperature equal to the temperature class rating of the transformer.

Upon completion of burn-in, all initial measurements are repeated. In evaluating test data, not only is consideration given to conformance to original limits, but to changes in parameter values. Normally, some change in some of the values is to be expected, but a knowledge of the inductive part will reveal when the delta change is excessive and indicative of failure, or incipient failure, in the component.

E. Guidance and Control

1. Power Subsystem

a. Power profile. The *Mariner* Mars 1969 spacecraft proof-test model (PTM) was tested at the Spacecraft Assembly Facility at JPL during June and July 1968 to evaluate its steady-state power requirements during various operational modes. Measurements were taken at various test locations on the spacecraft. These readings were compared with spacecraft telemetry values where applicable; wattmeter measurements were also compared with power magnitudes calculated from telemetered parameters. With system test tolerances considered, the PTM telemetered values compared within reasonable and acceptable limits to those obtained by "hard line."

The power source was external to the spacecraft for all modes of operation during these tests. The external power supply potential was adjusted to the estimated nominal values of the solar array or battery. The power requirements for the various operational modes of the PTM spacecraft are given in Table 2.

The "minimum guaranteed" *Mariner* Mars 1969 solar array power output given in the table includes uncertainty factors amounting to 2% due to sun intensity magnitude, and a 15°C tolerance of the nominal solar array temperature. These uncertainty factors are applied to provide the worst-case array output magnitudes at given operating conditions during the mission. The uncertainty factors cause the minimum guaranteed power to be approximately 8% less than the nominal power at the maximum power point at about midpoint during the mission where the sun intensity is 100 mW/cm² and the array temperature is nominally 28°C, approximately 9% less near earth at 145 mW/cm² at 60°C nominal temperature, and approximately 5% less near Mars at 69 mW/cm² at 2°C nominal temperature.

Also included in the table is the estimated output of the minimum guaranteed *Mariner* Mars 1969 array after radiation degradation by the Van Allen belt, and a 6-mo interplanetary flight near the peak sun-spot activity. The integrated flux used for this evaluation during this mission period is 4.4×10^9 protons/cm² having energy greater than 30 MeV. It is estimated with 80% probability that the *Mariner* Mars 1969 array power loss due to radiation degradation will not exceed 17%; the data provided in the table reflects this degradation magnitude.

Table 2. PTM spacecraft steady-state power requirements

Spacecraft operational modes	Power requirement, W
Near earth[a]:	
Countdown and launch (T −10 min to booster separation)	284.0
Roll search (near earth)	279.0
Earth cruise (battery charging)	253.0
Earth cruise (battery not charging)	250.0
Maneuver	278.0
Near Mars[b]:	
Mars cruise (battery charging)	257.5
Mars cruise (battery not charging)	253.0
Roll search (near Mars)	280.0
Far-Mars encounter (scan motors on)	297.5
Near-Mars encounter (scan motors on)	291.5
Near-Mars encounter (scan and gyro motors on)	314.0
Playback	288.0

[a]Minimum guaranteed array power near earth: 780 W with no radiation degradation; 647 W with maximum expected radiation degradation.

[b]Minimum guaranteed array power at Mars: 449 W with no radiation degradation; 373 W with maximum expected radiation degradation.

For steady-state conditions, it appears that the worst-case load for the PTM spacecraft is 314 W near Mars, with scan and gyro motors on. Under these circumstances, a failure mode is assumed whereby Canopus acquisition by the spacecraft had been lost, and gyros are energized to stabilize the attitude of the spacecraft. The power capability of minimum guaranteed array that is radiation-degraded to its maximum expected extent during the mission is shown to exceed spacecraft power demands in this operative mode by almost 16%.

b. Battery flight-acceptance vibration tests. The basic philosophy of flight-acceptance testing *Mariner* Mars 1969 batteries is to combine appropriate environmental conditions with performance-level testing of such magnitude that hardware defects can be detected without the test being destructive or degrading in nature. The environmental conditions and performance levels are designed to simulate the expected flight conditions, as opposed to battery type-approval test conditions (SPS 37-52, Vol. I, p. 25), where the design limits of operation are evaluated. Before the *Mariner* Mars 1969 batteries were flight-acceptance-tested, extensive developmental testing resulted in a redesign of certain areas within the battery cells and the battery chassis to ensure better vibration resistance than on previous *Mariner* batteries. Since the *Mariner* Mars 1969 spacecraft are to be launched on an *Atlas/Centaur* vehicle, the expected vibration levels are of greater magnitude than experienced on past *Mariner* missions, which used the *Atlas/Agena* vehicle. The design modifications definitely increased the operational limits of the battery in a vibration environment during type-approval testing. Flight-acceptance tests now have provided an additional comparison of previous battery performance to the performance of the *Mariner* Mars 1969 design.

Batteries 100, 105, and 106 were vibration-tested at the JPL Environmental Test Laboratory in accordance with all applicable *Mariner* Mars 1969 project requirements for flight-acceptance testing. The vibration test consisted of 20 s of random noise at a level of 10.8 g rms in each of three orthogonal axes. None of the batteries showed anomalies or defects of any kind during the testing. As part of the simulated launch conditions, the batteries were discharged with a 273-W load during the vibration runs. A continuous oscillograph recording of terminal voltage variation, due to plate-pack movement, was made. Analysis of these voltage variations is indicative of the relative magnitude of plate-pack displacement.

While the *Mariner* Venus 67 batteries performed to specification and were successfully flown, a great improvement in vibration resistance is expected with the new *Mariner* Mars 1969 design. The variations in terminal voltage of the *Mariner* Mars 1969 batteries, at a slightly higher g level (10.8 g rms) than the *Mariner* Venus 67 batteries, were almost nondetectable (< 1 mV), which is indicative of the existence of virtually no plate-pack displacement during vibration. This in turn means that a much higher degree of reliability has been obtained in the new *Mariner* Mars 1969 design to operate without failure under expected and abnormal vibration conditions.

2. Command Generation Program

The command generation (COMGEN) data processing software system for the *Mariner* Mars 1969 spacecraft contains the programs required to support the central computer and sequencer (CC&S) during launch and flight operations. Among the flight operations software are programs to: (1) prepare total or partial CC&S programs and radio commands for inflight reprogramming of the CC&S memory; (2) reconstruct, from telemetry data, the actual memory and perform a comparison with the expected memory contents; and (3) simulate the logic of the CC&S and generate a time sequence of events controlled by the CC&S. Command generation is also used for preparing eight-level paper–Mylar tape for the initial CC&S memory load and verification on the launch pad.

The *Mariner* Mars 1969 CC&S is a computer with a 128-word memory that must be programmed for operation. Its memory may be changed inflight by earth-based radio commands. Radio commands are also available for readout of the memory through spacecraft telemetry. During a midcourse maneuver, redundancy to the computer portion of the CC&S is provided by a fixed sequencer similar to the maneuver sequencer on *Mariner* Mars 1964 and *Mariner* Venus 67. This maneuver-fixed sequencer must also be programmed inflight with maneuver event time durations.

The programs that comprise the COMGEN software system include assembly, translation, simulation, launch tape format, command format, and memory readout data processing links. The assembler accepts as input a total or partial CC&S program in a symbolic language. Symbolic memory locations are assigned decimal values and a decimal machine language program is output.

The translator accepts as input a flight sequence of events and also generates a decimal machine language

program. A flight sequence is input in the form of equations. An elementary compiler solves the equations and defines the unknown symbols. These symbols are operated on by a set of conversion algorithms to generate information for insertion into a skeleton CC&S program that had been previously loaded into the translator.

The CC&S simulator accepts as input the decimal machine language program and generates a sequence of events. The logic of the CC&S is simulated in sufficient detail to accurately predict the state of the computer at any future time. The simulation results are inspected to verify the flight program that is initially loaded into the memory. Effects of radio commands may also be simulated to confirm that the desired response will be obtained.

Launch tape preparation programs accept as input a CC&S program and punch paper–Mylar launch tapes. These tapes are used by the launch complex equipment to load the CC&S memory just prior to launch.

The command format program accepts as input memory data in a convenient decimal format. These memory data are input to the CC&S simulator to generate a sequence of events and correct for transmission delays. If the desired sequence is confirmed, a command tape is written. Commands are encoded as a teletype message and sent to the Deep Space Network for transmission to the spacecraft.

The CC&S memory may be programmed or commanded to output its memory contents through spacecraft telemetry. The telemetry data stream is decoded and formatted into binary memory words for input to COMGEN. The memory readout retrieval programs convert the binary memory data to decimal machine language. These data may be input to the simulator for verification or may be compared with previously simulated memory data.

The COMGEN program has been designed and is in the final stages of implementation. Preparation of launch tapes will commence during the latter part of 1968. All programs will be completed before March 1969 and will be used to support flight operations.

3. Sun Sensors

a. Introduction. The *Ranger* and *Mariner* spacecraft have all used the sun as a celestial reference for pitch- and yaw-axis attitude control. The *Ranger* and *Mariner II* used reflected earth light as a reference to stabilize the roll axis. All subsequent spacecraft have used the star Canopus as a roll-axis reference. For pitch and yaw stabilization, the sun sensor outputs are fed into the attitude-control logic circuit, which controls the spacecraft by means of the attitude-control gas jets.

All JPL flight sun sensors have operated on the same basic principle. The configuration and operating characteristics of sun sensors change from mission to mission depending on the particular field of view and the associated dynamic constraints.

A flight set of sun sensors for all *Mariner* spacecraft has consisted of the acquisition sun sensors, the cruise sun sensors, and the sun gate.

b. Theory of operation.

Acquisition and cruise sun sensors. The operation of the acquisition and cruise sensors is illustrated by Figs. 27 and 28. Figure 27 illustrates the mechanical arrangement of the photodetectors; Fig. 28 is an electrical diagram for the detectors.

The photodetectors contain cadmium sulfide as the light-sensitive material. Each detector is essentially a light-sensitive resistor, which has a fully lit resistance of approximately 800 Ω at earth (1 solar constant) increasing to approximately 1215 Ω at Mars (0.433 solar constant).

The method of operation of a single axis can be visualized as follows: when the sun-lit area of cruise detectors A and B is equal (Fig. 27), the resistance of each detector is equal. This is the sun-acquired position and results in a null output voltage. When the spacecraft rotates slightly from the position shown, the sun-lit areas of cells A and B become unequal, resulting in unequal resistances. This in turn causes unequal voltage drops across detectors A and B, resulting in an output signal. A clockwise spacecraft rotation produces a negative output signal and a counterclockwise rotation produces a positive signal.

For large angles of rotation the acquisition detectors C, D, E, F, G, and H must be considered, since they are electrically energized by relay R1 at error angles of approximately 5 deg or greater. For clockwise error angles between approximately 5 and 89 deg, detectors A and C are both sun-lit. Under this condition a negative output signal will result, since both detectors have a negative excitation voltage and their paralleled resistance is less than the paralleled resistance of detectors B, D, F, and H, which are not sun-lit. At any error angle, two or more detectors are sun-lit and the single-axis system depicted generates an output signal curve as shown in Fig. 29. Another axis, oriented 90 deg about the spacecraft sun line to the one depicted, makes up a complete

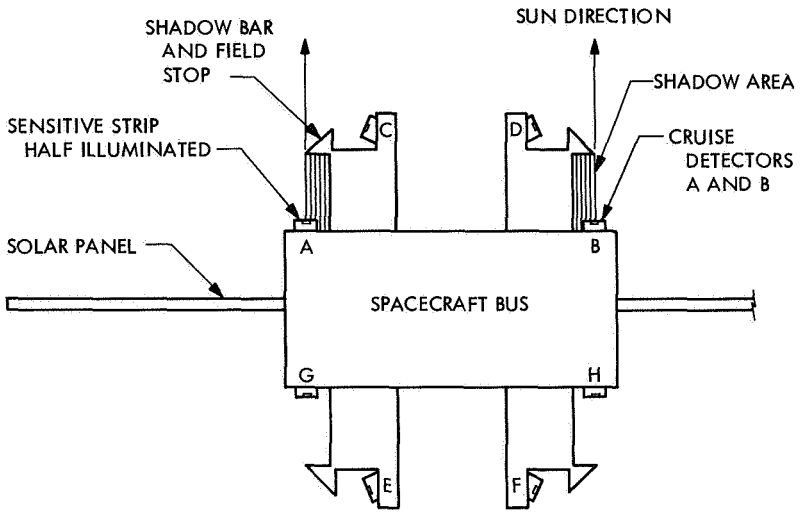

Fig. 27. Detector mechanical arrangement (single axis)

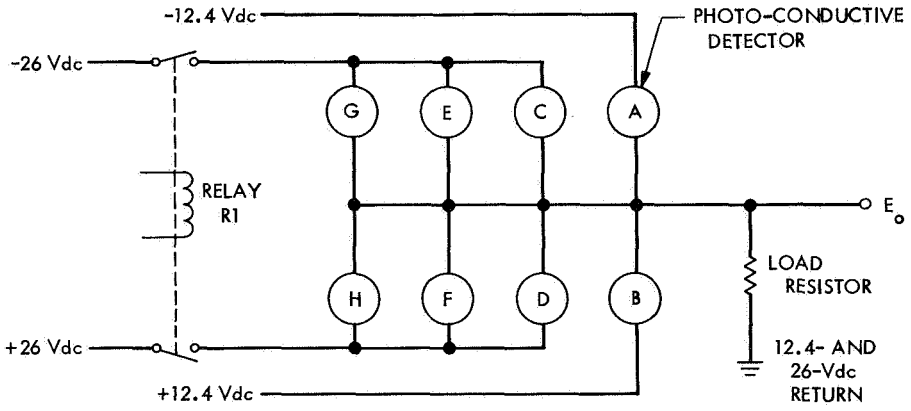

Fig. 28. Detector electrical diagram (single axis)

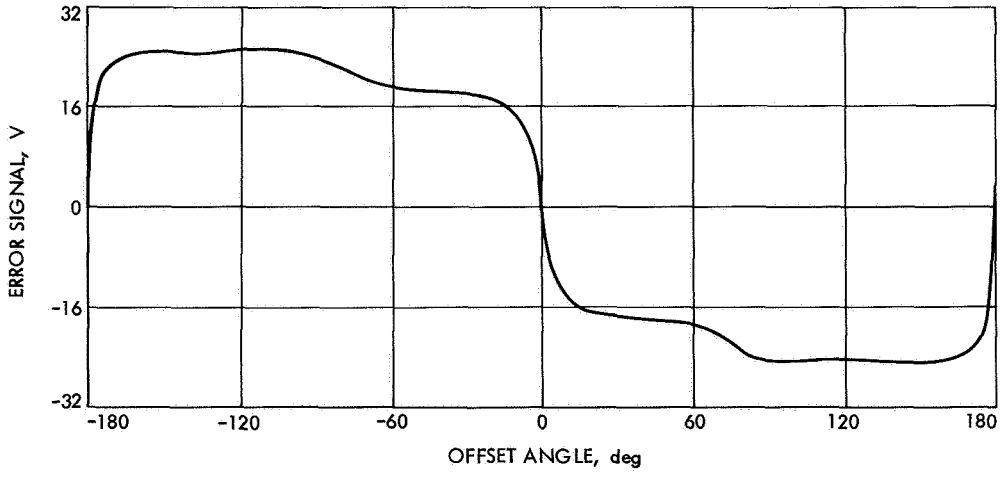

Fig. 29. Sun sensor system output curve

sun sensor system. The complete system provides a 4π steradian field of view that allows sun acquisition from any spacecraft position.

Sun gate. The operation of the sun gate is very simple. The structure provides a light-tight enclosure for each of two detectors of the same type used in the cruise and acquisition sensors. Each detector enclosure is provided with a 0.070-in.-diam aperture. This aperture is accurately adjusted to allow solar energy to activate the detector whenever the spacecraft roll axis is aligned to within 8 deg of the spacecraft sun line. The minimum resistance occurs at 0-deg error angle as shown by the output resistance curve in Fig. 30. The output resistance of the sun gate is monitored by the attitude-control logic circuit. This circuit indicates sun acquisition whenever the resistance is below a predetermined value (approximately 13 kΩ). One of the events caused by a sun-acquisition signal is the de-energization of the acquisition sun detectors through relay R1 (Fig. 28).

Two detectors wired in parallel are provided to increase the reliability of the sun gate. An "open" failure of either detector would change the level of the resistance curve as shown in Fig. 30. This will alter the angle at which sun acquisition is indicated but proper operation will continue. A shorted detector is considered many times more unlikely than an "open" since each detector is hermetically sealed and contains a sensitive area that is 0.050 in. wide.

c. Design.

Acquisition and cruise sun sensors. The design of the cruise sun sensor assemblies is the same as the *Mariner* Mars 1964, except that a modification was made to incorporate a different photodetector. An improved detector, which is housed in a TO-5 size transistor can, with a window to admit solar radiation, is used for all *Mariner* Mars 1969 sun sensors. Two cruise sensors (Fig. 31a) were used. These were mounted on pedestals extending upward from the bay IV and VIII positions of the spacecraft octagon structure. Each cruise sensor assembly contains

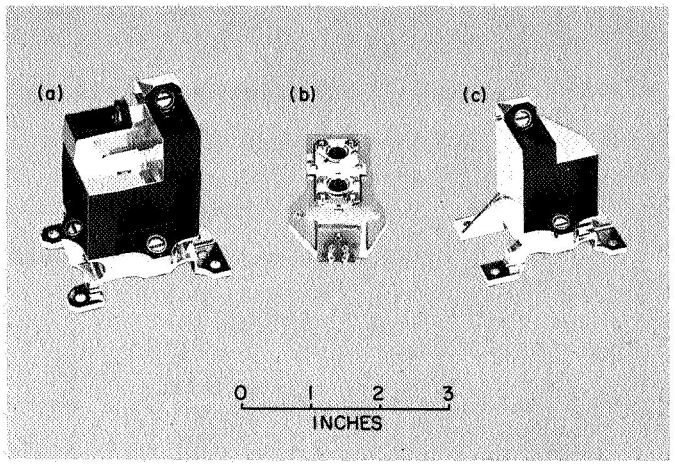

Fig. 31. Sun sensor flight set: (a) cruise sensor, (b) sun gate, (c) acquisition sensor

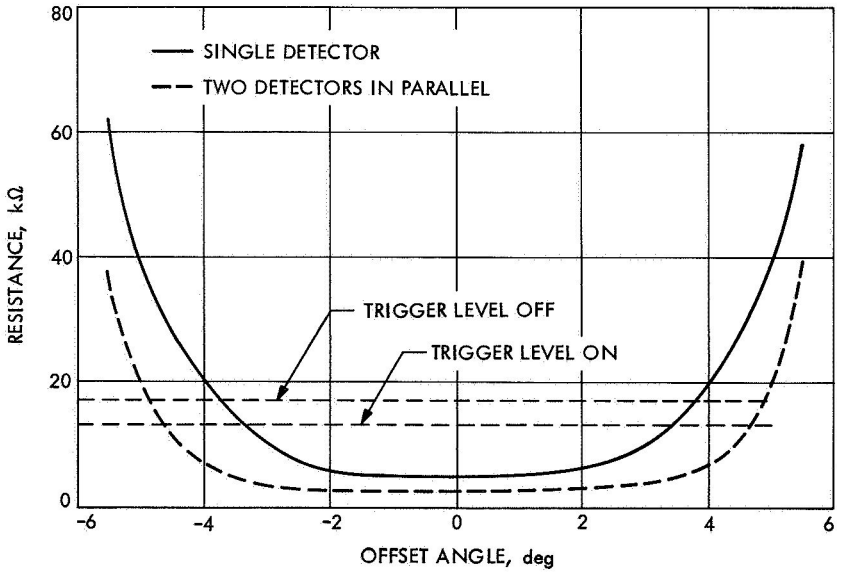

Fig. 30. Sun gate resistance curves

two acquisition detectors as well as two cruise detectors. The cruise detectors are located nearest to the base plane.

The cruise detector excitation voltage was reduced from the 16 V used in *Mariner* Mars 1964 to 12.4 V. This was done to reduce the power dissipation and, consequently, to improve reliability.

Four acquisition sensor assemblies (Fig. 31c), containing two detectors each, were mounted in bays I, III, V, and VII on the lower ring of the octagon structure. Four assemblies were required, compared to two for *Mariner* Mars 1964, because of more severe field-of-view constraints imposed by the size and configuration of the scan platform.

Sun gate. The *Mariner* Mars 1964 sun gate design was modified to incorporate the same detector used in the acquisition and cruise sun sensors (Fig. 31b). The mounting surface was made perpendicular to the optical axis, instead of parallel to it, to allow the gate to mount on the same pedestal surface as the bay IV cruise sensor assembly. This resulted in a simplification of the pedestal design. These changes also allowed an improvement in the terminal board configuration. The photodetector leads were routed directly to the solder terminals of the terminal board. This eliminated four solder joints, between the terminal board and detectors, and simplified the assembly.

Initial functional tests revealed that additional baffling was needed to prevent stray light from reducing the resistance at angles greater than 5 deg. The needed baffling was accomplished by adding a black paint pattern on the face of the detector assembly window. This pattern provided a transparent aperture parallel to and 0.008 in. wider than the detector sensitive strip.

d. Environmental testing.

Acquisition and cruise sun sensors. The initial type-approval vibration test of a cruise sun sensor assembly resulted in a failure of an acquisition detector. The construction of a photodetector is illustrated in Fig. 32. An analysis of the failed detector revealed that the ceramic detector wafer had moved in relation to the other parts of the assembly. This vibration-induced motion had fractured the indium solder joints connecting the electrical leads to the detector wafer. Movement of the wafer is normally prevented by electrical leads, which are crimped over to hold the wafer against the header assembly.

A special test was run to determine the vibration level to which these detectors were being subjected. It was found that at a resonant frequency of 1200 Hz the detectors were experiencing approximately 550 *g* rms.

A resilient detector mount was designed in an attempt to damp out the high *g* levels at the resonant frequency of the sensor housing. Silicon rubber rings, having a Shore durometer hardness of 35, were used to isolate the detectors from the housing. This design modification was incorporated into the engineering prototype sun sensor hardware for evaluation. The vibration screening was raised from 35 Ω to 70 *g* rms for the photodetectors; 70 *g*

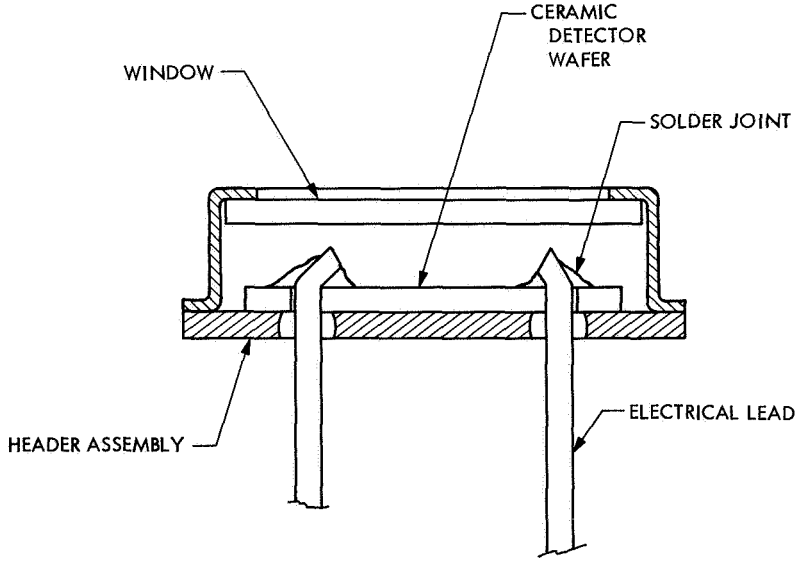

Fig. 32. Detector configuration

was used because the vibration equipment was not capable of producing the higher levels necessary to simulate the expected vibration level of 550 *g*.

No failures were experienced when the engineering prototype sensors were evaluated at type-approval vibration levels or at 160% of type-approval levels. These sensors included a total of 14 cells and it appeared that the resilient mount had effectively prevented vibration-induced detector failures. The proof-test model sensors were then modified to incorporate the resilient mount in preparation for the continuation of formal type-approval testing.

A backup effort was also initiated to prevent vibration-induced failures. This effort was directed at improving the mechanical design of the detector assembly to increase its vibration resistance. Three design changes in the construction were made. First, the header lead pins were left uncrimped. Second, the ceramic detector wafer was adhesively bonded to the header plate. Third, a conductive paint, in place of indium solder, was used to make the electrical connection between the detector wafer and header leads.

An evaluation of five adhesives and two conductive paints was made to determine the optimum choice as judged by the following criteria:

(1) Adequate mechanical strength throughout the expected temperature change.

(2) Sufficient chemical stability during the expected environmental conditions.

(3) Compatibility with the cadmium sulfide material. (Many adhesives contain materials that diffuse into the cadmium sulfide and permanently alter the operating characteristics.)

The test results indicated the Eastman 910 would best meet the requirements for an adhesive. Hanovia 13 was selected for the conductive paint. Sufficient component parts were procured from the vendor to allow construction of flight detectors. This effort was undertaken at JPL to have flightworthy detectors available at the earliest possible date, and to ensure that the JPL-developed construction techniques were rigidly followed.

A specially designed resonant beam vibration fixture was designed and developed to amplify the *g* level available from the standard vibration machine. This fixture allowed 3-axis screening of the ruggedized detectors at 650 *g* rms at 850 Hz. It was decided that this test, which exceeds the expected vibration level but only allows for one frequency, was preferable to the previous screening test, which swept from 50 to 2000 Hz but was limited to 70 *g*. The natural resonant frequency of the detector wafer and header leads was calculated to be approximately 16,000 Hz, indicating that the assembly was less sensitive to frequency than vibration level. An exploratory test on 12 non-ruggedized detectors at 650 *g* resulted in two failures out of 12. No vibration failures resulted during the screening of 160 ruggedized detectors.

The screening of the ruggedized detectors was completed in time to incorporate them into all flight sensors subsequent to the proof-test model sensors. The uncertainty of the vibration resistance of individual non-ruggedized detectors resulted in a decision to use the ruggedized detectors for the flight sensors.

Two additional non-ruggedized detector failures were encountered during the subsequent type-approval vibration testing of the proof-test model sensors. In each case the failed detector was replaced with a ruggedized detector and the testing was continued successfully.

One out-of-tolerance null condition was experienced on the first set of flight sensors. This was found during the post-environmental functional test. The null offset at 0 deg was 68 s compared to the tolerance of ± 54 s. It was found that a null offset can be caused by depressing the detector assembly toward one side of the resilient mount. This indicates that vibration or thermal stresses can change the null by altering the "at rest" position of the detector assembly relative to the sensor shadow edges. The tolerance of 54 arc sec represents a shift in detector position of 0.00066 in.

The sensor assembly was reworked by lapping the mounting feet to change slightly the mounting plane relative to the shadow edges and detector position. The flight-acceptance test was rerun and the post-environmental test revealed "in tolerance" conditions.

Another anomaly appeared after type-approved thermal shock testing. The post-environmental functional tests revealed that the pitch null was 79 arc sec compared to the 54-s tolerance. It was decided to repeat this test with closer controls to prevent an inadvertent side force on one of the detectors which could cause a null offset.

The thermal shock test was repeated after the out-of-tolerance null was corrected by reworking the sensor.

The post-environmental functional test revealed a pitch null offset of 107 s and a yaw offset of 112 s. These results indicate that thermal shock can induce thermal stresses that cause the detectors to come to rest at a different position within the resilient mount after testing.

Sun sensors used on prior missions also used resilient-mounted detectors, but the configuration provided much more restraint. These sensors did not exhibit any measurable null offset due to environmental testing.

An examination was made of the feasibility of increasing the null offset tolerance in lieu of a costly redesign and retest effort. The midcourse maneuver pointing error is composed of a number of separate errors. The sun sensor contribution to the pointing error was 0.2% in yaw and 0.08% in pitch. Changing the null offset from 54 to 144 s allows for a worst-case null shift of 112 s (due to thermal shock) plus an inherent null offset of 32 s, which is the largest inherent null offset that exists for the flight sensors. An increase of the tolerance to 144 arc sec changes the variance in pointing error, due to sun sensors, to 0.93% for yaw and 0.38% for pitch. This slight increase in total pointing error was judged to be acceptable to the mission requirements. The functional specifications were accordingly changed to call out these new tolerances.

Sun gate. Although no failures were encountered during environmental testing of the sun gate, the resilient detector mount and the ruggedized detectors were incorporated to ensure against possible failures.

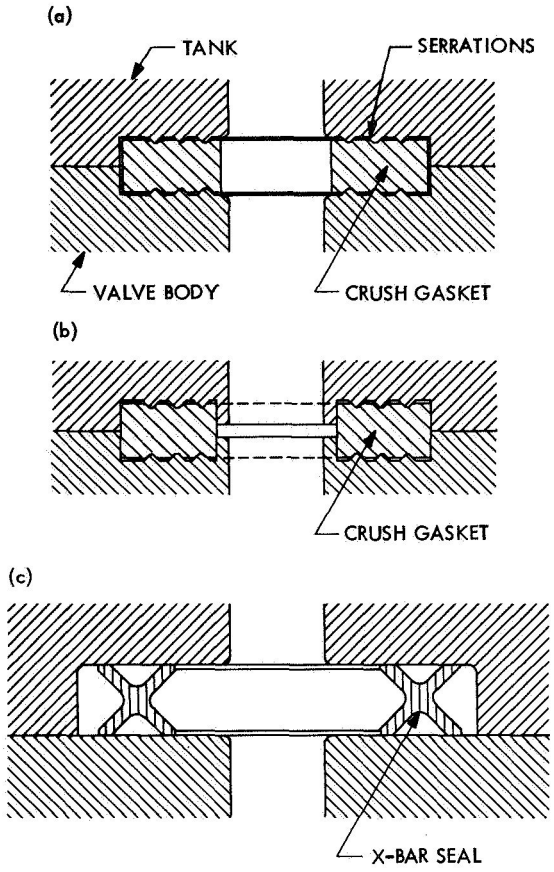

Fig. 33. Cross section of high-pressure seals: (a) present design, (b) machined pocket design, (c) X-bar design

4. Gas System Crushable Seal

a. Introduction. The gas system for the *Mariner* spacecraft, which provides the thrust necessary for attitude control, is made up of two separate sets, each consisting of a fill valve, a tank (for the gaseous nitrogen supply), a regulator (for lowering the pressure from the supply of 2650 to 15 psi), and a system of six thruster valves. Each half system is primarily an integrally welded assembly. However, several mechanical joints are incorporated, including a crushed-aluminum high-pressure seal between the flight fill valve and the supply tank. Figure 33a shows a cross-sectional view of this seal as installed in the flight hardware.

b. Design and performance. Three concentric serrations (with sharpness specified at a maximum 0.001-in. flat or 0.003-in. radius, depending on the type of machining used in manufacture) are machined into both the fill valve and the tank mounting boss (Fig. 33a). Both surface finishes are specified to be 16 rms or better. The surface finish of the aluminum seal is 4 rms as presently specified. Since the seal is fully annealed to be very soft, this surface finish is difficult to maintain. During assembly the machined serrations embed into the soft aluminum seal and form a triply redundant, metal-to-metal seal configuration.

Some difficulty was associated with maintaining the surface finish as well as scratch-free surfaces on the sides of the serrations. A rework procedure was developed whereby a die was made of the configuration, and a cleanup operation by electric-discharge machining was successfully used on the fill valve. This resulted in an approximately 6-rms finish on the reworked serrations. The surface could be described as having a matt finish (not characteristic of a cutting-tool-turned surface).

Photographs were taken, using scanning electron-beam photography, both before and after electric-discharge machining. Figure 34 shows the scratched surface of a

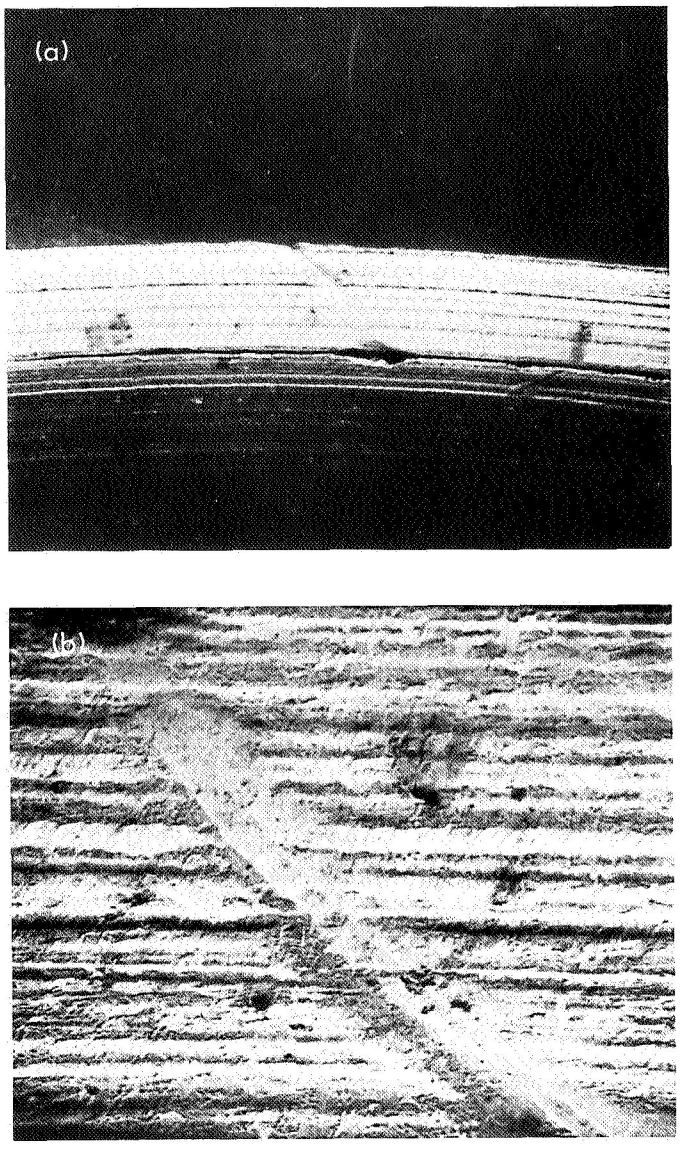

Fig. 34. Scratched surface of machined serration impression of middle groove: (a) 100×, (b) 500×

serration left by the impression of the fill-valve machined serrations in the soft aluminum seal that had failed due to leakage. Note the circumferential lay of the machining marks and the sharp deep groove left by the impressing serration (cross section shown in Fig. 35a).[2] Both of these characteristics were felt to be critical to the sealing capabilities of this type seal. Such scratches were encountered during fabrication of the *Mariner* Mars 1969 hardware, where eight similar failures required assembled hardware to be disassembled, repaired, reassembled, and retested.

Figure 36 is a similar serration surface as Fig. 34 after being cleaned by electric-discharge machining. The matt finish and lack of a sharp deep groove can be seen (see also Fig. 35b). Note the fidelity with which the soft aluminum has taken on the impression of the surface imperfections of the original surface, a requirement of this type seal.

During investigations, it was noted that the outer diameter and the inner diameter of the seal were not supported during the impressing of the serrations and

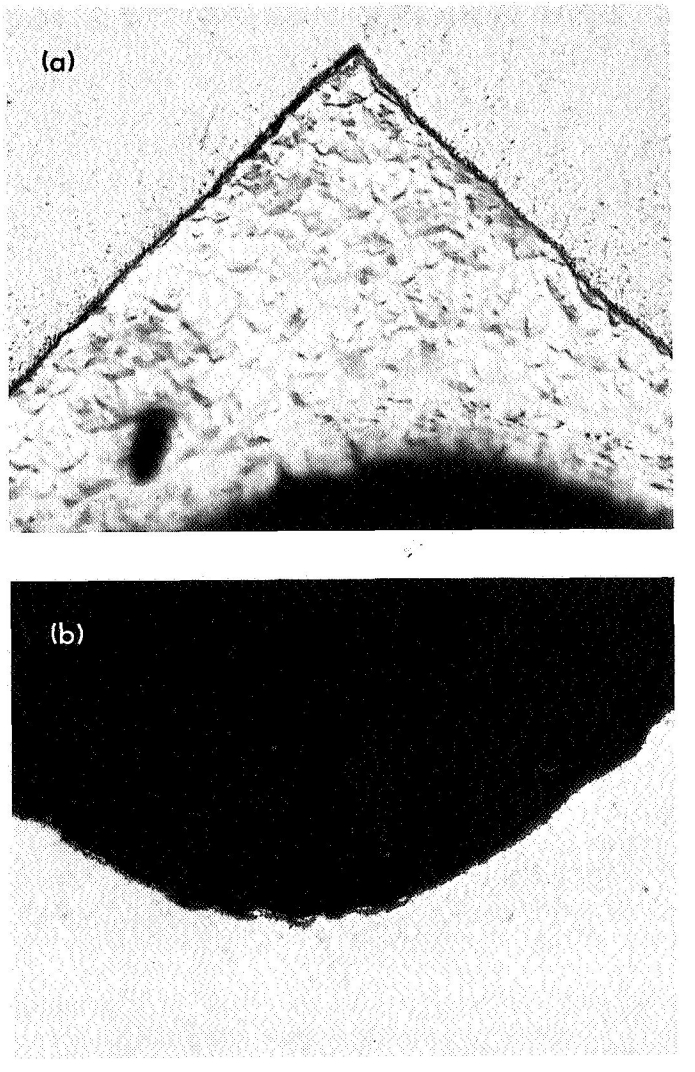

Fig. 35. Cross section of center serration impression (500×): (a) machine-turned, (b) electric-discharge-machined

[2]The material filling in the "V" of the cross section in Fig. 35a is a conductive coating required by the scanning electron-beam photographic method and does not mask or in any way detract from the metallurgical view.

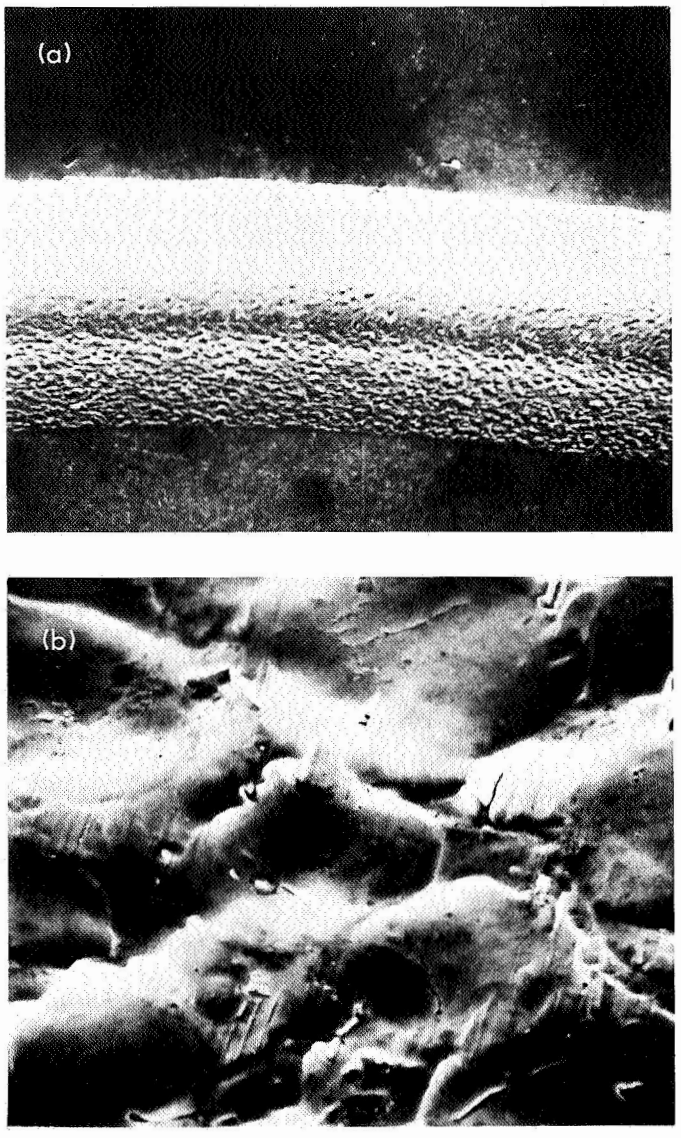

Fig. 36. Electric-discharge-machined serration impression of middle groove: (a) 100×, (b) 2000×

apparently allowed the surface material of the seal to cold-flow parallel to the surface of the serration. If this were the case, it would allow axial scrubbing of the material up the side of the serration to the final seating position. This scrubbing action would allow leakage paths up the sides of both the inside and outside serrations, thereby eliminating the two halves of those serrations as leak-deterrent configurations. Some indication of this was noticed by microscopic inspection. However, it was not until the scanning electron beam photographic investigation that proof of this action was obtained. Figure 37 shows the scrubbing action in the inside serration.

A partial remedy was incorporated in the *Mariner* Mars 1969 structure by making the outer diameter of the seal fit snugly within the pocket of both tank and fill valve. With this technique, the cold-flow was contained, thus serving as a backup to the impressing serration and the scrubbing action noted previously did not occur.

c. Future design improvements. The development of seals for future application should include an investigation of a seal configuration based on the present design, wherein the inner diameter as well as the outer diameter

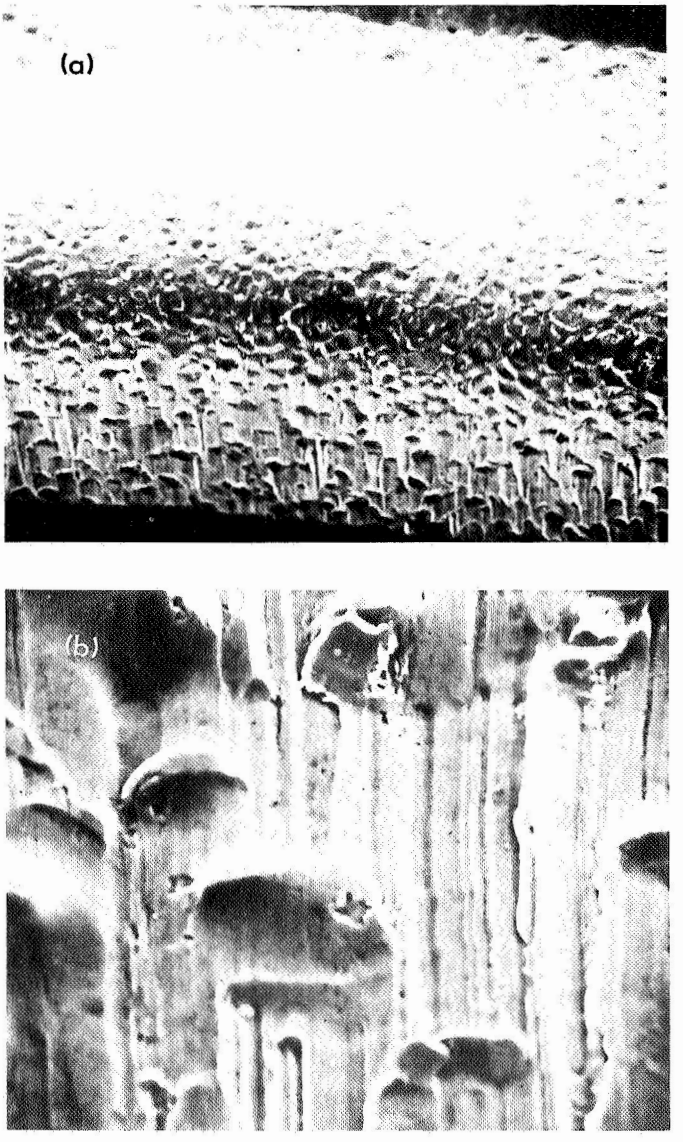

Fig. 37. Electric-discharge-machined serration impression of inner groove: (a) 200×, (b) 2000×

fits snugly within the pocket machined in both the tank and fill valve. This would squeeze the material of the seal against both the inner and outer rings as well as the center ring, and should achieve a seal that would require less handling and rework (Fig. 33b).

A second and parallel effort should investigate the possibility of using a separate metal seal similar to that used between the thruster valves and the valve manifolds, which is an X-bar configuration (Fig. 33c). Several of these types of seals are commercially available. Basically, they are of K, X, or O cross-sectional configuration, spring-loaded, and soft-alloy-coated. The sealing surfaces conform to the surface irregularities of the mating parts and, in addition to being spring-loaded, are pressure-loaded by the contained gas. This approach should result in an overall configuration that would be more reliable at less cost.

F. Space Sciences

1. Hydrogen Embrittlement of Inconel 718 Pressure Vessels on the Infrared Spectrometer

a. Introduction. The Rocketdyne Division of North American Aviation, Inc., has found a hydrogen-embrittlement effect with Inconel 718 that was not previously suspected.[3] During a NASA program to screen several metals and alloys for such an effect, unnotched tensile specimens of Inconel 718 showed much lower ductility values in ultrapure 10,000-psig hydrogen than in air. Further tensile tests with severely notched specimens (10-to-1 stress concentration) gave strength values nearly 50% lower then those obtained during tests in air.

The two-stage Joule–Thomson cryostat used to cool one of the sensors of the *Mariner* Mars 1969 infrared spectrometer requires a high-pressure hydrogen vessel for the second stage. Present vessels are 6-in.-diam spheres made by forging, welding, and heat-treating hemispheres of Inconel 718. Since the reliability of these vessels is essential, the Rocketdyne work emphasized the need for more extensive fracture-toughness data for Inconel 718 in a high-pressure hydrogen environment.

A two-part accelerated test program was initiated with The Boeing Company. One part (Phase I) was contracted by the University of California at Berkeley and involved the testing of existing Inconel 718 vessels having known surface flaws induced by electro-discharge machining. The other part (Phase II) was contracted with Boeing by JPL and involved the testing of flawed sheet specimens cut from a selected Inconel 718 forging of similar composition to that used for the vessels. Phase II is discussed first because most of the data were taken in this effort.

b. Testing fracture toughness of sheet specimen (Phase II).

Objectives. This part of the program was undertaken to generate fracture-toughness data and to establish threshold flaw-size curves for Inconel 718 under sustained stress in a high-pressure, high-purity hydrogen environment. With these data the extent of hydrogen embrittlement with existing Inconel 718 vessels could be determined.

Description. Boeing's approach (Refs. 1 and 2) involves the testing of large sheet or plate specimens whose thickness is approximately that of the intended vessel wall and whose width is several times the induced-flaw length in order to avoid specimen size effects. In this case Inconel 718 sheet specimens were cut from the forging, machined to a nominal cross section of 0.140×3.00 in., and heat-treated.[4] Using electro-discharge machining, a sharp notch is cut in the thickness direction and the notch length lies normal to the tensile axis. A fine fatigue crack extending from the root of the notch is introduced by low-cycle tension fatigue at ~50% of the fracture stress.

Several specimens with differing semi-elliptical flaw sizes are loaded to failure in tension. The data determine the critical stress intensity in plain strain (K_{1c}) as a function of flaw size, as shown by the upper curve in Fig. 38. Threshold stress intensity is obtained with the same type of specimen, holding flaw size relatively constant and varying the sustained load, or varying the flaw size and holding load constant, or by both means. If the specimen does not fail or leak, it is "flaw marked," pulled to failure, and examined for flaw growth or the no-growth condition that defines the threshold. The environment of high-pressure hydrogen at room temperature is contained by stainless-steel cups with O-rings clamped over the flawed surface after the sustained load value has been reached.

Preliminary results. In Fig. 38 the upper curve shows critical fracture stress as a function of flaw size a/Q, where a is the crack depth in inches and Q is a flaw shape parameter. The critical stress intensity value is estimated to be $\simeq 120$ (klb/in.^{2})$\sqrt{\text{in.}}$ The lower curve

[3]Chandler, W. T., and Walters, R., unpublished data under NASA contract NAS 8-19, Task 7, Apr. 1968.

[4]Heat treatment: anneal 1 h at 1750°F, air cool, reheat to 1325°F for 8 h, furnace cool to 1150°F at 100°F/h, hold at 1150°F for 10 h, and air cool.

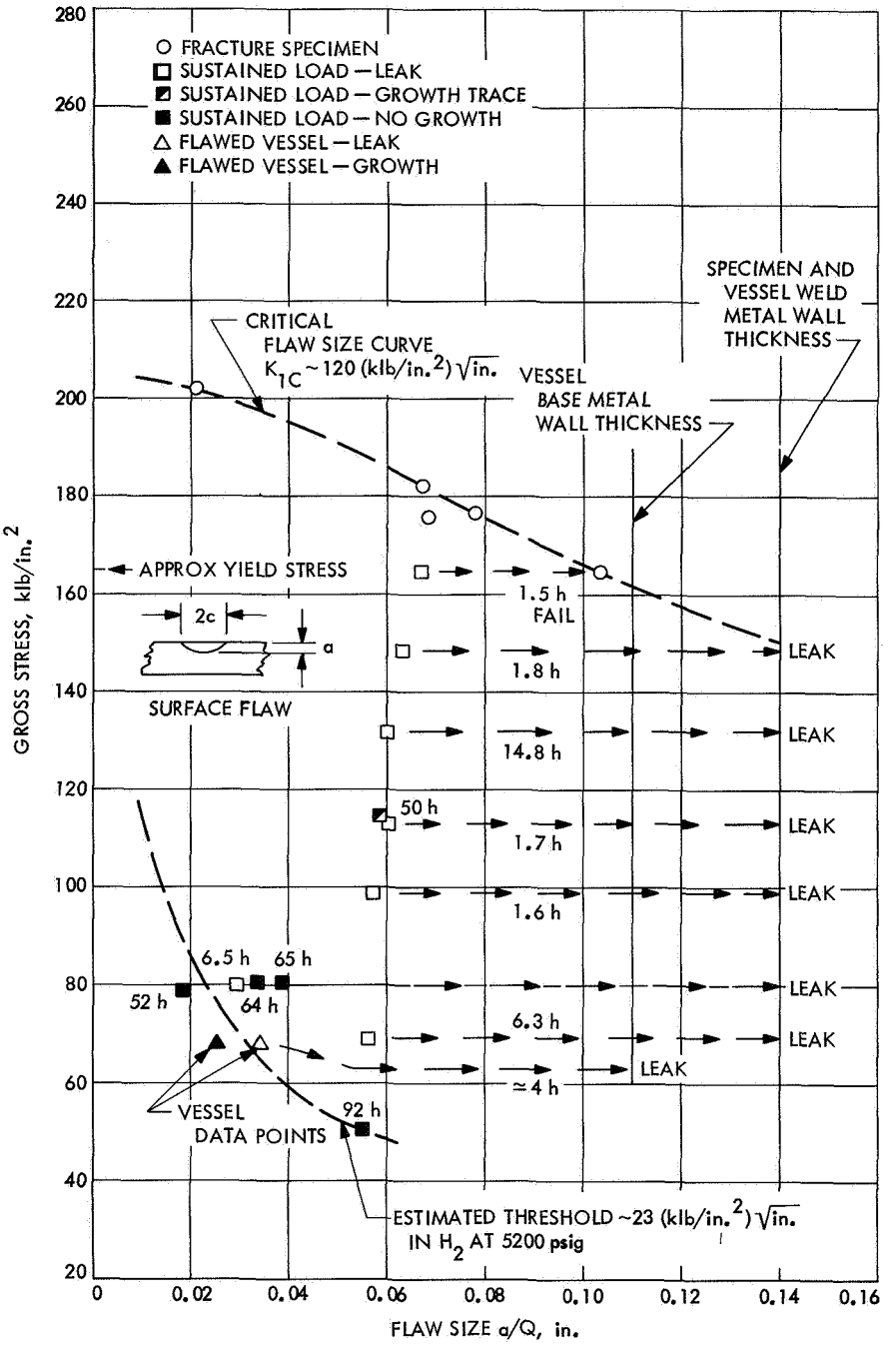

Fig. 38. Preliminary critical and threshold flaw-size curves for Inconel 718

gives threshold stress versus flaw size; i.e., the curve defines the approximate upper limit combination of stress and flaw size for a time-independent condition of no flaw growth and no failure. The threshold stress intensity K_{TH} is estimated to be 23 (klb/in.^{2})$\sqrt{\text{in.}}$

In Fig. 39 the time-independent threshold becomes more obvious in the plot of stress versus time for the same specimens as shown in Fig. 38. The specimen data scatter may be traced to metallurgical variation along the forging as well as to heterogeneity of microstructure in a given specimen.

c. Testing fracture toughness of vessels (Phase I).

Objective. Paralleling the Phase II effort, the objective of Phase I was to obtain sustained-stress flaw-growth data

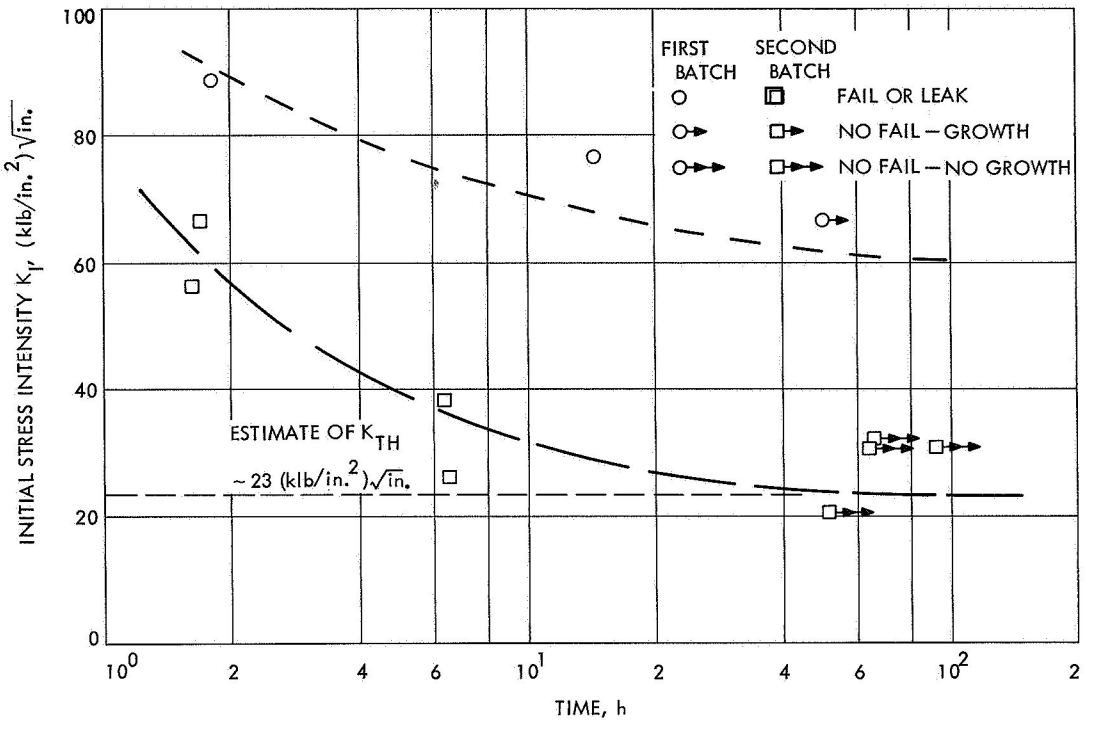

Fig. 39. Sustained stress life data

with two of the existing Inconel 718 vessels, which were heat-treated, after welding, in the same manner as the Phase II specimens (see Footnote 4).

Description. Semi-elliptical flaws were electro-discharge-machined (EDM) in the outer wall of two spherical vessels. Each flaw was located in the thin-wall portion (~0.110 in.) at a latitude of approximately 60°N with the weld zone being the equator. Fatigue crack extension of the EDM notch or flaw was obtained by low-cycle, low-load hydraulic pressurization of the vessels. Flaw depth, including the fatigue crack extension, was nominally 0.040 in. in one vessel and 0.060 in. in the other. The vessels were subjected to a net membrane wall stress of ~69,000 psi by pressurizing with oil at 10,000 psig inside and holding the hydrogen at 5200 psig on the outside, all being contained by another pressure vessel. The test condition was 30 pressurization cycles with 3-h holds, or a total time of 90 h at maximum stress.

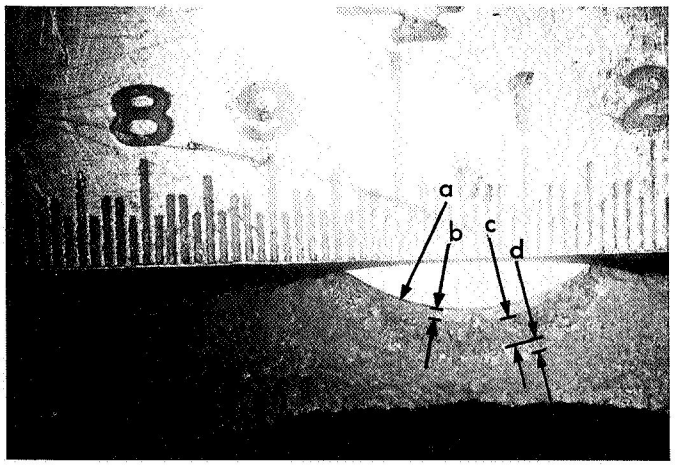

Fig. 40. Fracture section of Inconel 718 vessel wall showing: (a) initial EDM notch, (b) cyclic fatigue crack extension, (c) flaw growth, (d) cyclic marking

Results. The vessel containing the nominal 0.060-in. flaw leaked in about 4 h or during the second hold cycle; the second vessel with the nominal 0.040-in. flaw did not leak after 90 h. After cyclic loading to mark the flaw, the second vessel was burst and examined in order to determine flaw growth. The photomacrograph of Fig. 40 shows sustained flaw growth of ~0.025 in. in 90 h for this vessel. Data points for both vessels appear in Fig. 38 as the open triangle (first vessel) and the closed triangle (second vessel). It is evident that the vessel data corroborate the low-threshold flaw-size data of the as-received but heat-treated forging of a different heat number.

d. Discussion. It will be evident in studying Fig. 38 that a successful hydrostatic proof test at equivalent stresses approaching the yield stress indicates that a flaw may exist which did not quite reach through the wall thickness. On the other hand, in the high-pressure hydrogen environment of 5200 psig at room temperature, equivalent to ~69,000-psi membrane stress (see triangular data points), a flaw size of $a/Q = 0.030$ in. could be expected to grow through to leak in less than 100 h. The flaw shape parameter Q for this work lies between 1.2 and 1.4. If the average of 1.3 is taken, $a/1.3 \simeq 0.030$ in. or $a \simeq 0.039$ in. The threshold stress intensity for weld metal is lower, ~20 $(\text{klb/in.}^2)\sqrt{\text{in.}}$, than that for parent or base metal. In the Boeing experience, searching for tightly closed cracks of this size (such as may exist in a weld-heat-affected zone) by non-destructive testing methods gives no assurance that *all* have been found. Boeing, therefore, recommended that the existing vessels not be used on the *Mariner* Mars 1969 spacecraft. However, another material was recommended and Boeing is currently manufacturing the new vessels under a contract with the University of California at Berkeley.

References

1. *Fracture Toughness Testing and Its Applications,* STP 381, Symposium of the American Society for Testing Materials, Chicago, Ill., June 21–26, 1964.
2. Tiffany, C. F., Lorenz, P. M., and Shaw, R. C., *Extended Loading of Cryogenic Tanks,* Report NASA CR-72252. Prepared for NASA under contract NAS 3-6290, The Boeing Company, Seattle, Wash., Mar. 1967.

G. Environmental Sciences

1. Six-Channel Spectrum Averager for Environmental Acoustic Testing

a. Introduction. To meet the *Mariner* Mars 1969 proof-test-model type-approval acoustic test requirements, a new means was required to obtain and shape the specified acoustic spectrum. The spacecraft was to be subjected to reverberant-field wide-band-spaced acoustic noise whose spectral levels within each ⅓ octave band would be determined by a six-microphone average of the specified spectrum. An averager was constructed to calculate the strict rms average ⅓ octave spectrum bands in real and near-real time. The average ⅓ octave spectrum was then manually adjusted to meet the required acoustic test specification.

b. Functional description. Special acoustic microphones pick up the high-intensity acoustic noise from within the reverberation acoustic chamber (Fig. 41). The microphone signals feed into cathode-follower-type amplifiers. The outputs of the amplifiers are sequentially sampled, one at a time, by a switching commutator. The output of the switching commutator at any given time represents a time sample of the total broad-band rms noise spectrum picked up by one of the six microphones. The microphone sample time (commutator dwell time) can be adjusted within the encoder/decoder. Each microphone signal is sequentially sampled for the same length of time. After the last microphone signal has been sampled, the process is begun again, either automatically or manually, by resetting a switch located on the front panel of the encoder/decoder.

The time signal from the switching commutator goes to a spectrometer, an electronic device used to break up a broad-band frequency spectrum into several narrow frequency bands whose center frequencies are listed in Table 3. The spectrometer is of the ⅓ octave filter type and is external to the averager. The ac signal output from the spectrometer is dependent on the particular ⅓ octave filter selected and on the ⅓ octave frequency content of the total broad-band spectrum being analyzed. The

Table 3. Acoustic test specifications

⅓ octave band center frequency, Hz	Sound pressure level[a] in ⅓ octave bands, dB	Tolerance band, dB	
80	130.5	+4	−4
100	136.0	+3	−3
125	136.0	+3	−3
160	136.0	+3	−3
200	136.0	+3	−3
250	141.0	+3	−3
315	141.0	+3	−3
400	141.0	+3	−3
500	138.0	+3	−3
630	135.0	+3	−3
800	131.5	+3	−4
1000	128.5	+3	−4
1250	125.5	+3	−4
1600	122.0	+5	−4
2000	119.0	+6	−4
2500	116.0	+6	−5
3150	113.0	+6	−5
4000	109.5	+6	−5
5000	106.5	+6	−5
6300	103.0	+6	−5
8000	100.0	+6	−6
10000	97.0	+6	−6

[a]Decibel reference: 2×10^{-4} μbar.

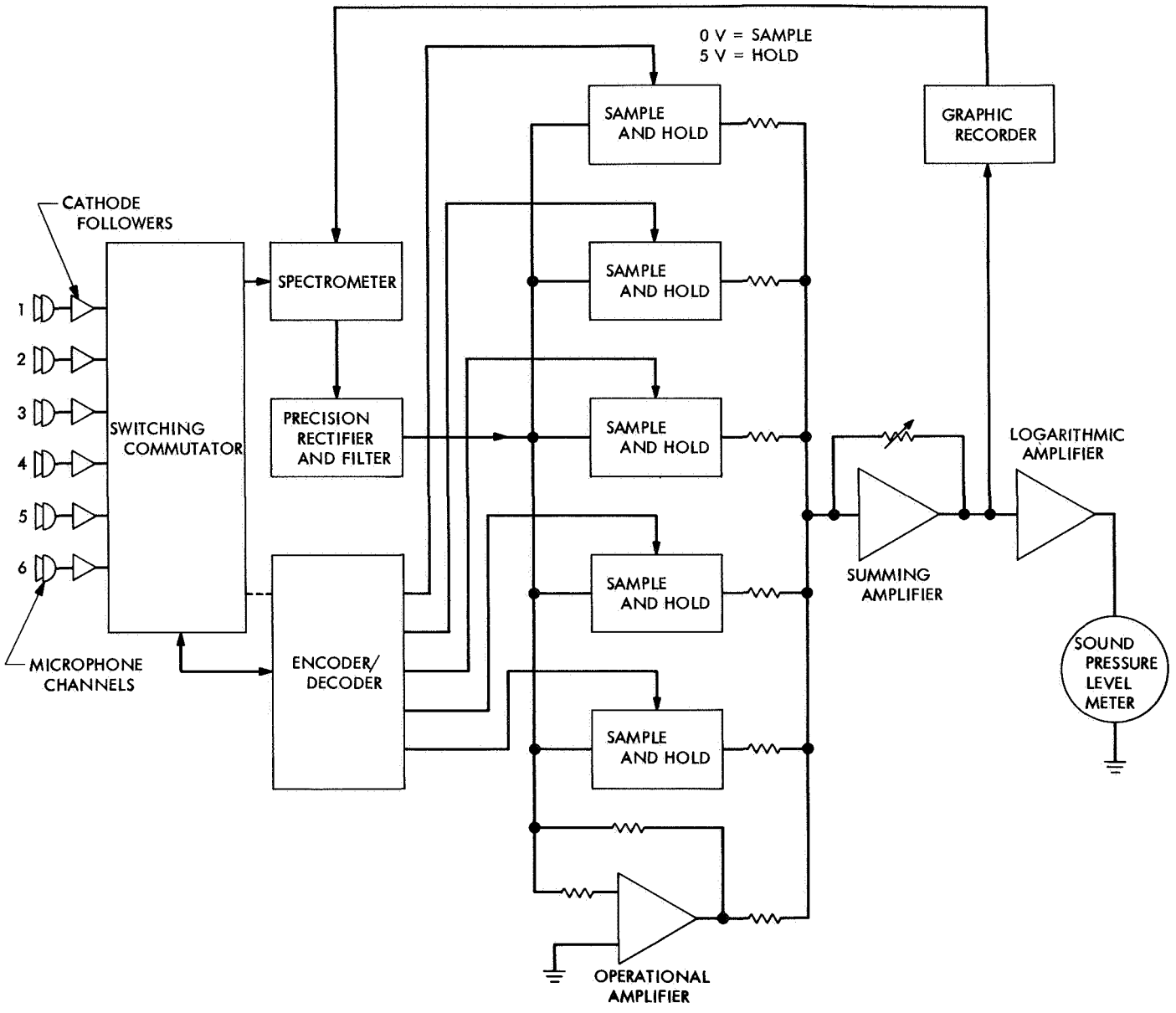

Fig. 41. Six-channel acoustic signal averager

spectrometer can be programmed to automatically switch through each ⅓ octave filter, one at a time, from the low-frequency spectrum end to the high-frequency spectrum end. The spectrometer switching is controlled by the encoder/decoder.

Each microphone signal is sequentially gated through the same filter of the spectrometer to a precision rectifier and smoothing filter (low-pass filter). The dc signals are then stored in sample-and-hold circuits associated with each microphone channel.

Initially, for example, the channel 1 microphone signal is gated through to the spectrometer, which has been preset to the first ⅓ octave filter. The spectrometer output represents an analysis of a narrow-band portion of the total frequency spectrum sensed by microphone 1. This ac signal is converted to dc and stored in the first sample-and-hold circuit, at which time microphone 1 is automatically disconnected from the spectrometer and microphone 2 is gated through to the spectrometer. Next, the signal from the second microphone is analyzed for the same ⅓ octave band and this signal is converted to

dc and stored in the second sample-and-hold circuit. The process is continued for each microphone, the encoder/decoder giving the switching commands to the switching commutator and the sample-and-hold circuits. The last channel requires only an operational amplifier, since, shortly after the last microphone channel is connected to the spectrometer, a command is given by the encoder/decoder to sum all the dc signals in a summing amplifier.

The summing amplifier sums 1/6 of the individual dc signals that represent the energy content for a particular 1/3 octave band of frequencies. It is necessary to use 1/6 of the signals to stay within the permissible maximum differential-input common-mode voltage range of the summing amplifier.

The output of the summing amplifier represents the average rms spectrum density (sound pressure level) picked up by the six microphones for a 1/3 octave frequency band. This value is plotted by a recorder in a coordinate system whose ordinate axis is rms sound pressure level in decibels, and whose abscissa is log frequency. The recorder is synchronized to the master clock of the encoder/decoder.

After a mark is made on the recorder paper, the encoder/decoder commands the spectrometer to switch to the next 1/3 octave filter and the process starts over. Each 1/3 octave analysis and averaging takes approximately 5 s. Degrees of freedom and statistical errors are listed in Table 4.

Table 4. Acoustic averager degrees of freedom, N, for 0.625-s sampling time

1/3 octave band center frequency, Hz	Bandwidth, BW, Hz	$N = 2BW \times (0.625)$	Approximate error, $\% = (N/2)^{-1/2} \times 100$
100	23	29	26.0
125	29	36	24.0
160	37	46	21.0
200	46	58	19.0
250	58	72	17.0
315	73	91	15.0
400	92	115	13.2
500	116	145	11.8
630	146	182	10.4
800	183	229	9.4
1000	230	288	8.3
1250	290	362	7.4
1600	370	462	6.6
2000	460	575	5.9
2500	580	635	5.2
3150	730	913	4.7

A special meter, calibrated in decibels, indicates the average rms sound pressure level for that 1/3 octave band. The meter has a 30-dB range, with 0 dB representing the total overall rms sound pressure level. The meter is driven by a logarithmic amplifier to obtain decibel units of sound pressure level.

Figure 42 shows the encoder/decoder electronics and Fig. 43 illustrates the sample-and-hold electronics, summing amplifier, and logarithmic amplifier.

c. Test description and results. Figure 44 shows the *Mariner* Mars 1969 spacecraft inside the acoustic chamber. Generally, if the test specimen is less than one-tenth of the inside dimensions of a properly constructed reverberation chamber, the generated acoustic field anywhere within the chamber will be quite uniform. However, in the case of an extremely large structure, the uniformity of the acoustic field is questionable. For this reason, the acoustic test requirement stipulated a noise spectrum whose spectral levels within each 1/3 octave band would be determined by a six-microphone average of the specified spectrum.

Table 3 lists the spacecraft acoustic test requirement, expressed in sound pressure levels per 1/3 octave center frequencies. Table 5 shows the test results in tabular form. The analog average of channels 1 through 6 was obtained by the averager and compares quite closely to the result from a digital computer analysis performed on the raw data recorded during the test.

Figure 45 is a 1/3 octave analog plot from the averager. The dashed lines on this plot represent the tolerances allowed for the test. The solid straight line would be the ideal spectrum required to meet the test specification. Of primary concern for this acoustic test was the frequency range from 100 to about 800 Hz.

Table 5. Acoustic test results

Microphone channel	rms sound pressure level, dB	
	Analog	Digital
1	149	149.79
2	149	149.40
3	148	146.97
4	149	149.69
5	150	151.16
6	149	149.75
Average	149	149.61

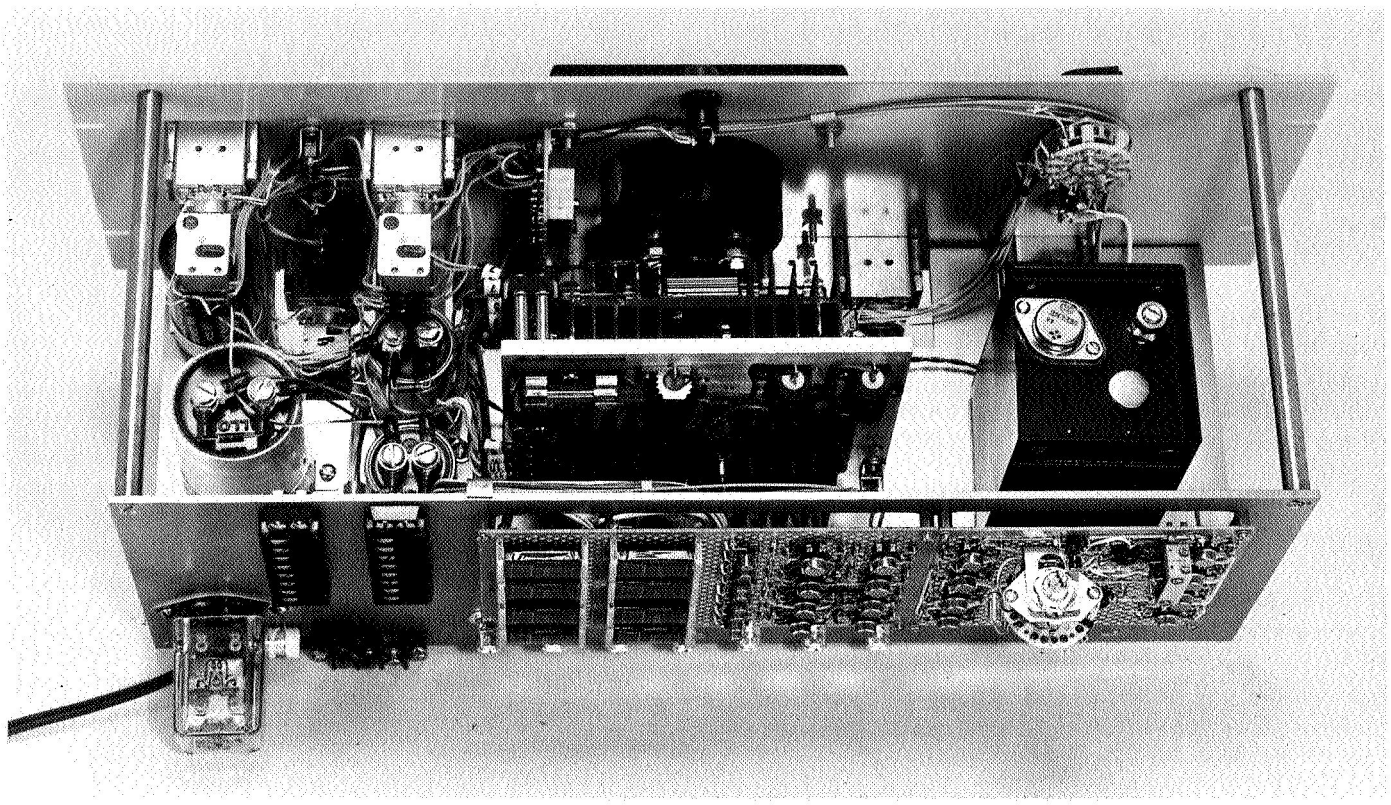

Fig. 42. Encoder/decoder electronics

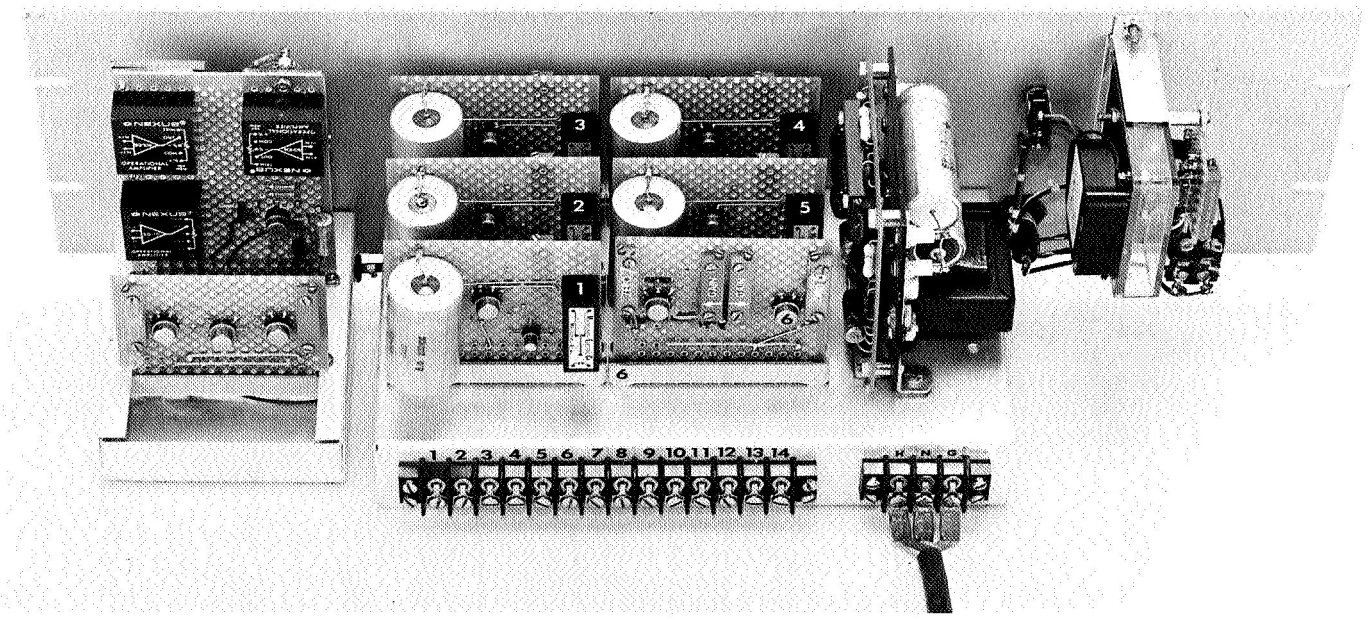

Fig. 43. Acoustic averager electronics

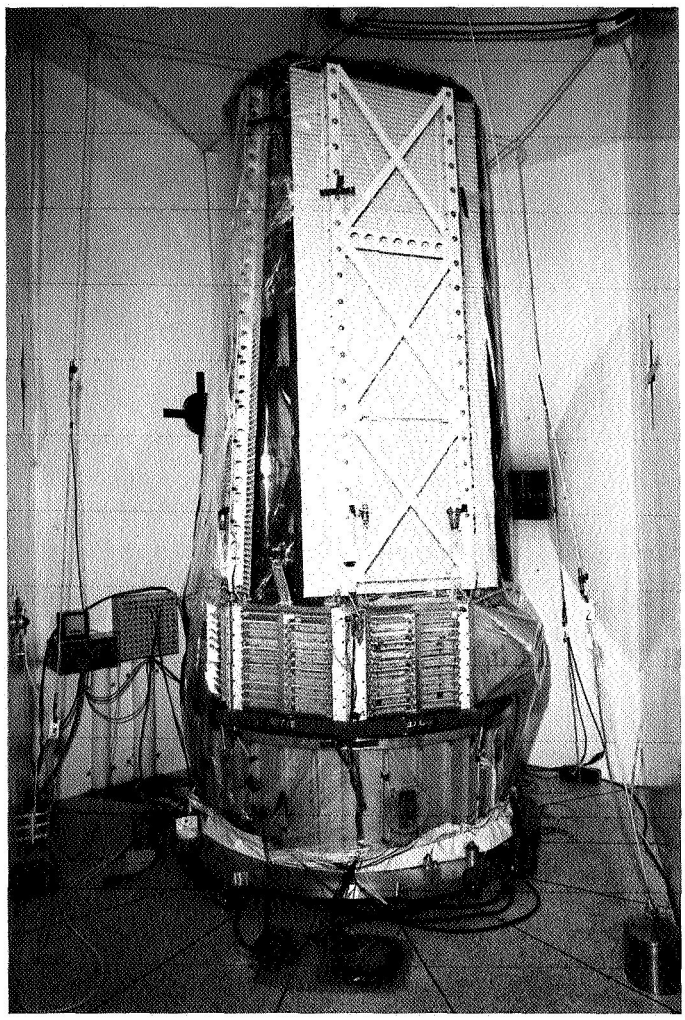

Fig. 44. *Mariner* Mars 1969 spacecraft in acoustic reverberation chamber

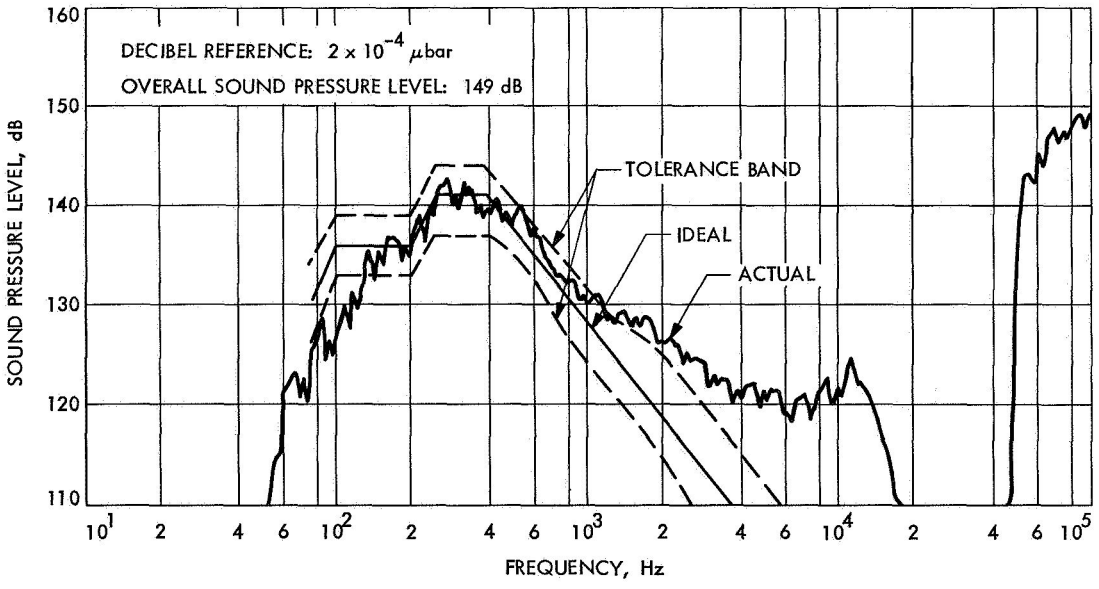

Fig. 45. One-third octave sound pressure level analog plot

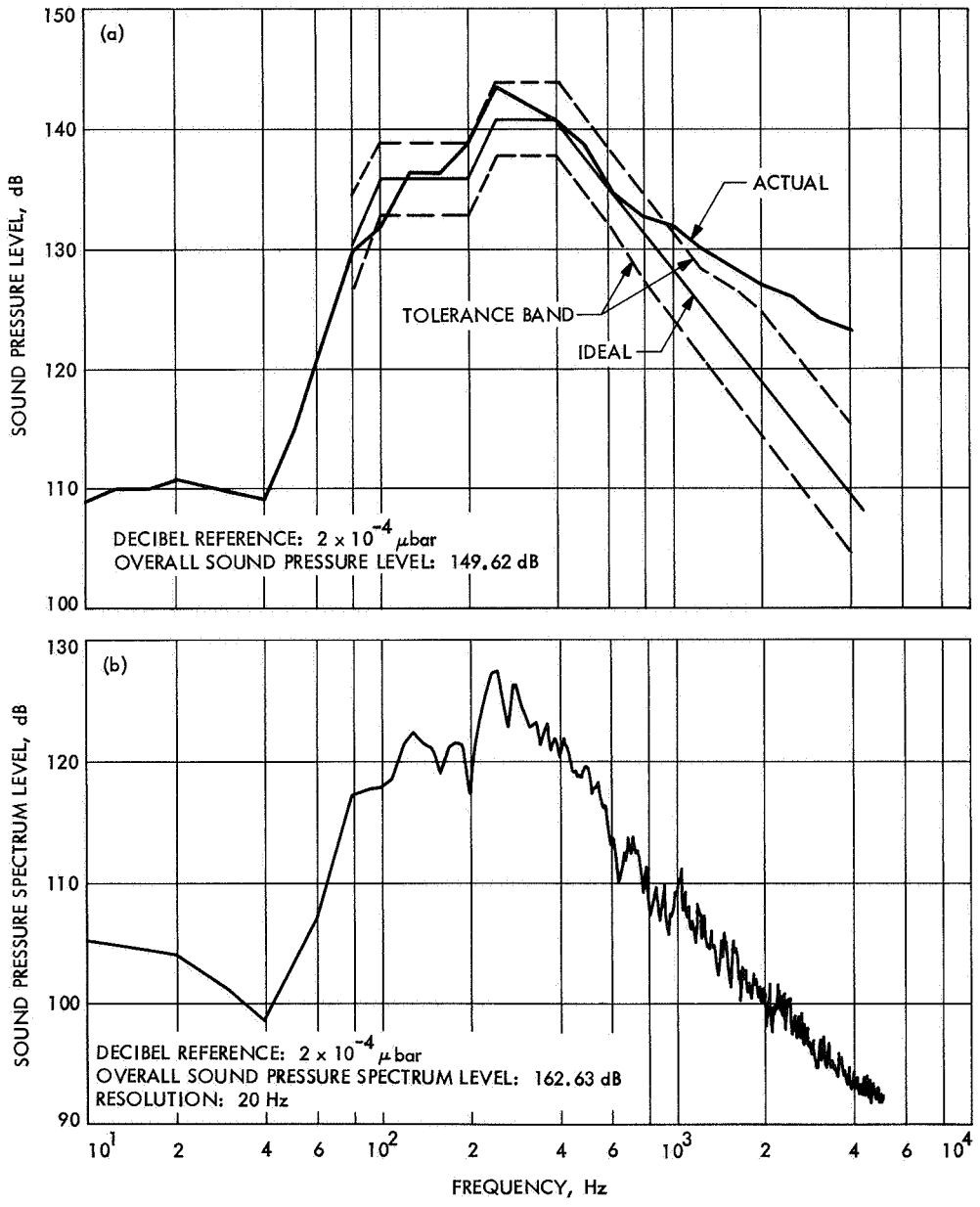

Fig. 46. Digital plots: (a) ⅓ octave sound pressure level, (b) constant bandwidth sound pressure spectrum level

Figure 46a is a digital ⅓ octave analysis similar to the analog analysis of Fig. 45. The overall sound pressure levels of both types of analyses are almost identical. Again, the dashed lines represent the tolerance band and the solid thin line represents the ideal spectrum.

Figure 46b displays the results of the acoustic test employing a constant bandwidth (rather than ⅓ octave) analysis of frequency versus sound pressure spectrum level.

The accuracy of the averager is a function of the analog sample rate (dwell time), precision rectifier linearity, sample-and-hold circuit drift rate and stability and operational amplifier characteristics. The precision rectifier dc response for constant-amplitude ac sine wave input was very nearly linear (within 0.01 Vdc) over a frequency range of 10–2000 Hz. Figure 47 shows the negligible drift characteristics of the sample-and-hold circuits. The operational amplifier errors are insignificant. Thus, the acoustic test results indicate that averager provides a strict spectrum average that is as accurate as the digital analysis spectrum average.

d. Other applications. The design of the averager can be extended to include many more input channels. Besides acoustic-type environmental tests, this type of averager be used for multipoint-control vibration tests and other types of probabilistic and deterministic signal averaging.

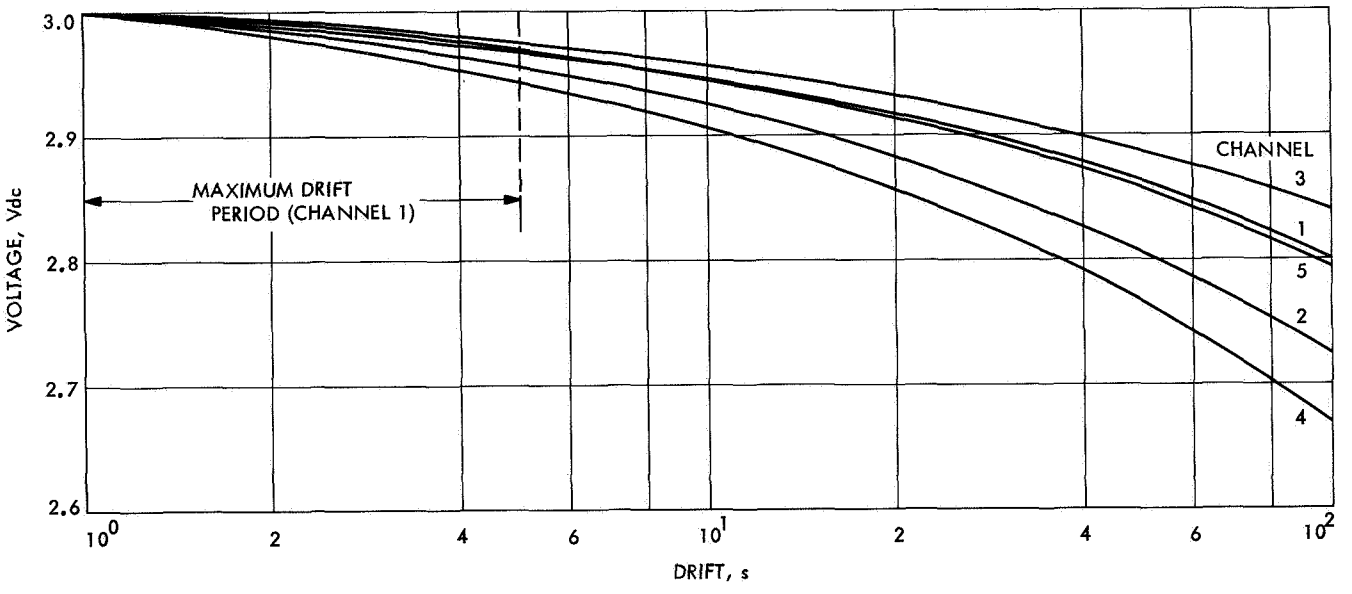

Fig. 47. Drift characteristics of sample-and-hold circuits

II. Advanced Planetary Missions Technology

ADVANCED STUDIES

A. Introduction

An Advanced Planetary Missions Technology Program has been established under the cognizance of the JPL Assistant Laboratory Director for Flight Projects. Mission and system studies and scientific and engineering work are being performed to support planning and advance the state-of-the-art applicable to future planetary missions. The current technological activities are reported in this chapter of the SPS, Vol. I.

B. Guidance and Control

1. Power Subsystems

a. Introduction. Future planetary mission studies related to operation of a scientific package on the Mars surface indicated a need for quantitative and qualitative information on power subsystems that could provide power to the system for an extended period of time. The long life and planetary environmental conditions limit the selection of sources of available power. The sources available that appear capable of providing the required power are solar cells, radioisotope thermoelectric generators (RTG), and batteries.

A comparison study was made of these power sources to determine the operating characteristics and performance capabilities of each while operating within the Mars surface environment. Using a computer program which was developed specifically to determine the optimum sizes of the power sources, the study indicated that a hybrid power subsystem that used a solar array and an RTG with a small sterilizable battery not only achieved the maximum return of scientific data but was also the lightest weight configuration. Table 1 summarizes the characteristics of the power subsystems studied for a softlander (Ref. 1).

To identify the state of the art of the power sources used in the study, work being investigated in JPL research and advanced development programs is being utilized. Studies relative to science subsystems interference from the radiation field produced by the RTG or a radioisotope heater for thermal control are being extended to the lander science instruments. In addition, tasks that were performed to determine the ability of solar cells to survive sterilization and high-level-impact loads were evaluated. A contract to study planetary arrays (SPS 37-49, Vol. III, pp. 112–114) has been modified to meet the needs of the Advanced Planetary Missions Technology (APMT) requirements. This effort will provide a definition of environmental effects on a solar array, test data to verify effects such as sterilization on the electrical and mechanical properties of cells, and specific structural designs of arrays to meet the requirements defined in APMT studies.

Table 1. Comparison of power subsystems characteristics

Characteristic	Power subsystem		
	Oriented solar panel/ battery[a]	RTG/ battery[a,c]	Oriented solar panel/ RTG/ battery[a,c]
RTG power output, W	—	65	37
RTG weight, lb	—	81	46.5
Solar panel area, ft²	50	—	30
Solar panel average power, W	220	—	104
Solar panel weight (total)[b], lb	81	—	47
Battery energy (required), W-h	450	295	57
Battery energy (total), W-h	1400	740	142
Battery weight (Ag–Zn sterilized), lb	70	37	7
Conversion and distribution weight, lb	41.5	37	41.8
Total subsystem weight, lb	192.5	155	142.3
Percent of total vehicle weight (900 lb), %	22	17.2	15.9

[a]Combination sized for one complete diurnal cycle operation assuming no degradation due to clouds, dust, wind, etc.

[b]1.3 lb/ft² plus motor and mechanism.

[c]80-lb credit for thermal control elimination of isotopic heaters and insulation not included.

b. Mission study. A 1973 Mars mission using a survivable hardlander was investigated by APMT. The design concept of a *Mariner* 1971 spacecraft orbiter was modified to accommodate an 1100-lb capsule/lander. The mission plan described the release of the capsule/lander at a predetermined altitude from the surface of the planet. As the capsule speed approaches transonic levels, the lander is extracted from the capsule and descends to the planet surface on a parachute. The lander is expected to impact the surface at a terminal velocity of 115 ft/s.

c. Solar panel performance. Because a severe weight and packaging problem existed with a postulated 1973 Mars hardlander, a maximum of 24 ft² of array area was allocated for this mission. A conceptual configuration of a five-disc impactable solar panel installed on the hardlander concept is shown in Fig. 1.

A preliminary solar panel performance analysis was conducted for a December 15, 1973 landing at zero latitude and slope and at 20°S latitude on a 20-deg slope. The panel performance factors assumed for the preliminary analysis are consistent with the state of the art of panel manufacturing. An 8-mil N/P 2-Ω-cm silicon solar cell was used for the study.

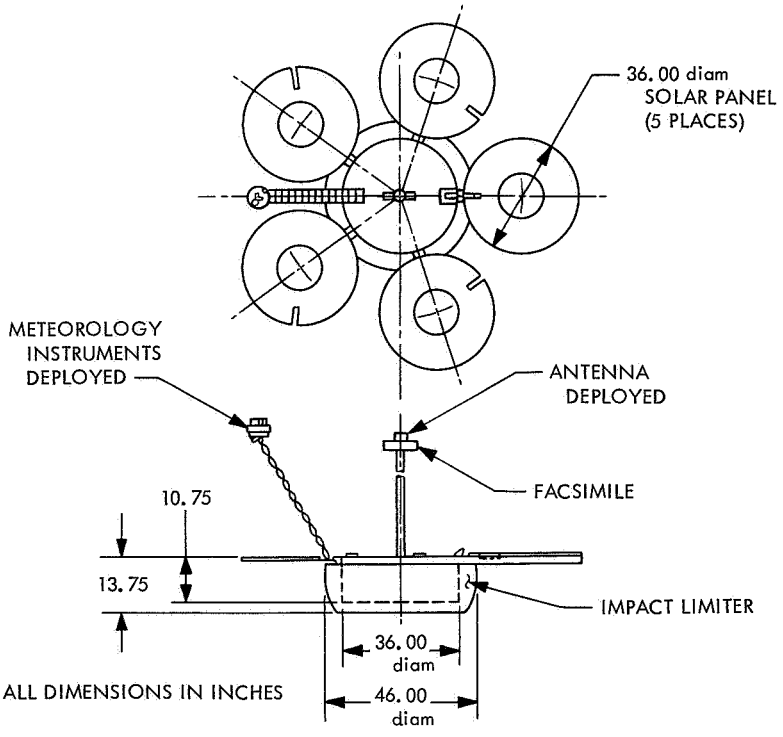

Fig. 1. Impactable solar panel configuration for a 1973 Mars survivable hardlander

Using modified *Voyager* environmental models VM-8 and VM-10, a thermal analysis was performed to determine the average operational temperatures of the array. The results of this analysis, combined with panel available power per time of Martian day, are shown in Fig. 2 for zero latitude and slope. Panel output of the VM-10

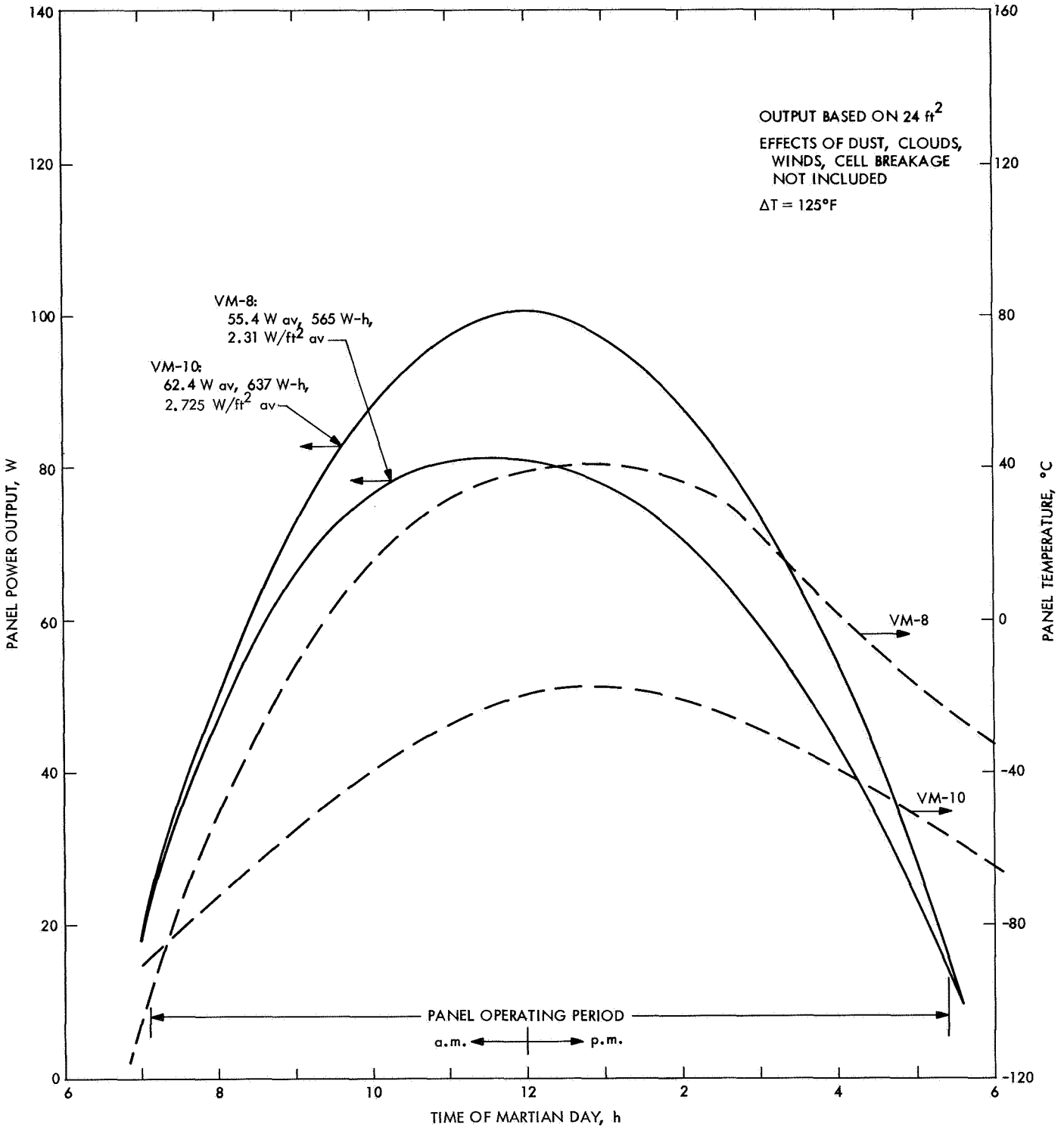

Fig. 2. Impact solar panel available power and panel temperature vs time of Martian day (December 15, 1973; 0° lat; 0 slope; 1.5 AU; 62.5 mW/cm²)

is approximately 17% greater than the VM-8 output for the atmospheric/surface temperature differential of 125°F. Panel power output was also determined for atmospheric/surface temperature differentials of 63 and 0°F. The results are plotted and compared with a desired mission power profile in Fig. 3. The range of power variation for the VM-10 is 11%. However, there is an approximately 4% difference between the VM-8 with $\Delta T = 125°C$ and the VM-10 with $\Delta T = 0°F$. Further analysis of Fig. 3 shows that the available solar panel output in all cases will restrict transmission time. In addition, a change in duty cycles, including a reduction in peak loads, would be required. During the transmission period, it is assumed that battery charging is not interrupted.

The preliminary performance of the array compared to power required per time of day for a 20°S latitude landing on a 20-deg slope showed that the average VM-10 power is reduced by approximately 5% for each of the three atmospheric/surface temperature differentials. At this latitude and slope, the duty cycle must be revised accordingly irrespective of the fact that there is an increase in the communication window to earth. Estimated total weight of the panel configuration including hinges, structure, substrate, adhesive, cells, etc., stressed for a high-impact survivable landing, is approximately 60 lb.

d. Battery. The power subsystem battery required for a 1973 Mars hardlander mission must be a high-impact

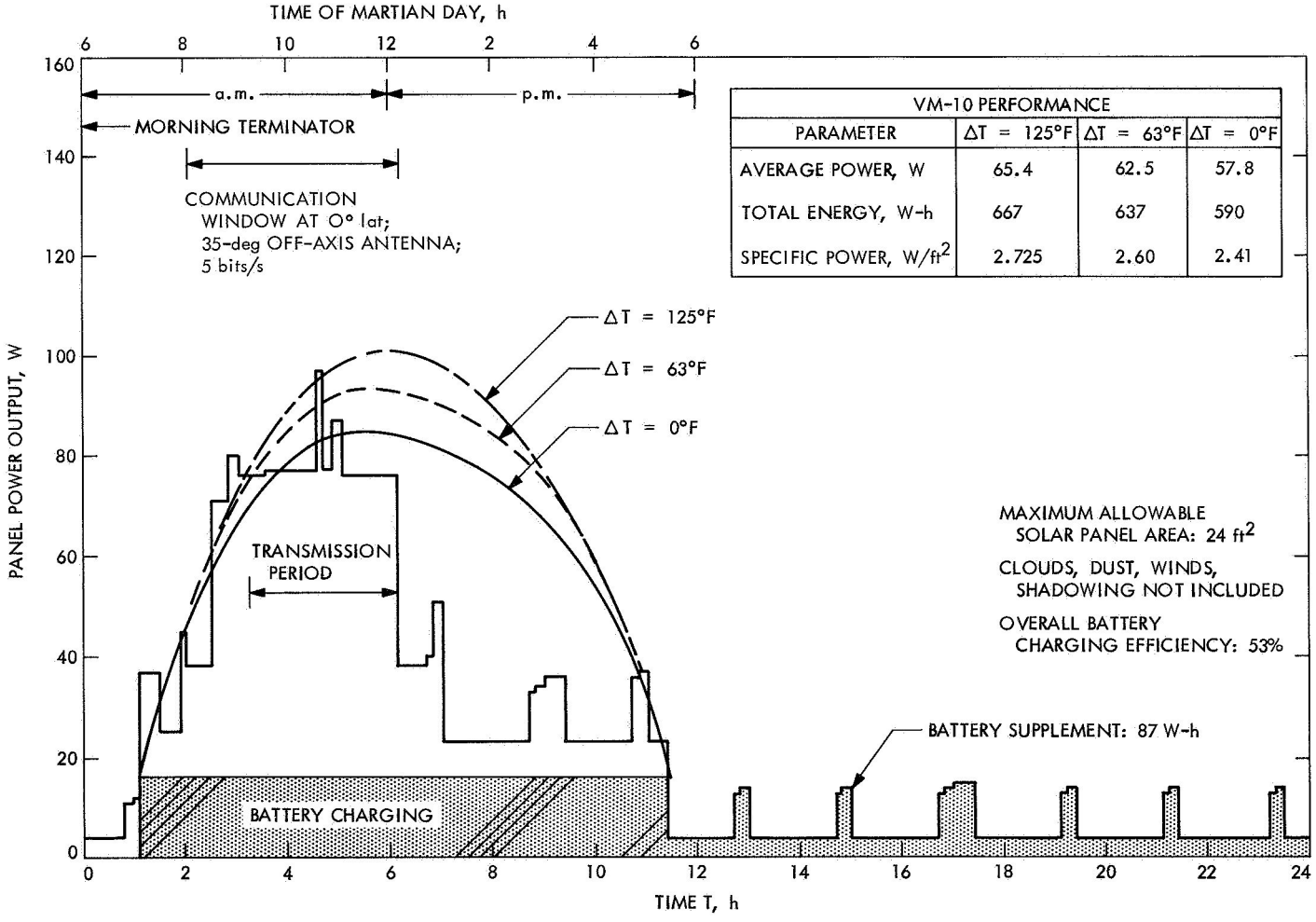

Fig. 3. Comparison of VM-10 fixed solar panel output, at various atmospheric/surface temperature differentials, with 1973 Mars mission power profile (*Titan* 3C; survivable hardlander; December 15, 1973; 0° lat; 0 slope; 1.5 AU; 62.5 mW/cm²)

sterilized secondary silver–zinc type. A primary, impactable, sterilizable silver–zinc battery will provide a specific energy density rating of 10–15 W-h/lb per cell less case weight. The specific energy density of a high-impact sterilized secondary silver–zinc battery was assumed to be 7.3 W-h/lb for the 1973 mission design study, which requires an energy of 217 W-h. Included in the total energy requirements are a 50% depth-of-discharge and a 50% actual-energy requirement for uncertainties of payload characteristics and sterilized batteries. With these assumptions, the total battery weight is 30 lb.

e. Power conditioning. The recent success of the JPL-developed capsule system advanced development[1] hardlander has provided sufficient evidence that sterilized high-impact electronic components are within the present state of the art. The power subsystem for a 1973 Mars hardlander mission requires a battery charger. Estimated total weight of the power conditioning established for this mission is approximately 8 lb.

Reference

1. Swerdling, M., "Power System Configurations for Extended Science Missions on Mars," Paper 689085, presented at the Intersociety Energy Conversion Conference, Boulder, Colo., Aug. 1968.

C. Environmental Sciences

1. High-Velocity Shock Tester

a. Design and development. The high-velocity shock test machine is designed to provide repeatable shock accelerations in the range of 2,000 to 25,000 g with impact velocities of 200 ft/s, for testing at the failure levels of spacecraft components or specimens. Test shocks are produced by impacting a hard steel cylindrical tool against a plastically deformable copper target. The tool velocity at impact determines the rise time and duration of the shock pulse. The diameter of the tool determines the level of acceleration.

The machine consists of a carriage-mounted tool that rides horizontally on 18-ft-long guide rails toward the impact point. Figure 4 shows the overall view. The carriage is powered by two cables of bungee cord. Various diameters, such as ½-in., ¾-in., and 1-in., are employed, depending on specimen weight and velocity requirements. The cord is anchored at one end to a block 18 ft behind the impact block. The cord passes through the impact block and is attached at the other end to the carriage. A windup cable powered by an electric winch pulls the carriage back against the tension of the bungee spring. An air-powered remote-control mechanism releases the carriage. The test specimen rides on the carriage to impact. The target, made of annealed copper and mounted in the impact block, is expendable and is replaced after each test.

The tester was developed about 6 yr ago at JPL, and about 1 yr ago a duplicate machine was built. Since that time, improvements have been made to the tester, resulting in more efficient and effective operation.

One improvement made to the tester was the method of releasing the carriage. In the original design, a cutting tool was electrically actuated to cut the windup cable and release the carriage. This method had more than one disadvantage. After each test, the windup cable had to be redressed. A special threaded stud had to be replaced on the cut end of the cable with a swagging jig. Windup cable was wasted and time was lost for each test. The cutting tool also had to be maintained in sharp and honed condition.

This method has been replaced by a remote-operated quick-release arrangement that uncouples the carriage from the windup cable. Figure 5 depicts the release device. Compressed air pushes a piston, which offsets the tension of a return spring and shifts the release pin within the male member of an Avdel Ball-Lok quick-release coupling mechanism. Shifting of the release pin allows latching balls to retract and unlatch the male member from its female counterpart. This releases the carriage to be pulled to impact by the bungee spring.

Longitudinal waves propagate along the bungee spring as the carriage moves toward impact. These waves have a rather large transverse displacement which causes the carriage to move away from the copper block after impact and rebound back into the copper block. This causes additional shocks to the test specimen. To minimize this problem, the spring must be under tension throughout the carriage travel. Slack near the point of impact can result in cord interference between the moving carriage and the impact block.

In the original design, the bungee spring is installed on the tester and then stretched 18 in., using the movable pulley arrangement shown in Fig. 6. This method has limitations. For example, the various diameter springs used on the machine have optimum pretension settings.

[1]*Capsule System Advanced Development Program Report,* July 15, 1968 (JPL internal document).

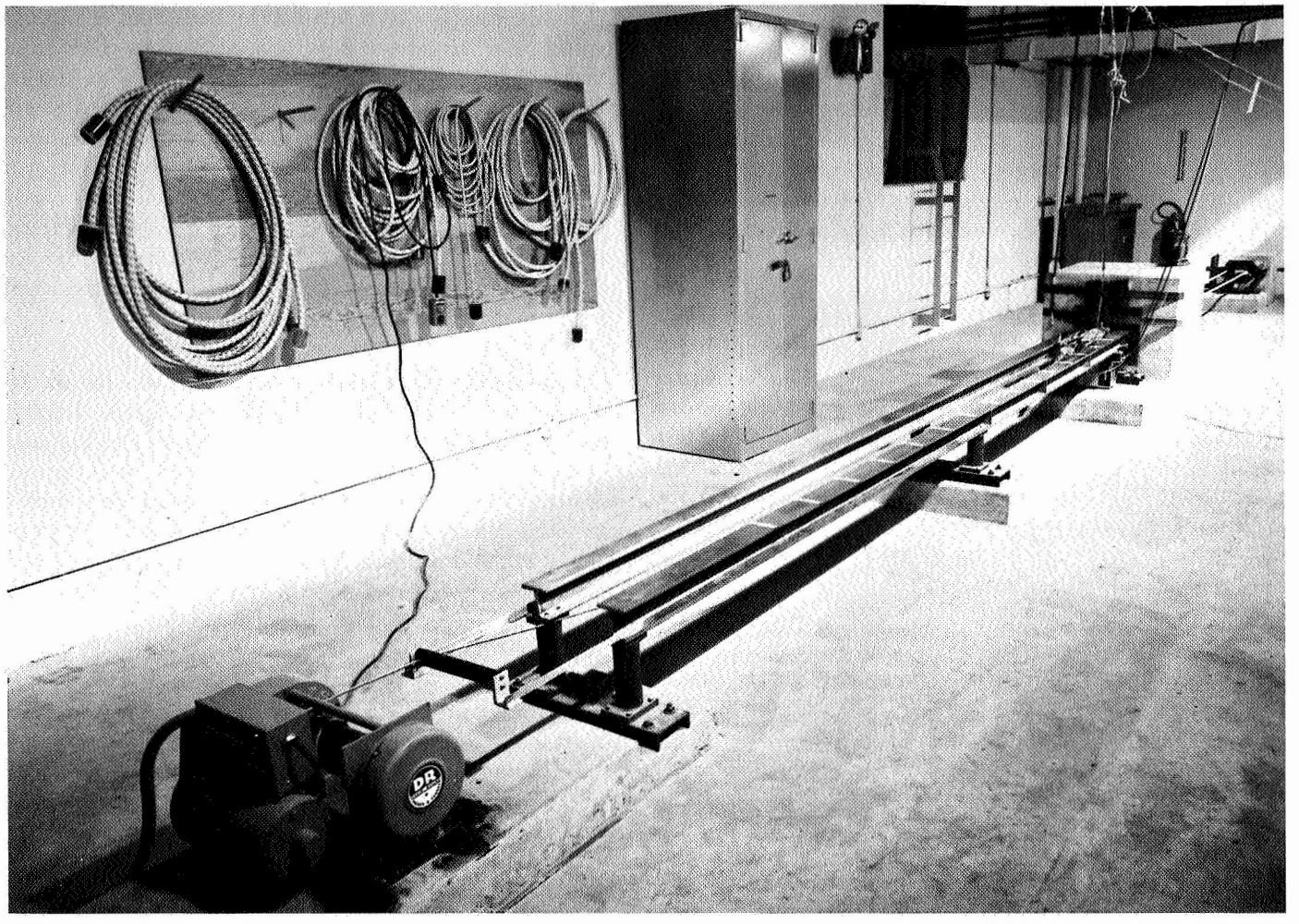

Fig. 4. Overall view of shock tester

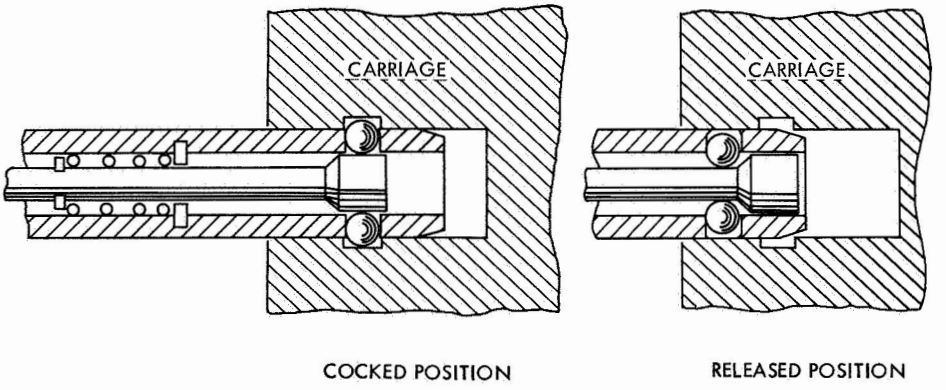

Fig. 5. Cutaway view of carriage release mechanism

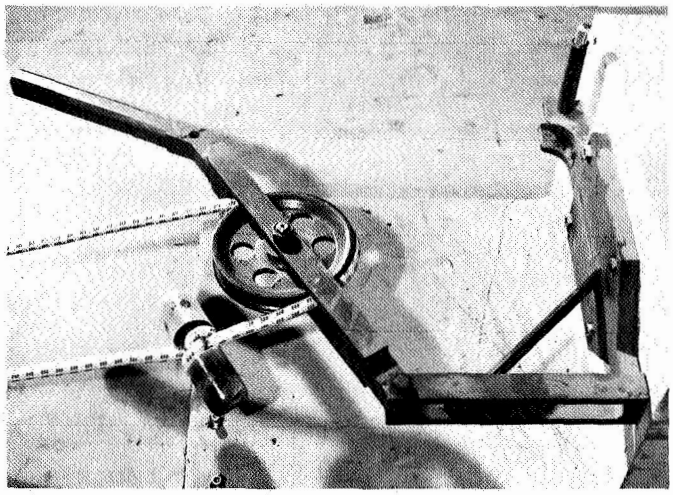

Fig. 6. Original pretension mechanism in relaxed position

Furthermore, since the same spring is used for several tests, its pretension requirements change because of stretch. The present device cannot accommodate the variations in pretension requirements. A new mechanism under development is depicted in Fig. 7. Several settings are available, permitting a total adjustment length of 30 in.

b. Instrumentation. Three methods have been employed to determine the acceleration level of the shock pulse. The first method assumes that the pulse is rectangular. A calculation of the acceleration level is made by recording the impact velocity V with a pair of photocells and a digital counter, then measuring the depth of penetration d into the copper impact block. Acceleration then becomes $A = V^2/2d$. Since a rectangular pulse has the smallest peak value of any pulse for a given depth of penetration, this value will always be a conservative estimate of the acceleration level.

The second method employs piezoelectric shock accelerometers. The accelerometer output is amplified and placed on a memoscope. The output is simultaneously recorded on magnetic tape for playing back through different bandpass filters for analysis.

The third method uses a strain gage to measure the decelerating force during impact. A full bridge is mounted on the nose of the impact tool. The bridge is dc-excited and its output is amplified, placed on a memoscope, and recorded on magnetic tape. Calibration is performed by static loading. Since this method determines the force level by monitoring strains, not acceleration, the record

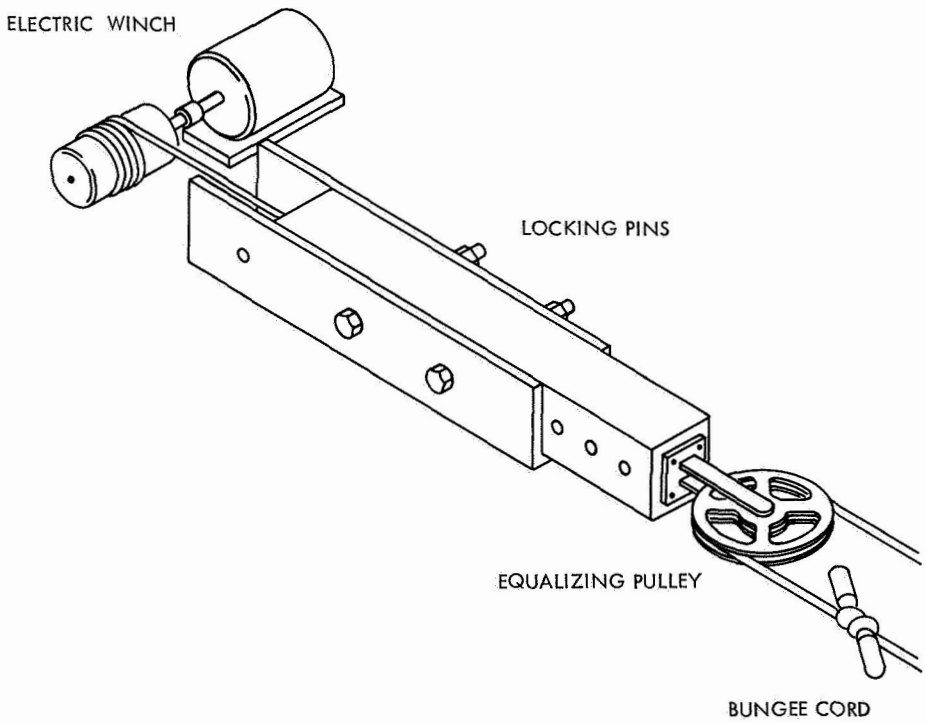

Fig. 7. Redesigned pretension mechanism

is relatively ring-free and more accurately read. The acceleration level is obtained by dividing the force by the carriage mass.

Although it is now possible to obtain good measurement of acceleration levels considerably in excess of 10,000 g, very few shock tests have been performed at these levels using strain gages. Comparison of the strain-gage method and the accelerometer method, however, indicates force readings are more desirable for verifying acceleration levels. The strain-gage method provides a better quality wave shape.

Reliable measurement of the highest acceleration levels is difficult with any of these three methods. Additional work remains to be completed to achieve agreement between the force and accelerometer techniques.

D. Propulsion

1. Thermal Sterilization of Mild Detonating Cord Used to Fracture Capsule Sterilization Canister Separation Joint

The data obtained from the separation joint tests performed by Lockheed Missiles and Space Company (SPS 37-49, Vol. III, pp. 248, 249) were evaluated and resulted in three conclusions:

(1) There was no discernible contamination caused by firing the mild detonating cord (MDC).

(2) Velocities imparted to the test sections as they were fractured and separated averaged approximately 6 ft/s. This is considered satisfactory.

(3) At least one sample of three of the four kinds of MDC tested (HMX, HNS, and Dipam) showed definite degradation of separation performance when exposed to one thermal sterilization cycle. The only sample of NONA was not degraded by the sterilization cycle, but the energy released by it was much lower than any of the other explosives. Table 2 shows a comparison of separation velocity before and after one thermal sterilization cycle of 64 h.

Since the high-temperature explosive material used in the cords should theoretically not be degraded by temperatures below 260°C, the Lockheed results indicated the desirability of further investigation in the area of thermal sterilization of MDC. It was desirable to determine if the degradation which had occurred was due to high temperatures, temperature cycling, or some other cause.

Table 2. Separation velocity of fractured test sections

Explosive material	Load, gr/ft	Sterilization time at 135°C, h	Test panel weight, lb	Panel separation velocity, ft/s
HNS	3.00	64	1.05	7.15
HNS	3.00	none	1.04	7.80
Dipam	2.5	64	1.03	4.90
Dipam	2.5	none	1.01	7.05
HMX	2.5	64	1.05	3.1
HMX	2.5	none	1.04	3.7
NONA	2.5	64	1.03	2.1
NONA	2.5	none	1.02	2.1

Tests of similar MDC made by the Naval Ordnance Laboratory at White Oak, Maryland, had shown that the explosives could be seriously degraded by chemical vapors and that the amines were especially bad. Since amines are used as hardeners for epoxy resins, it is important to keep the cords away from epoxy curing ovens and other sources of chemical vapors.

To attempt to identify the failure mechanism which had resulted in the degradation of the MDC, a test program was initiated at JPL. To prevent possible contamination, containers were fabricated from ¼-in.-diameter new refrigeration grade copper tubing that had been cleaned inside and sealed at both ends. Three pieces of the same kind of MDC, each 15 in. long, were enclosed in each piece of copper tubing. One container of each kind of MDC to be tested[2] was set aside and served as a control. The remaining containers were placed in a previously cleaned oven and heated to 135°C for 39 ±3 h. After this, the containers and oven were cooled to ambient temperature. One container of each kind of MDC was then removed from the oven, marked, and set aside. This sequence of heating, cooling, and removing samples from the oven was continued through six cycles. At the end of this series, all of the samples had been removed and were ready to be fired.

Firing to measure the propagation rate of the cords was accomplished in the following manner. Two notches were made in the cover of each piece of MDC, 12 in. apart. When ready for firing, one piece was suspended in a steel fixture in a vertical position. A blasting cap

[2]At the time these tests were conducted, no MDC loaded with HMX was available for testing.

was attached to the top end to act as the initiator. One turn of small enamel insulated wire was wrapped around the MDC in each of the two notches. The two wires and the cover of the MDC formed the start and stop circuits of a Hewlett-Packard 1-megacycle counter. When the initiator was fired, the MDC was ignited and burned down to the start wire. The fire through the small notch ionized the air at that point and formed a conductive path to the start wire, allowing a capacitor to discharge and start the counter. The counter continued to count at a rate of 1 million counts/s until the same action at the stop wire caused it to stop. Thus, it was possible to read the burning time of 12 in. of MDC directly from the counter in microseconds. To establish the accuracy of the system, several strands of Pyrocore[3] were fired, and its propagation rate was measured. Its rate was found to be approximately the same as given by the manufacturer (14,000 ft/s). The rate of burning was read to 0.1 μs-ft. This sequence was repeated with each piece of MDC until all the samples had been fired.

No significant change in propagation (detonation) rate was noted. The largest change which occurred was in the propagation rate of Dipam, which was increased approximately 6% by the sterilization sequence. The test results, summarized in Table 3, indicate that all three kinds of MDC may be subjected to the entire thermal sterilization sequence with no degradation. These test results would also indicate that the degradation noted in the Lockheed program was not due to temperature changes.

Table 3. Average propagation rate in feet per second

Explosive material	Number of sterilization cycles						
	0	1	2	3	4	5	6
HNS	20533	20661	20408	20744	20920	20576	20408
Dipam	20040	21413	21551	21008	21505	20876	21321
NONA	22075	22675	21739	21834	22172	22026	21645

2. Chemical Heat Sources

a. Introduction. SPS 37-52, Vol. I, pp. 34–41, presented the results of some preliminary experiments carried out with one class of exothermic chemical reaction—the so-called *solid-solid* reaction. Both the reactants and products are in the solid state at room temperature in these reactions. Thus, they are of interest for spacecraft heaters because no liquids or gases under pressure need to be stored, and no gaseous products need be vented to a planetary atmosphere.

The results of those experiments were favorable, demonstrating the feasibility of several different solid-solid reactions. The gasless nature of the reactions was verified, and it was shown that they could be carried out in completely sealed metallic containers without melting, burnthrough, or other kinds of failure. The mixtures were readily ignited by glowing wires, with and without primers, and reacted essentially to completion. The feasibility of using solid-solid reactants in configurations wherein a number of discrete charges are prepackaged in close proximity to each other was also demonstrated. After screening a number of reactions, that between aluminum and copper oxide,

$$2Al + 3CuO \rightarrow 3Cu + Al_2O_3, \qquad \Delta H_r = -0.972\ \text{kcal/g} \tag{1}$$

was selected for further development.

This article will present the results of additional experiments conducted with the Al/CuO system. Specifically, it was recognized that the method of sealing a loading port or the passage for electric igniter wires through the wall of any reaction container would provide a potential leak path for the initially molten reaction products. Indeed, several instances of failure in the earlier-reported work were traceable to the method of introducing these igniter wires. Accordingly, a number of different configurations for simultaneously sealing the reaction containers (after loading with the chemical mixture) and introducing the lead wires were fabricated and tested. In addition, it was of interest to determine whether the Al/CuO reaction could be initiated after the reactants (and the sealed container enclosing them) had been sterilized by heating to 275°F for 36 h.

b. Apparatus. Four basic seal configurations were evaluated. In each case, the test fixture was a cylindrical copper block, 4 in. in diameter and 1.25 in. high. A ½-in.-diameter hole in the center of each block formed the receptacle for the chemical heat source—a mixture of aluminum and copper oxide containing 18.4 wt % aluminum. The igniter elements were commercial grade "electric matches,"[4] coiled lengths of nichrome resistance wire, or pyrotechnic initiators.

[3]Pyrocore, manufactured by du Pont, is a type of MDC containing PETN (pentaerythritol tetranitrate), barium peroxide, and aluminum.

[4]Model 1060, Flare–Northern Division of Atlantic Research, Saugus, Calif.

Test configuration 1 is shown schematically in Fig. 8. The electric match was positioned in the receptacle by means of an asbestos gasket and sealed with a potting compound.[5] Care was taken to assure that the potting filled the space between the lead wires and the hole in the gasket. Finally, an asbestos insulator and aluminum cover were put into place to hold in the igniter assembly against any possible pressure generated within the receptacle during the reaction. Each of the seven retaining screws was tightened to a torque of 28 in.-lb. The assembled test fixture was then held at 300°F for 2 h to cure the resin. This temperature ignited neither the electric match nor the chemical mixture.

Test configuration 2 is illustrated schematically in Fig. 9. Closure was effected by means of a threaded aluminum plug to which an electric match was potted.[6] The screw threads were relied on to resist any internal pressure, as well as to provide a labyrinthine, leak-resistant seal against the molten reaction products. The electric match lead wires were first inserted through the hole in the aluminum plug. Then the potting compound was poured into the match-well, and the match was positioned securely within the potting. Care was taken to assure that the wire passageway through the plug, as well as the match-well, were filled with potting compound. The plug/match assembly was then inserted into the receptacle containing the chemical mixture and tightened to a torque of 80 in.-lb. The potting was cured for 1 h at 250°F. This temperature did not ignite the electric match or the chemical mixture.

The basic arrangement of test configuration 3 is shown in Fig. 10. This was similar to test configuration 2, except that the plug/igniter assembly, made by modifying a standard squib,[7] had the lead-in wires sealed in a ceramic material within the plug. In what will be known here as modification 1 (Fig. 10), the igniter was made from an expended squib by connecting a ¼-in.-long piece of nichrome wire to the bridgewire terminals. In modification 2, an unmodified squib was used in place of the nichrome wire version. In modification 3, the igniter was again nichrome wire as in modification 1, but five ½-in.-diameter holes surrounded the central receptacle (Fig. 11). These were positioned along radii 72 deg apart, but located at varying radial distances from the center of the test fixture so that the minimum thickness of material between the central receptacle and each outer hole varied between 0.035 and 0.100 in. (Fig. 11). This was to gain additional information regarding the minimum separation possible between such holes in a "multiple-module" heater configuration (SPS 37-52, Vol. I) without local burnthrough.

[5]Epoxylite 8705, product of Epoxylite Corp., South El Monte, Calif.
[6]Ceramabond 503, Aremco Products, Briarcliff, N.Y.
[7]JPL part 10000029-1.

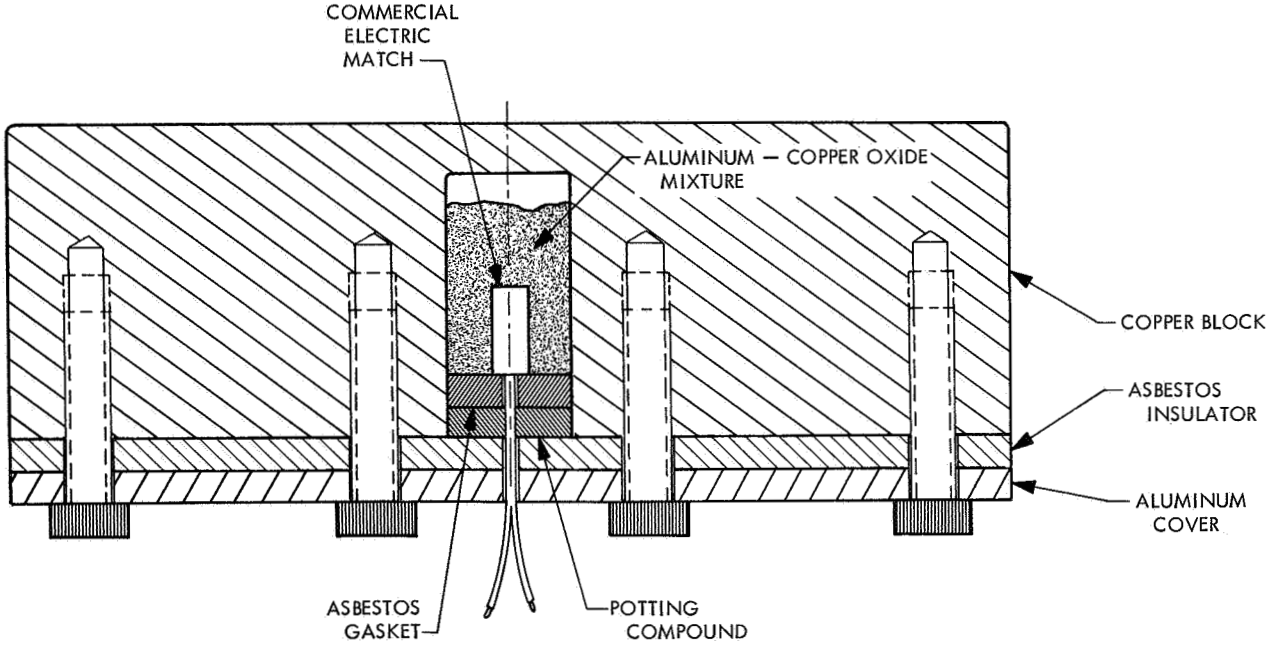

Fig. 8. Test configuration 1

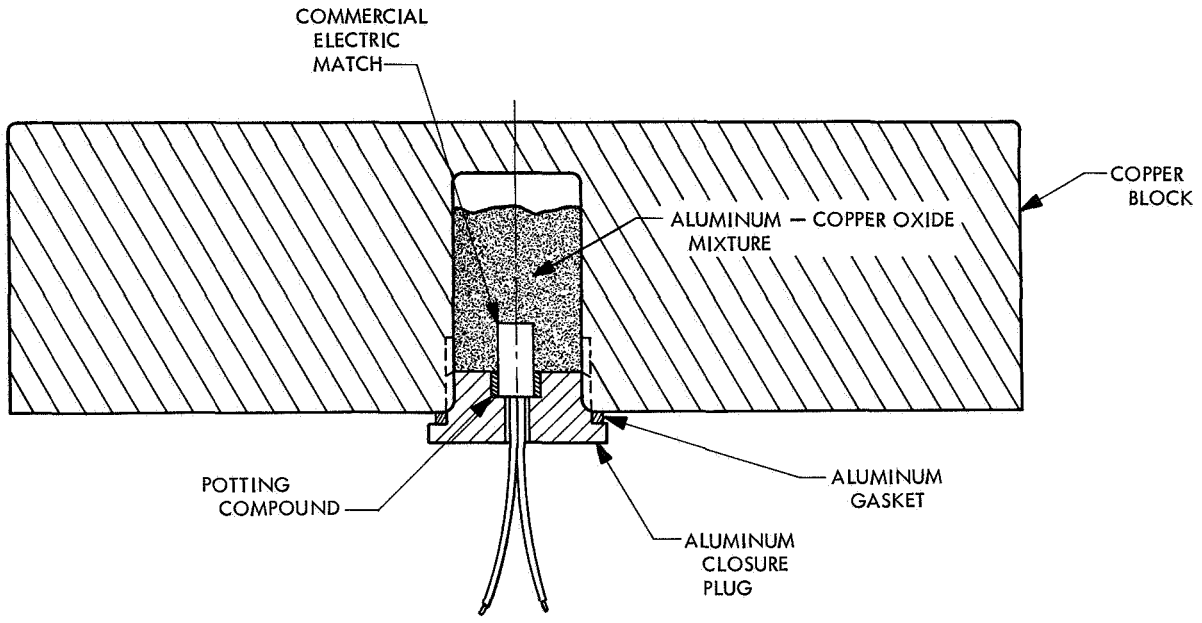

Fig. 9. Test configuration 2

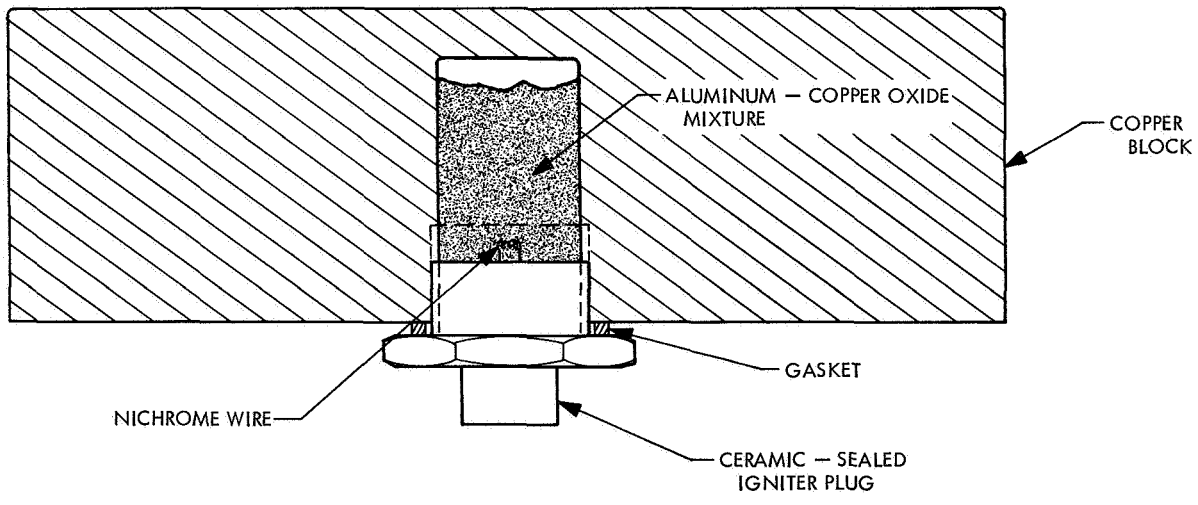

Fig. 10. Test configuration 3

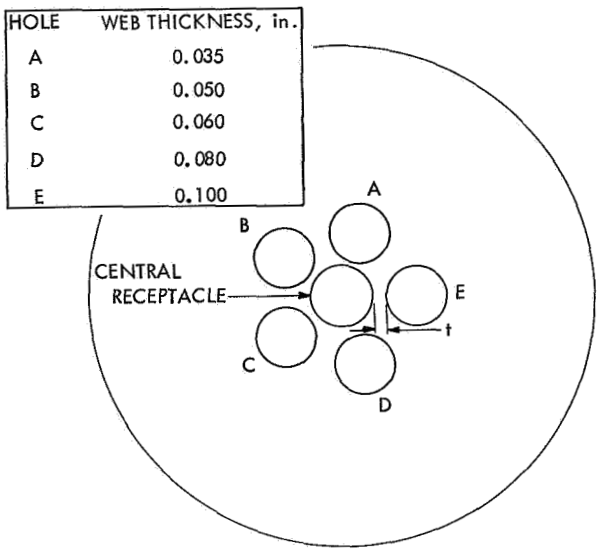

Fig. 11. Arrangement of supplementary holes in modification 3 of test configuration 3

The fourth and final seal test configuration is depicted in Fig. 12. The electric match was again held within the chemical mixture receptacle by a threaded plug, with the lead wires passing through a hole in the center. This time, however, the seal was effected by electroforming a 0.125-in.-thick layer of copper over the plug. A special coating, sprayed onto the insulation of the lead wires, made it externally conductive so that these wires were firmly embedded in the electroformed copper matrix. For test purposes, the opposite end of the receptacle (top in Fig. 12) was closed with a simple, screw-in filler plug so that the chemical charge could be loaded after electroforming. In a flight design, this end of the device would be completely closed (e.g., as in Fig. 10), and the electroforming would be accomplished with the charge in place.

The apparatus used for each of the two sterilization tests was a single steel capsule of the type described in SPS 37-52, Vol. I. This device is depicted in Fig. 13. Nichrome wire comprised the igniters. The test device was filled essentially to capacity with the chemical charge, which was lightly tamped in place.

c. Test procedures. Testing was accomplished on A-stand at JPL's Edwards Test Station. Each seal test fixture was set on ¼-in.-high wooden blocks on a table covered with ¼-in.-thick aluminum plate. The fixtures were all positioned so that the seals to be evaluated were on the bottom and would be subjected to maximum contact with the molten reaction products due to gravity. The two sterilized[8] test fixtures were mounted on a small bracket like that shown in Fig. 13, except that in the present tests they were inverted (wires entering from the top) to keep molten material *away* from the seal. This was done because past experience (SPS 37-52, Vol. I)

[8]275°F for 36 h.

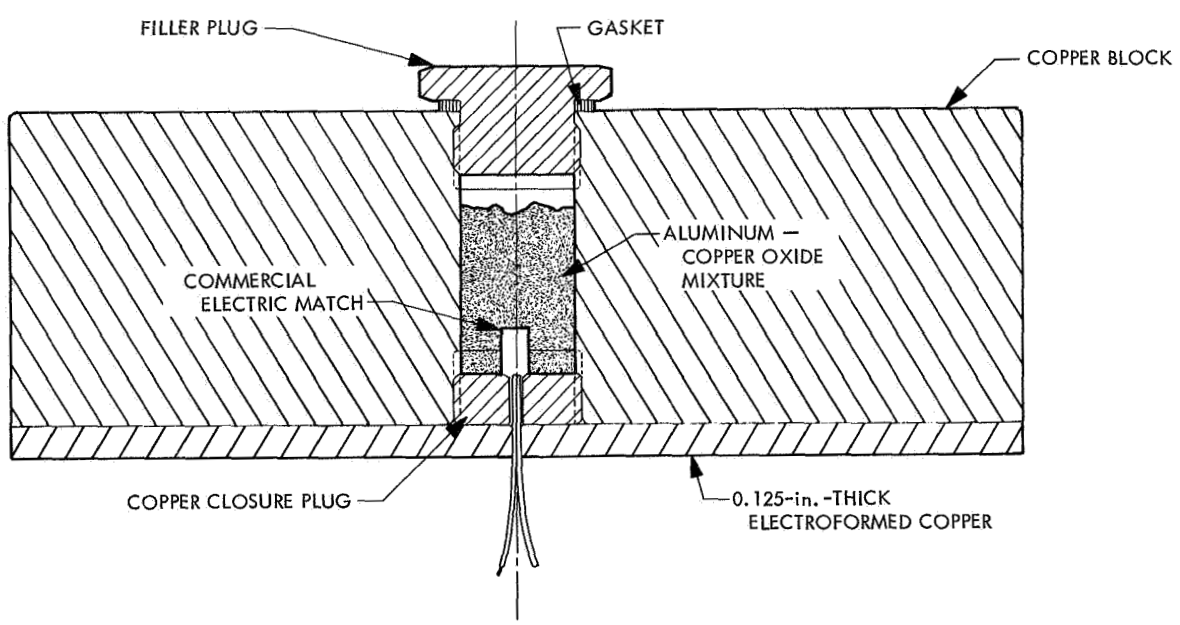

Fig. 12. Test configuration 4

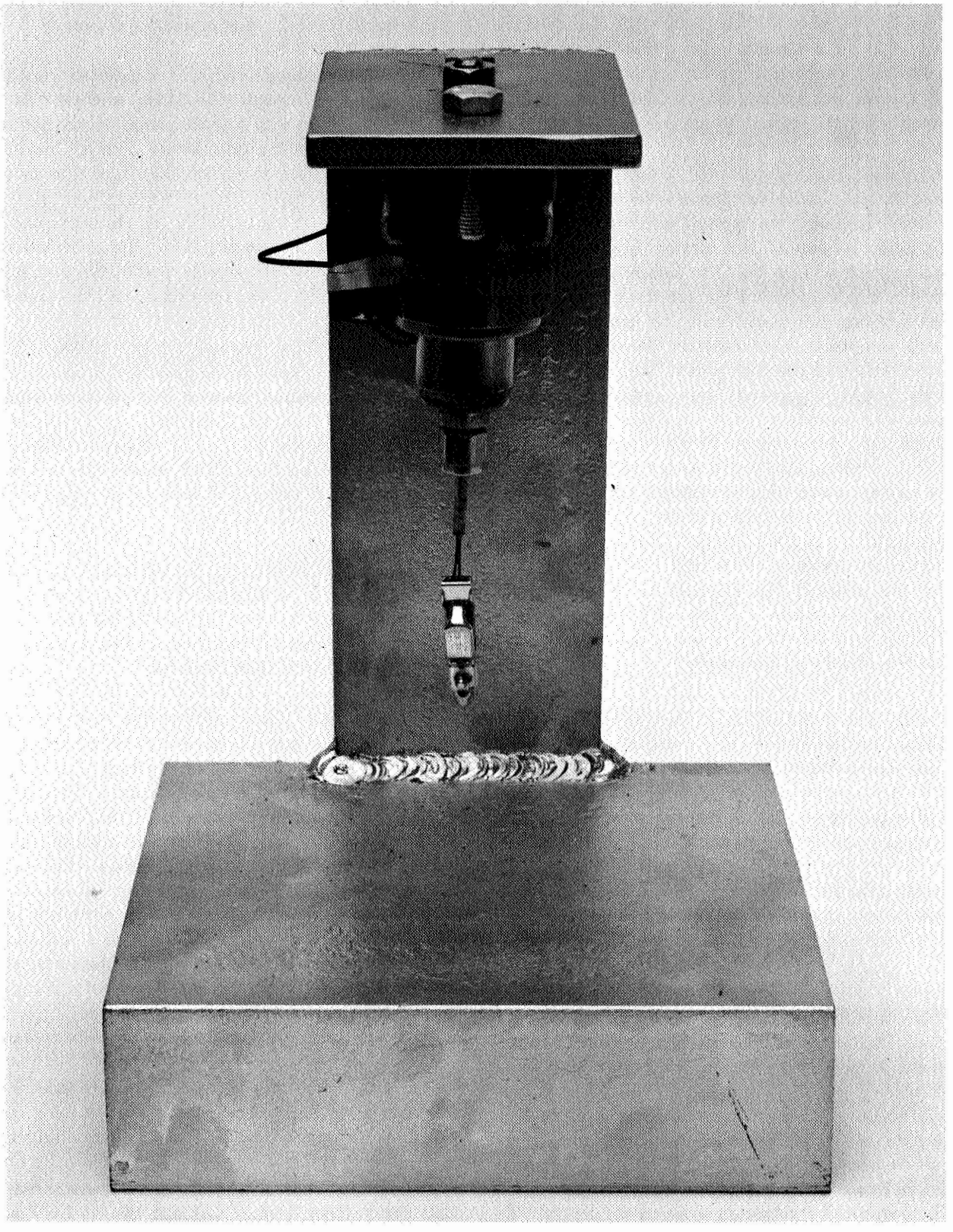

Fig. 13. Stainless steel capsule positioned on mounting bracket

showed that the relatively crude seals would fail due to faulty welds. The object of the tests with the sterilized devices was to see if ignition after sterilization was possible, and *not* to evaluate any seals; so the orientation of the test fixtures was immaterial. In both cases, the devices were remotely ignited by means of a 28-V direct current.

d. Results and discussion. The seal on test configuration 1 failed, expelling the molten reaction products. A metallographic section of this device is shown in the photomacrograph of Fig. 14a. The failure appears to be located at a single point on the interface between the solidified potting compound and the copper wall of the charge receptacle. This may have been due to some local imperfection or piece of foreign matter which prevented the potting compound from wetting the wall at that point. The molten reaction products subsequently burned through the asbestos insulator and aluminum cover. There was no infiltration of the molten products into the passage containing the igniter wires, or at any other point around the periphery of the solidified potting. Although a failure occurred in this case, it is believed that further development could lead to a workable seal based on this concept. The selection of the most satisfactory potting compound, and the establishment of surface finishing and cleanliness specifications, are among the items that should be considered.

Test configuration 2 also failed when fired. The failure was confined to the aluminum closure plug (Fig. 14b), and there was no detectable infiltration of molten products into the screw threads. The potting compound surrounding the electric match was apparently breached, permitting passage of the molten products through the match-well and the wire passage, both of which were appreciably enlarged in the process. Either the Ceramabond was not capable of resisting the molten copper–slag mixture, or not enough of it was used in test configuration 2.

All three modifications of test configuration 3 were successfully fired, achieving complete containment of the reaction products. The post-test appearance of modification 3 is shown in Fig. 14c, where it may be seen that there was no penetration of the products through either the screw threads or the ceramic seal around the wires. There was a clean and well-defined interface between the solidified mixture and the top edge of the igniter plug. There was no burnthrough between the central hole and any of the five surrounding holes on modification 3. However, a dark spot was observed at one point on the inner wall of hole *A* (Fig. 11), indicating that a web thickness of 0.035-in. is marginal for copper.

Test configuration 4 was also completely successful in containing the molten Cu–Al_2O_3 mixture. As shown in Fig. 14d, there was no penetration of this mixture into the threads of the copper closure plug, or into the wire cavity. The degree to which the electroformed copper adhered to the original copper surface, and to which the igniter wires were embedded in the electroformed copper matrix, may be seen in Fig. 14d. The solidified copper–slag mixture remained wholly within the charge cavity, again maintaining a clean interface with the closure plug.

In all cases, there was no evidence of the inclusion of any unreacted material in the solidified products. Sections through the metallic portion of the product showed a very homogeneous material, uniformly bronze-like in color, which is apparently an alloy of copper containing a low percentage of aluminum. Such results are in agreement with those of the chemical analysis of such residues reported in SPS 37-52, Vol. I.

Both sterilization tests were successful. In each case, heating at 275°F for 36 h did not prematurely ignite the chemical mixtures. Upon removal from the oven, however, both devices were successfully ignited by the application of 28-V direct current.

e. Conclusions. The results of this work have demonstrated that it is possible to seal chemical heater charge containers against the molten products (Cu and Al_2O_3) that are formed during the exothermic reaction of Al and CuO. Both the threaded joints and a solid matrix of electroformed copper enabled complete containment of the products. Threaded joints would probably be favored for reasons of simplicity. Seals consisting all or in part of epoxy resins or potting compounds were not effective against the molten products, although it seemed likely that one of these seal concepts could be perfected through additional development effort. The use of a ceramic seal to effect passage of the igniter wires into the charge receptacle was found to be successful in every case.

It is also possible to successfully ignite stoichiometric mixtures of Al and CuO after exposure to heat sterilization cycles presently required for planetary landers.

The chemical heater work conducted to date has shown that combustion devices utilizing the Al–CuO reaction are gasless, sterilizable, readily ignited, and thermally efficient. They will operate in any position, and may be

(a) TEST CONFIGURATION 1

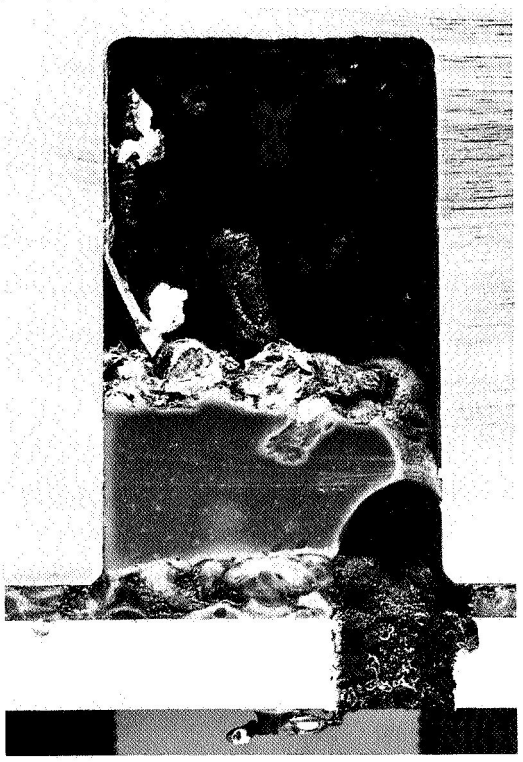

(b) TEST CONFIGURATION 2

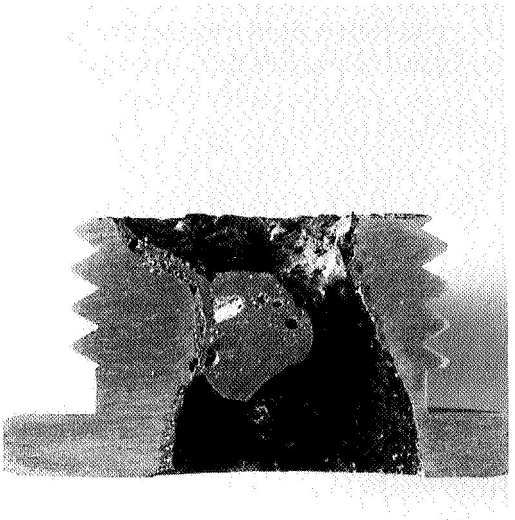

(c) TEST CONFIGURATION 3

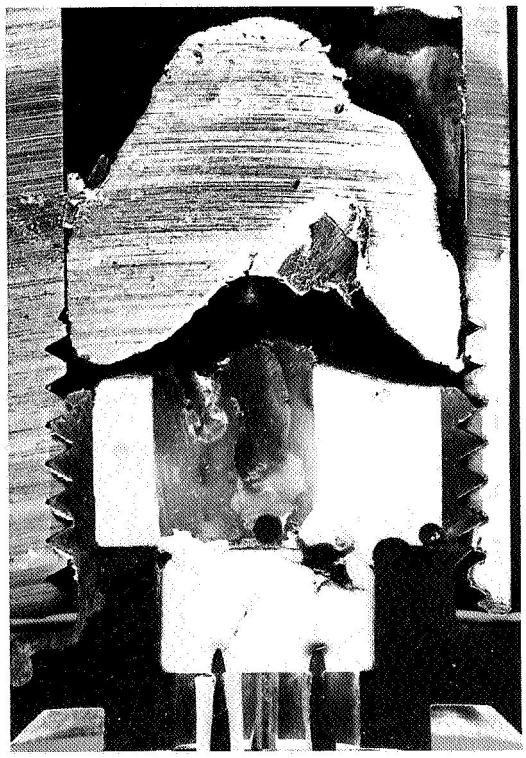

(d) TEST CONFIGURATION 4

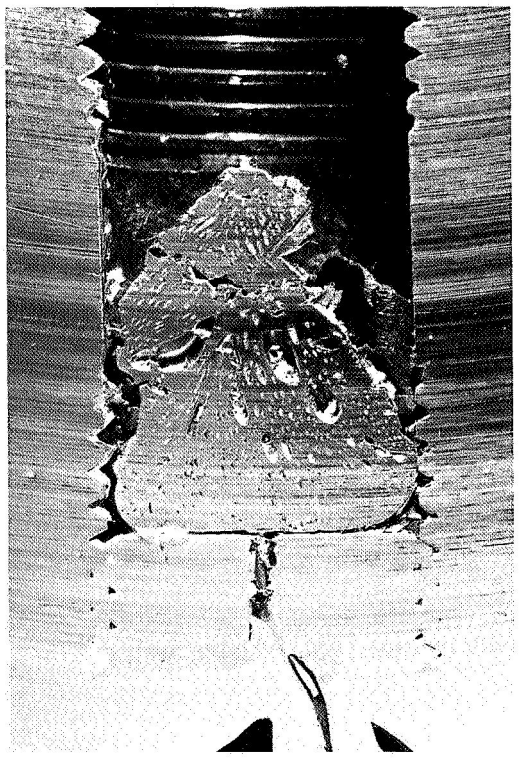

Fig. 14. Post-test sections of four test configurations

completely contained in sealed containers, provided that sufficient attention is paid to seal design and thermal stress analysis. This, plus their potential impact resistance, lack of moving parts, and absence of any stored gases or liquids under pressure, makes them appear particularly attractive for use as chemical heat sources for planetary landers. Their development to flight prototype status appears to be both feasible and desirable.